DEVELOPMENT OF EPPT1 TARGETED BIOCOMPATIBLE DRUG DELIVERY SYSTEM AND INVESTIGATION OF ITS ANTICANCER ACTIVITY

MSc. Thesis

Ezgi KARACA

Graduate School of Engineering and Natural Sciences

Biomedical Engıneering and Bioinformatics

September 2020

DEVELOPMENT OF EPPT1 TARGETED BIOCOMPATIBLE DRUG DELIVERY SYSTEM AND INVESTIGATION OF ITS ANTICANCER ACTIVITY

A THESIS SUBMITTED TO

THE GRADUATE SCHOOL OF

ENGINEERING AND NATURAL SCIENCES

OF ISTANBUL MEDIPOL UNIVERSITY

IN PARTIAL FULFILLMENT OF THE REQUIREMENTS FOR

THE DEGREE OF

MASTER OF SCIENCE

IN

BIOMEDICAL ENGINEERING AND BIOINFORMATICS

by

Ezgi KARACA

September, 2020

Development Of EPPT1 Targeted Biocompatible Drug Delivery System And Investigation Of Its Anticancer Activity

By Ezgi Karaca

September 2020

We certify that we have read this thesis and that in our opinion it is fully adequate, in scope and in quality, as a thesis for the degree of Master of Science.

Assoc. Prof. Dr. Yasemin Yüksel Durmaz (Advisor)

Assist. Prof. Mehmet Hikmet Üçışık

Assist. Prof. Dr. Ömer Aydın

Approved by the Graduate School of Engineering and Natural Sciences:

Assoc. Prof. Dr. Yasemin Yüksel Durmaz
Director of the Graduate School of Engineering and Natural Sciences

Foreword

As the world moves further into the sophisticated nanotechnology age, multidisciplinary research gains importance for medical research areas too. This thesis content comprises the fundamentals of chemistry, nanotechnology, and biomedical science. Drug delivery system (DDS) design and an investigation were developed for breast cancer treatment at the nano level. Receptor-mediated, Graphene (G) based DDS was designed with the pH-triggered functionality with the help of a unique copolymer coating on it. Results show that an optimized carrier which is peptide conjugated and, targeted is biocompatible and drug-carrying capacity is tunable so that is a promising material for further conjugations to become an artificial vector for gene delivery.

I hereby, declare that this thesis is my own work and that, to the best of my knowledge and belief, it contains no material, which has been accepted or submitted for the award of any other degree or diploma. I declare that where necessary I have obtained the appropriate copyright permission for any material from the thesis that has previously been published for its inclusion in the thesis. I also declare that this thesis contains no material previously published or written by any other person except where due reference is made in the text of the thesis.

Name, Surname: EZGİ KARACA

Signature:

Acknowledgment

Foremost, I would like to express my sincere gratitude to my thesis advisor Dr. Yasemin Yüksel Durmaz for her continuous support during the past two years.

My dear friends Nur Damla Korkmaz, Fatma Koç and Gizem Keçeloğlu, Hanife Pekel, Metehan İlter for our laboratory and office neighborship and their moral support,

Dear Ahmet Enes Duranay, Haji Muhammed Furqan Madni, and Bilal Janjua for their endless support,

Amore-mio Elif Nur Yılmaz, who suddenly became more than a lab fellow over the past year,

My dear husband and my best friend Kaan Başavcı for his lifelong partnership,

Last but not least, my family Emine and Cemal Karaca as the pillar of my life, for always believing in my way of life,

And my angel brother Doruk.

Contents

1. INTRODUCTION 1

2. BACKGROUND 8

2.1 Cancer 8

2.2 Cancer Treatment Options 10

2.2.1 Radiotherapy 10

2.2.2 Surgery 11

2.2.3 Chemotherapy 11

2.2.4 Controlled Drug Delivery System 12

2.2.4.1 Passive Accumulation In Tumor 13

2.2.4.2 Active Accumulation In Tumor 14

2.2.5 Targeted Drug Delivery System 15

2.2.5.1 Peptides as Targeting Ligands 17

2.3 Graphene-Based Targeted Drug Delivery System 19

3 EXPERIMENTAL SECTION 21

3.1 Materials 21

3.1.1 Chemicals and Reagents 21

3.2 Methods 22

3.2.1 Synthesis of PEG Containing poly[(ethylene glycol methacrylate)-*co*-(methyl methacrylate)-*co*-(1-pyrene methacrylate)-*co*-(3-azido propyl methacrylate) Graft Copolymer (P(PEGMA-*co*-AzPMA-*co*-MMA-*co*-PMA)); *PAMP* 22

3.2.1.1 Synthesis of 1-Pyrenemethyl Methacrylate Monomer; PMA 23

3.2.1.2 Synthesis of Azido-1-Propyl Methyl Methacrylate Monomer; AzPMA 24

3.2.1.3 Synthesis of Benzyl Group Containing Initiator (2-bromo-2-methyl propionate) 25

3.2.2 PAMP Coating on Reduced Graphene Oxide and *in situ* Reductions of Graphene Oxide; PAMP-rGO 25

3.2.3 Preparation of EPPT1 Targeting, PAMP Coated Nano platform by Cupper Catalyzed Azide-Alkyne Click Reaction; PAMP-rGO-EPPT1 26

3.2.4 Capping Remaining Azide Groups with Propargyl Alcohol; PMP-rGO-EPPT1 27

3.2.4.1 Synthesis of Alkyne-PEG-EPPT1 28

3.2.5 Drug Loading on EPPT1 Targeted PAMP Coated rGO Nanoplatforms; PAMP-rGO-EPPT1-Dox and PMP-rGO-EPPT1-Dox 29

3.2.6 Drug Loading on PAMP Coated rGO Followed by Conjugation of EPPT1 Peptide; PAMP-rGO-Dox-EPPT1 31

3.2.7 In-Vitro Drug Release Study 32

3.2.7.1 Cell Viability Analysis 33

3.2.7.2 Cellular Uptake Studies 34
4 RESULTS 36
4.1 Preparation of EPPT1 Targeting, Drug Loaded, and PAMP Copolymer Coated rGO-based Nano platform 36
4.2 Synthesis and Characterizations of PAMP Copolymer 37
4.3 The PAMP Copolymer Coating and *in-situ* Reduction of Graphene Oxide *in-situ*: PAMP-rGO and Its Characterization 39
4.4 Conjugation of EPPT1 Peptide on PAMP-rGO or PAMP-rGO-Dox Nano platform: (PAMP-rGO-EPPT1) 41
4.5 Drug Loading on EPPT1 Targeted PAMP Coated rGO Nanoplatforms: PAMP-rGO-EPPT1-Dox and PMP-rGO-EPPT1-Dox 46
4.6 The Effect of Copolymer Features in Drug Release Profile at Physiological and Acidic Environment 54
4.6.1 Investigation of the Effect of Azide Groups and PEG Brush Length of Copolymer on Drug Release Profile 54
4.6.2 Investigation of the Effect of Presence and Order of EPPT1 Peptide Conjugation on Drug Release 56
4.7 Anticancer Activity of Targeted Nano platform 61
4.7.1 MTS Assay 61
4.7.2 Resazurin Assay 63
4.7.3 Investigation of Selective Cellular Entry of Biocompatible Targeted and Non-Targeted GO Based Nano platform 67
4.7.3.1 Confocal Microscopy Imaging of Cellular Entry of Targeting Nanocarriers . 67
4.7.3.2 Flow Cytometry Analysis of Cellular Entry of Targeted Nanocarrier 68
5 DISCUSSION 70
5.1 Synthesis and Characterization of Targeted Drug Carrier 70
5.2 Drug release Profiles of Dox Loaded Targeted and non-targeted Nanocarriers 76
5.3 In-Vitro Experiments 78
6 CONCLUSIONS AND FUTURE WORK 81
7 BIBLIOGRAPHY 83

List of Figures

Figure 1.1: Properties and applications of graphene derivatives 1
Figure 1.2: Schematic of the formation of reduced graphene oxide (rGO) and graphene oxide (GO) from graphene (or graphite). Picture owner is InvestorIntel & 2017 InvestorIntel Corp. 2
Figure 1.3: Schematic representation of the hypothesis of the project 7
Figure 2.1: Numbers of the deaths by cause, World, 2017. IHME, Global Burden of Disease. 9
Figure 2.2: The distribution of cancer types worldwide from 1990 to 2017. IHME, Global Burden of Disease. 9
Figure 2.3: EPR effect representation [49]. 14
Figure 2.4: Types of nanoparticles used in targeted drug delivery [56]. 15
Figure 2.5: Schematic representation of active targeting mechanisms by which nanocarriers can deliver drugs& image agents to the target cells. (A) Ligands on the surface of the nanoparticles attach to a special receptor on the target cells; (B) Starting internalization of the nanoparticle–receptor complex by receptor-mediated endocytosis and vesicular transport through the endosomes; (C) Internalize into the cell and release its cargo into the target cell [56]. 16
Figure 3.1: Schematic representation of PAMP coating and in-situ reduction to rGO. 26
Figure 3.2: Schematic representation of EPPT1 peptide conjugation on the PAMP-rGO surface 27
Figure 3.3: Schematic representation of capping remaining azide groups on PAMP-rGO-EPPT1. 28
Figure 3.4: Symbolic representations of drug loading on PAMP-rGO-EPPT1 and PMP-rGO-EPPT1 30
Figure 3.5: Symbolic representation of order of drug loading and EPPT1 pepdite conjugation on PAMP-rGO to obtain PAMP-rGO-Dox-EPPT1 and PMP-rGO-Dox-EPPT1 32
Figure 4.1: Schematic representation of EPPT1 targeting, drug-loaded PAMP coated rGO nanoplatforms 36
Figure 4.2: Chemical reactions of a) the initiator, b) PMA, c) AzPMA, and d) ATRP copolymerization of monomers. 38

Figure 4.3 TGA curves of **a)** GO, rGO, $(P_{15}A_{10}MP)_{2000}$, $(P_{15}A_{10}MP)_{2000}$-rGO, and **b)** GO, rGO, $(P_{26}A_{16}MP)_{500}$, $(P_{26}A_{16}MP)_{500}$-rGO compositions. 40
Figure 4.4 AFM analysis of **a)** GO and **b)** PAMP-rGO 41
Figure 4.5: Schematic illustration of EPPT1 peptide conjugation 42
Figure 4.6: ^{1}H NMR spectrum of a) Alkyne-PEG-NHS, b) EPPT1 and, c) Alkyne-PEG-EPPT1 43
Figure 4.7: Calibration curve for the Ellman's Assay 44
Figure 4.8: FTIR spectrum of a) AzPMA, b) $PAMP_{500}$, c) $PAMP_{500}$-rGO, d) PMP_{500}-EPPT1 45
Figure 4.9 a) UV-Visible full-spectrum scanning **b)** Absorption calibration curve through different concentration of Dox-HCl 47
Figure 4.10 Drug loading efficiency (LE) chances depend on temperature. 47
Figure 4.11: SEM images of **a)** GO, **b)** rGO, **c)** $P_{23}MP_{500}$-rGO, **d)** $P_{23}MP_{500}$-rGO-Dox, **e)** $P_{15}MP_{2000}$-rGO-EPPT1-Dox with low magnification, **f)** $P_{15}MP_{2000}$-rGO-EPPT1-Dox with high magnification and, **g)** SEM-EDX analysis of some compositions 49
Figure 4.12: TEM images of **a)** $(P_{15}A_{10}MP)_{2000}$-rGO-Dox, **b)** $(P_{15}A_{10}MP)_{2000}$-rGO-EPPT1, **c)** $(P_{15}A_{10}MP)_{2000}$-rGO-EPPT1-Dox and, **d) (**$P_{15}A_{10}MP)_{2000}$-rGO-Dox-EPPT1 50
Figure 4.13 TGA curves of **a)** GO, rGO, Dox, $(P_{26}A_{16}MP)_{500}$, $(P_{26}A_{16}MP)_{500}$-rGO, and $(P_{26}A_{16}MP)_{500}$-rGO-Dox, $(P_{26}A_{16}MP)_{500}$-rGO-Dox-EPPT1 **b)** GO, rGO, Dox, $(P_{15}A_{10}MP)_{2000}$, $(P_{15}A_{10}MP)_{2000}$-rGO, $(P_{15}A_{10}MP)_{2000}$-rGO-Dox, $(P_{15}A_{10}MP)_{2000}$-rGO-Dox-EPPT1 compounds. 51
Figure 4.14: Raman spectra of a) GO, b) rGO, c) PAMP-rGO, d) PAMP-rGO-Dox compounds. 52
Figure 4.15: DLS and Zeta analysis of carriers. 53
Figure 4.16 In-vitro drug release profile of **a)** $(P_{15}A_{10}MP)_{2000}$-rGO-Dox, $(P_{15}MP)_{2000}$-rGO-Dox **b)** $(P_{26}A_{16}MP)_{500}$-rGO-Dox, $(P_{26}MP)_{500}$-rGO-Dox at pH 5.5 and 7.4**.** Values represent mean+ SEM from three independent experiments. 55
Figure 4.17: In- vitro drug release profiles of the $(P_{26}A_{16}MP)_{500}$-rGO-Dox, $(P_{25}A_{17}MP)_{2000}$-rGO-Dox, and $(P_{15}A_{10}MP)_{2000}$-rGO-Dox at pH 5.5 and 7.4. Values represent mean+ SEM from three independent experiments. 56
Figure 4.18: In-vitro drug release profiles of **a) (**$P_{15}A_{10}MP)_{2000}$-rGO-Dox, $(P_{15}A_{10}MP)_{2000}$-rGO-Dox-EPPT1 and **b)** $(P_{26}A_{16}MP)_{500}$-rGO-Dox, $(P_{26}A_{16}MP)_{500}$-rGO-

Dox-EPPT1 at pH 5.5 and 7.4. Values represent mean+ SEM from three independent experiments. 57
Figure 4.19: In-vitro drug release profiles of **a) (**$P_{15}MP)_{2000}$-rGO-Dox-EPPT1, $(P_{15}MP)_{2000}$-rGO-EPPT-Dox and **b)** $(P_{15}A_{10}MP)_{2000}$-rGO-Dox-EPPT1, $(P_{15}A_{10}MP)_{2000}$-rGO-EPPT1-Dox at pH 5.5 and 7.4. Values represent mean+ SEM from three independent experiments. 58
Figure 4.20: In-vitro drug release profiles of **a) (**$P_{15}MP)_{2000}$-rGO-Dox, $(P_{15}A_{10}MP)_{2000}$-rGO-Dox, $(P_{15}MP)_{2000}$-rGO-EPPT1-Dox, $(P_{15}A_{10}MP)_{2000}$-rGO-EPPT1-Dox and **b)** $(P_{26}MP)_{500}$-rGO-Dox, $(P_{26}A_{16}MP)_{500}$-rGO-Dox, $(P_{26}MP)_{500}$-rGO-EPPT1-Dox, $(P_{26}A_{16}MP)_{500}$-rGO-EPPT1-Dox at pH 5.5 and 7.4. Values represent mean+ SEM from three independent experiments. 59
Figure 4.21: In-vitro drug release profiles of **a) (**$P_{26}A_{16}MP)_{500}$-rGO-Dox-EPPT1, $(P_{26}A_{16}MP)_{500}$-rGO-EPPT1-Dox and **b)** $(P_{23}MP)_{500}$-rGO-Dox-EPPT1, $(P_{26}MP)_{500}$-rGO-EPPT1-Dox at pH 5.5. Values represent mean+ SEM from three independent experiments. 60
Figure 4.22 MTS assay analysis of $(P_{15}A_{10}MP)_{2000}$ derivatives on MDA-MB-231cancer cell line at **a)** 24h and **b)** 48h 62
Figure 4.23: Resazurin assay analysis of $(P_{15}A_{10}MP)_{2000}$ derivatives on MCF-7 cancer cell line at **a)** 24h and **b)** 48h 64
Figure 4.24: Resazurin assay analysis of $(P_{26}A_{10}MP)_{200}$ derivatives on MCF-7 cell line at **a)** 24h and **b)** 48h 66
Figure 4.25: Cellular uptake analysis of $P_{15}MP_{2000}$-rGO-Dox and $P_{15}MP_{2000}$-rGO-EPPT1-Dox with MCF-7 68
Figure 4.26: FACS analysis results of targeted $PAMP_{2000}$-rGO-Dox-EPPT1, non-targeted $PAMP_{2000}$-rGO-Dox nanoplatforms, and Free-Dox 69

List of Scheme

Scheme 3.1: Controlled polymerization with PEGMA, PMA, MMA, and AzPMA monomers..... 23
Scheme 3.2: Synthesis of the 1-pyrenemethyle methacrylate..... 23
Scheme 3.3: Synthesis of 3-azido-1-propanol 24
Scheme 3.4: Synthesis of azido-1-propyl methyl methacrylate (AzPMA)..... 25
Scheme 3.5: Synthesis of benzyl group-containing initiator..... 25
Scheme 3.6: Synthesis of alkyne-EPPT1-PEG 29

List of Equations

Equation 3.1: Calculation of LE and LC 30
Equation 3.2: Calculation of % Drug Release 32
Equation 3.3: Calculation of Cell Viability % from Absorbance. 33

List of Abbreviation

G: Graphene

GO: Graphene Oxide

rGO: Reduced Graphene Oxide

PEG: Poly(ethylene glycol)

PMA: 1-pyrenemethyle methacrylate

MMA: Methyl methacrylate

AzPMA: 3-Azidopropil methacrylate

PMDETA: N,N,N′,N″,N″-Pentamethyldiethylenetriamine

Dox: Doxorubicin-HCl

ATRP: Atom transfer radical polymerization

CuAAC: Copper(I)-Catalyzed Azide Alkyne Cycloaddition

FPT: Freeze-Pump-Thaw

DMF: Dicholomethane

DMAP: 4-Dimethylaminopyridine

EDC: 1-Ethyl-3-(3-dimethylaminopropyl)carbodiimide

DTNB: 5,5'-dithiobis-(2-nitrobenzoic acid), Ellman’s Reagent

THF: Tetrahydrofurane

MTS: 3-(4,5-Dimethylthiazol-2-yl)-2,5-diphenyltetrazolium bromidefor

DMEM: Dulbecco's Modified Eagle's Medium

TGA: Thermal Gravimetric Analysis

FBS: Fetal Bovine Serum

PBS: Phosphate-buffered saline

LE: Loading Efficiency

LC: Loading Content

^{1}H-NMR: Hydrogen Nuclear Magnetic Resonance

FTIR: Fourier Transformation Infrared

AFM: Atomic Force Microscopy

SEM: Scanning Electron Microscopy

EDX: Energy Dispersive Using X-Ray

DLS: Dynamic Light Scattering

RES: Reticuloendothelial System

List of Symbols

Π : pi bonding

μg: Microgram

μL: Microliter

ε :Absorptiviy coefficient

λ : wavelength

ÖZET

EPPT1 PEPTİDİ İLE HEDEFLENMİŞ BİYOUYUMLU İLAÇ TAŞIMA SİSTEMİNİN GELİŞTİRİLMESİ VE ANTİKANSER ETKİLERİNİN İNCELENMESİ

Ezgi KARACA

Biyomedikal Mühendisliği ve Biyoinformatik, Yüksek Lisans

Tez Danışmanı: Doç. Dr. Yasemin Yüksel Durmaz

Eylül, 2020

Son zamanlarda grafenin (G) diğer biyomalzemelere göre üstün öözellikleri onu antikanser ilaç taşıma sistemi, gen ve peptit taşınmasında önemli bir material haline getirmiştir. Bir diğer yandan toksit etkileri kullanımı sınırlandırabilir. Grafen oksit (GO) onu hidrofilik yapan çok sayıda fonksiyonel oksijen grubu bulundurur. Fakat GO`in sahip oldu sp^3 hibridize karbonları sebebiyle kusurlu yüzey oluşumu bulunmaktadır. GO üzerindeki oksijen grubunun azaltılmasıyla bu problem ortadan kalkabilir fakat çözünürlüğü kısmen azalır. Bunun için indirgenmiş grafen oksit (rGO) yapısı GO'in oksijence zengin gruplarının indirgenmesiyle elde edilir. rGO daha düzgün ve geniş yüzey alanı ve daha az toksisiteye neden olması rGO'yu biyolojik uygulamalar için daha cazip kılar. Fakat suda çözünürlüğünün ve biyouyumluluğunun düşük olması aşılması gereken bir sorundur ve bunun için genellikle yüzey kaplama stratejileri takip edilir. Poli(etilen glikol) (PEG) yüzey alanı kaplaması için kullanılan polimerlerden olup, kaplandığı nanoparçacığın kandaki dolaşım süresini uzatır ve immün hücreler tarafından karaciğer ve dalaktan atılımını engeller. Bu tez çalımasında, EPPT1 peptidiyle hedefli hale getirilmiş, rGO'nun biyouyumluluğunun iyileştirildiği grafen bazlı bir ilaç taşıma sisteminin geliştirimesi çalışılmıştır. Grafen oksidin yüzeyi indirgenirken poli [(etilen glikol metakrilat)-*ko*- (metil metakrilat)-ko-(1-pirenmetakrilat) -*ko*-(3-azido propil metakrilat)] P[PEGMA-co-MMA-co-PMA-co-AzPMA]'nın π-π etkileşimiyle yüzeye kaplanmasıyla biyouyumluluk arttırılıp, fonksiyonlanabilir hale getirilmiştir. Hedefleyici ajan EPPT1 peptidi grafen yüzeyinin sahip olduğu azit gruplarına click reaksıyonu kullanılarak aşılanmıştır. Kanser hücrelerin hücre zarında yüksek orandaki varlığı bilinen reseptorlerden olan uMUC1 reseptorünü tanıyan peptit konjugasyonuyla grafen tabanlı ilaç tasıma sistemi hedefli hale getirilmiştir. Hedeflenen biyouyumlu nanoplatform kaplanan kopolimerdeki PEG gruplarının uzunluğu (500 g/mol ve 2000 g/mol) ve iyonik azit gruplarının varlığının ilaş yükleme ve salım davranışına etkileri ayrıntılı olarak incelenmiştir. Ayrıca, ilacın kompozisyona yüklenme sırası ve yüzeyde hedefleyici ajanın varlığının ilaç salım davranışı üzerine etki ettiği gözlenmiştir. % 95'e kadar ilaç yükleme kapasitesine sahip sistemin asidik (pH:5.5) ve nötr (pH:7.4) ortamlarda ilaç salım profilleri ortaya koyulmuştur. Elde edilen taşıyıcıların antikanser aktivitesi, MTS ve Resazurin testleri kullanılarak MCF-7 ve MDA-MB-231 meme kanseri hücrelerinde test edildi. Bunun sonucunda daha uzun PEG'li kopolimerleri ilaç salımının yavaşlamasına ancak biyouyumluluğun ve çözünürlüğün artmasına sebep olduğu, azit grubu içeren kompozisyonların Doxorubisin (Dox) ilacıyla arasındaki iyonik etkileşim daha hızlı bir ilaç salım profili oluşturduğu, hedefleyici peptide EPPT1 konjugasyonu sonrası kompozisyonlarda her iki PEG uzunluğunda (500 g/mol ve 2000 g/ mol) yük dengeliyici etki gösterdiği ve ilaç salımını yavaşlattığı gibi etkiler gözlenmiştir. İlaç salım profilleri de belirlenen farklı kompozisyonalarla *in-vitro* deneyler yapılarak, MTS, Resazurin testi

meme fibroblast sekonder hücre hatlarında (MCF-7 ve MDA-MB-231) negatif kontrol, pozitif kontrol, boş taşıyıcı, hedefli ilaçsız ve hedefli Dox yüklü taşıyıcılar test edilmiştir. Sonuçlar ışığında Dox'un dalga boyu sebebiyle Resazurin testi en güvenilir test olarak seçilmiştir. PEG_{2000} içeren kompozisyonlar için 7.5 µg/ ml Dox içeren hedeflenmiş rGO nanotaşıyıcılarla etkileşmiş hücrelerin 48 saat sonrasında yalnızca % 24 oranında canlı kalabildiği aynı koşullarda Dox ile muamele edilen hücrelerin ise % 25'inin canlı kaldığını gözlemlenmiştir.. Son olarak kompozsiyonların seçici olarak hücreye giriş kabiliyetlerini gözlemlenmek amacıyla eş odaklı mikroskopi ve akış sitometrisi ile nitel ve nicel olarak kanser hücrelerindeki etkinliği gözlemlenmiştir. Bunların sonucunda EPPT1 peptit içeren taşıyıcıların seçici olarak diğerlerine göre hücre içinde birikiminin fazla olduğu kanıtlanmıştır.

Anahtar Kelimeler: Grafen oksit, PEG, pi-pi etkileşimi, Doksorubisin, Hedefleme, Nanotaşıyıcı

*Bu çalışmaya sağlamış olduğu maddi destek için Türkiye Bilimsel ve Teknolojik Araştırma Kurumu'na (TÜBİTAK) teşekkür ederiz (Proje No: 116Z534).

ABSTRACT

DEVELOPMENT OF EPPT1 TARGETED DRUG DELIVERY SYSTEM AND INVESTIGATION OF ITS ANTICANCER ACTIVITY

Ezgi KARACA

M.Sc. in Biomedical Engineering and Bioinformatics

Advisor: Assoc. Prof. Dr. Yasemin Yüksel Durmaz

September 2020

Recently, the superior properties of graphene to other biomaterials have made graphene an indispensable and unique material for anticancer drug delivery research, gene and peptide transport. On the other hand, the undeniable beneficial effects of graphene provided by a wide surface area could be limited by toxic effects. Oxidized formation of graphene (G) is a graphene oxide (GO) that comprises a lot of oxygen functional groups which make it hydrophilic. Unfortunately, despite GO with an excellent functionalization ability and good solubility in water conditions, defected areas hamper sp^3 hybridized carbon surface area. Partially reduction of some oxygen functionality on GO generates reduced graphene oxide (rGO) with less solubility but better graphene properties. Therefore, reduced graphene oxide is chosen due to a wider surface area and less toxicity associated with functional groups for several biological applications. Covering the wide surface area of rGO is a common strategy to have better water solubility and biocompatibility. Poly(ethylene glycol) is a commonly used polymer that provides an ability to nanoparticle prolonged circulation time with covering the unknown nanomaterial from immune cells and decreases the uptake by the spleen and liver-resident phagocyte. This thesis study focuses on the development of an EPPT1 targeted, biocompatible graphene-based drug delivery system that can address the biocompatibility problem of rGO and show the potential of selective drug delivery into the target cell. The surface of the graphene oxide was coated with a functional copolymer poly[(ethylene glycol methacrylate)-*co*-(methyl methacrylate)-*co*-(1-pyrene methacrylate)-*co*-(3-azido propyl methacrylate)] P[PEGMA-*co*-MMA-*co*-PMA-*co*-AzPMA] that enhances the biocompatibility and water dispersibility via its PEG brushes. The copolymer also contains the multiple pyrene units to enhance the π-π interactions with graphene surface and azide groups to do further targeting agent functionalization of the coated surface which ensures the recognition of uMUC1 receptors that is highly expressed on the membrane of breast cancer cells. Doxorubicin (Dox) as anticancer drug loading and releasing profile of the targeted, biocompatible graphene platform were deeply investigated by showing the effect of PEG brush length (500 g/mol and 2000 g/mol), the effect of having ionic azide groups on the surface, the effect of the order of drug loading and targeting agent conjugation on drug release rate. Anticancer activity was tested in two different breast-cancer cells of MCF-7 and MDA-MB-231 using MTS and Resazurin Assay. Once the drug release profiles of the carriers with the 95% drug loading capacity were investigated at acidic (pH:5.5) and the physiological conditions (pH:7.4), the results showed that longer PEG brushes slow down the drug release however it ensures the biocompatibility and aqueous medium solubility. Azide group containing carrier has a faster drug release profile because of the ionic interaction between positively charged Doxorubicin at acidic pH. EPPT1 peptide showed the charge balancing effect and slowed down the release even in the azide group containing carriers in both PEG brush molecular

weights (500, 2000 g/mol). After the investigation of the drug release profile of the nanocarriers system in a different copolymer and synthesis order variety, in-vitro experiments have been done. MTS and Resazurin assay have been performed with the empty carrier, non-targeted, and targeted Dox loaded carriers with negative and positive controls on MCF-7 and MDA-MB-231 breast cancer fibroblast secondary cell lines. Resazurin has chosen as the most reliable assay to work with Dox loaded therapeutics. The results showed that 7.5 μg/ml targeted, Dox loaded, PAMP coated rGO nanocarrier with PEG_{2000} brushes gives 24 % cell viability, while free Dox gives 25 % cell viability after 48h interaction with MDA-MB231 cells. Finally, the selective cellular uptake ability of the compositions was investigated qualitatively and quantitively by confocal microscopy and flow cytometry analysis and it is shown that EPPT1 targeted a graphene-based drug delivery system selectively can accumulate more into breast cancer cell lines.

Keywords: Graphene Oxide, PEG, π-π interaction, Doxorubicin, Biocompatible, Targeting, Drug Delivery System, Nanocarrier

* This study was supported by The Scientific & Technological Research Council of Turkey (TUBITAK) 1001 project number 116Z534.

CHAPTER 1

1. INTRODUCTION

Graphene (G) is consists of hexagonal structures 2-D material sp^2 hybridized carbon atom bonds. For 50 years because of the surface modification capability of this thin carbon layer and its derivates has been producing with the intent of the various applications in the area of materials science, electronics, and photonics ***Figure 1.1*** [1].

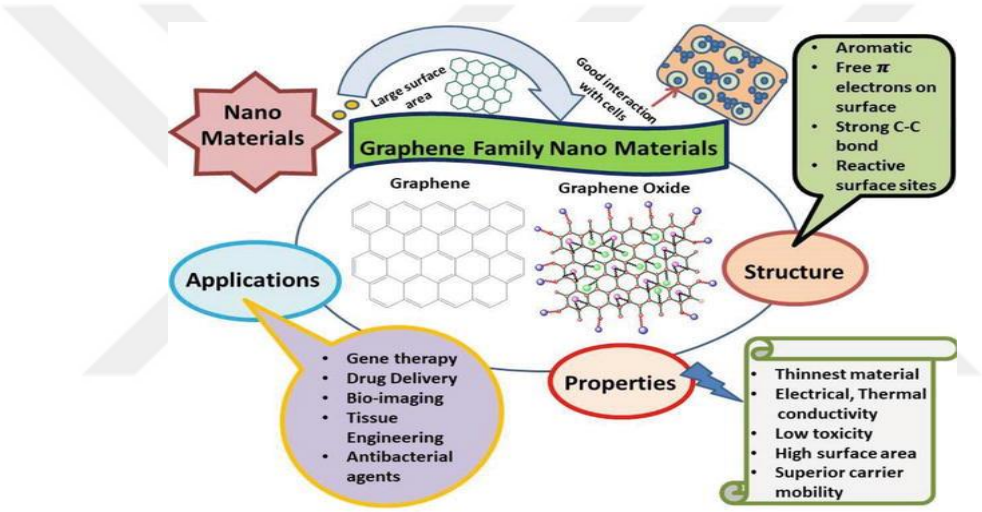


Figure 1.1: Properties and applications of graphene derivatives

In the favor of its large surface, physicochemical properties which are resulted from long-range π-π conjugation have been seen as a favorable material for the drug delivery systems [2-4] Greatly increasing attention on G derivatives since 2008 for the biomedical applications generally gathered on graphene oxide which is the product of the oxidation of the graphite several times [5]. Graphene oxide contains polar oxygen functional groups such as hydroxyl and oxygen groups inside the hexagonal structure and, also carbonyl and, the carboxyl group placed at the border of the layer effected the dispersion tendency in water is increased [6] ***(Figure 1.2)***. Unfortunately, despite its extraordinary wide surface that is able to be functionalized with desired molecules by lots of interactions such as covalent and non-covalent bonding, graphene shows low solubility and aggregation tendency because of the strong π-π stacking behaviors [7]. Stability of the GO and its

derivatives-based on the physiological conditions should be considered with regards to the decreased accumulation in the reticuloendothelial system (RES) and prolonged circulation time in the bloodstream to avoid cytotoxicity issues. GO has known as a highly soluble form of G derivatives in water, however, relocation through in the cell media GO extremely intend to interact with salt, ions, and biomolecules, it results in flocculation and aggregation of the adequately dispersed GO in a water environment [8,9] This problem is critical in physiological conditions with regard to the cytotoxicity issue while the GO-based DDS's journey starts from the injection to the tumor cell nucleus.

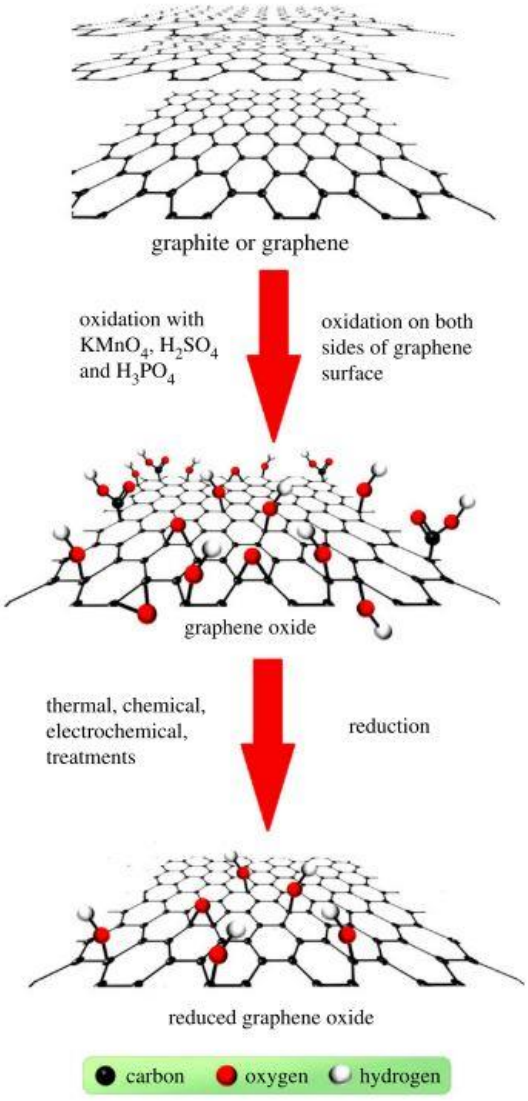


Figure 1.2: Schematic of the formation of reduced graphene oxide (rGO) and graphene oxide (GO) from graphene (or graphite). Picture owner is InvestorIntel & 2017 InvestorIntel Corp.

Owing to the electrostatic charge shielding and nonspecific binding of proteins, GO sheets aggregate at the physiological environment. To overcome those issues, the functionalization of reactive groups on GO is a toll to make it more dispersible and become a more effective material for DDS. Moreover, if those oxygen-containing reactive groups are not specifically functionalized for the desired system, those create the aggregation problem in the cell medium [10, 11] Controlled oxygen contribution on GO is derivated can be procured by the reduction of GO with chemical or thermal methods. GO itself comprises sp^2-hybridized carbon atoms packed into a honeycomb flat flakes and defection on the sp^3 bonded parts which allow epoxy and alcohol structure additionally, at the edge of flakes carboxylic acid formations occurs [14]. Defected areas that resulted from oxygen group functionality is with the hexagonal structures of the GO surface, is not convenient for the biological applications. Some problems such as less surface area for therapeutic loading can be occurred because of the defective areas on GO plates. On the other hand, reduced graphene oxide (rGO) shows better physical and optical characteristics and with the less defected surface, it is capable to make noncovalent bondings such as π-π stacking, Van der Walls forces, electrostatic interactions, and hydrogen bonding [12–14]

Nanocarriers are engineered for the extended therapeutics systemic circulation time to increase the opportunity for its targeted delivery into the specific tumor side. Although the prolonged circulation time of nanocarriers with therapeutics within the body creates opportunities for blood components such as opsonins to interact with it. GO has known that it has a wide surface area which greatly interacts with blood proteins and causes aggregation and toxicity when GO is administrated intravenously [15]. Even though the edge of GO is hydrophilic, the basal plane of it mostly hydrophobic and can absorb the blood proteins by interacting with the hydrophobic part of the protein. Accordingly, effective functionalization of graphene-based nanocarriers should have mandatorily functionalized by such as poly(ethylene glycol) (PEG) or its derivatives which is able to enhance the systems' water-solubility to overcome cell/macrophage reaction which is called opsonization. To overcome these problems with a hydrophilic nature PEG in an aspect of its trustable safety material confirmation by the Food and Drug Administration (FDA) can be used as a material to generate a hydrated cloud to hamper interaction with neighboring carriers and proteins in blood [16]. PEG is a polymer that is used as a coating material by sterically shielding its hydrophilic structure to avoid nanoparticle recognition

by immune cells. PEG provides an ability to nanoparticle prolonged circulation time by covering the unknown nanomaterial from immune cells and decreases the uptake by the spleen and liver-resident phagocytes[15]. According to the research of Klibanov and coworkers, PEGylated polymeric nanoparticles show outlasting blood-circulation half-life from less than 30 min to 5 h [17]. That's why PEG chains that have bonded with both covalently and noncovalent bonds contribute nanoparticle biocompatible characteristics.

Graphene and its derivatives demonstrate excellent and unique physiochemical property in terms of biological applications, such as broad surface area which allow therapeutic packing via different interactions, exceptional strength, and small size [18]. It was clearly declared by the study of Lie et al. graphene sheets and graphene oxide (GO) layers that have demonstrated an ability as a nano platform for the drug delivery system to carry therapeutics, antibodies, DNA, proteins, and genes. Graphene comprises the higher surface area (2600 m^2 g^{-1}) which is four times higher than other acceptable nanomaterials [19]. Drug loading capacity has been enriched by the wide surface area of GO and, that inspires interest with lots of interactions such as hydrogen bonding, electrostatic force, π-π interaction, Van Der Waals force, and hydrophobic interactions [20].

Moreover, their thickness has provided rigidity to the nanocarrier which is certainly required for cell penetration. Therefore, lateral dimensions of graphene-based nanocarriers have been considered as a limitation, since it leads to cell uptake, renal clearance, blood-brain barrier transport, biological degradation, most importantly cytotoxicity issue [12]. The effects of the plate-like structure of sheets on toxicity and the mechanism of the cellular uptake are not well understood yet. RES can recognize the nanoparticles with a size larger than 300 nm, and then they are not able to stay in the circulation for a long time in blood vessels [21]. Otherwise, anionic nanoparticles repulse the BSA protein in the blood with negative charges, driving to diminished protein retention and delayed circulation time [22].

Our previous work established effective PEGylation and reducing GO at the same time to make GO more biocompatible as an efficient drug delivery agent. The research has shown that the PEGylated GO with noncovalent bonds nano platform has excellent biocompatibility and a wide surface area that is an effective place for future therapeutics loading. Wang et al. investigated that the cytotoxicity on human fibroblast cells which interacts with the GO, their concentration restricted with 50 μg/mL. In our previous

study, it was demonstrated that high hemocompatibility and low cytotoxicity comparing the starting GO and copolymer show high solubility regardless of the PEG brush lengths [23]. Demirel et al. proved that on the results of MTS, LDH and, ROS assay, PEG-rGO was modified for safely used, according to the cell line tested on both HEK-293T and MRC-5 cells up to 150 μg/mL concentration.

The main point of this thesis is based on the development of biocompatible, targeted, controlled drug release profile favored the nano platform with high drug loading capacity. he optimization of the Dox loading process on GO and its derivates has been significantly pointed with regards to high drug loading efficiency, prevents burst release on the physiological environment, and selectively cell uptake ability. Aromatic drugs such as Camptothecin, Paclitaxel, and, Doxorubicin-hydrochloride are able to adsorb onto the nano platform via π-π stacking, electrostatic, and, hydrophobic interactions [24]. TIt is also known that the Dox loading environment, pH, and temperature are influential to the drug release profile at physiological pH (7.4) and acidic pH (5.5) [10]. Not only the pH triggers the negatively charging on GO which causes increasing adsorption of Dox on the GO layer but also the concentration of loaded Dox and contacts time regulates the drug loading efficiency [27]. As shown by Hashemi and coworkers' study, free Dox which is passively transported through the cell specified by the diffusion from the extracellular matrix to the intracellular matrix through a gap between the phospholipid membrane is susceptible to the efflux system [28]. Thus, a PEGylated GO-based drug carrier system is designed with prolonged drug release ability. Regulation of the monomer numbers inside the PAMP copolymer (P[PEGMA-*co*-MMA-*co*-PMA-*co*-AzPMA]) has been deeply examined with an in-vitro drug release system. PAMP copolymer coated GO-based targeted nanoparticle with a negatively charged surface designed for the repelling BSA from the adsorption on its surface to prevent cytotoxicity issue.

Nanoparticles that are designed for the DDS with nano levels size, generally because of the polar molecular structure of them, are capable of transportation into cells by crossing the cell membrane. The cell membrane is capable of entering small-sized and apolar molecules such as therapeutics itself from its phospholipid layers without any energy necessity[29]. Otherwise, endocytosis became a part of the polar and charged nanoparticle with a size of around 200-300 nm for internalization and transportation which is called active transport. In endocytosis, nanoparticles are surrounded by the cell membrane to form the vesicle called endosome to take the particle into the cell. It is a

process, engulfs the particles by the cell membrane which contains overexpressed receptors on it so that they are able to transport to inside the cell via receptor-mediated endocytosis. The vesicles are called an endosome which is the final placement inside the cell of the nanoparticles through the active transportation process.

Overexpression and underglycosylation 90% of an epithelial cell of the breast tumors of the underglycosylated mucin-1 antigen (uMUC-1), seems to be related to the tumor proliferation and effectiveness of the therapeutics [30]. MUC1 is an antigen and overexpression on breast cancer cells is able to use as a targeting property with the specifically synthesized peptides to recognize and biding on uMUC1 receptors to cargo DDS via active targeting. PAMP copolymer coated Dox loaded targeted carrier (PAMP-rGO-EPPT1-Dox) was designed with high efficient cellular uptake ability via receptor-mediated endocytosis via EPPT1 peptide which was synthesized to recognize overexpressed uMUC1 receptors on breast cancer cells. The following process comes with the design was the pH drop in endosome triggers the Dox release depending upon monomer quantity and distribution (PEG length, peptide presence or absence, and azide group existence). PAMP copolymer composition, ionic group interaction, and the presence of the peptide at the surface affects the release profile of the Dox in acidic conditions. Additionally, it was shown that there is no clear drug release in the physiological environment. As can be seen in ***Figure 1.3***, it was hypothesized that EPPT1 targeted Dox loaded rGO based nanoplatform can accumulate on the tumor environment through the EPR effect and it might have more interaction with cancer cells through EPPT1-uMUC receptor to enhance cellular uptake via receptor-mediated endocytosis. Once the carrier is in the endosome, it can sense the pH change to acidic pH and respond to it by accelerating the drug release.

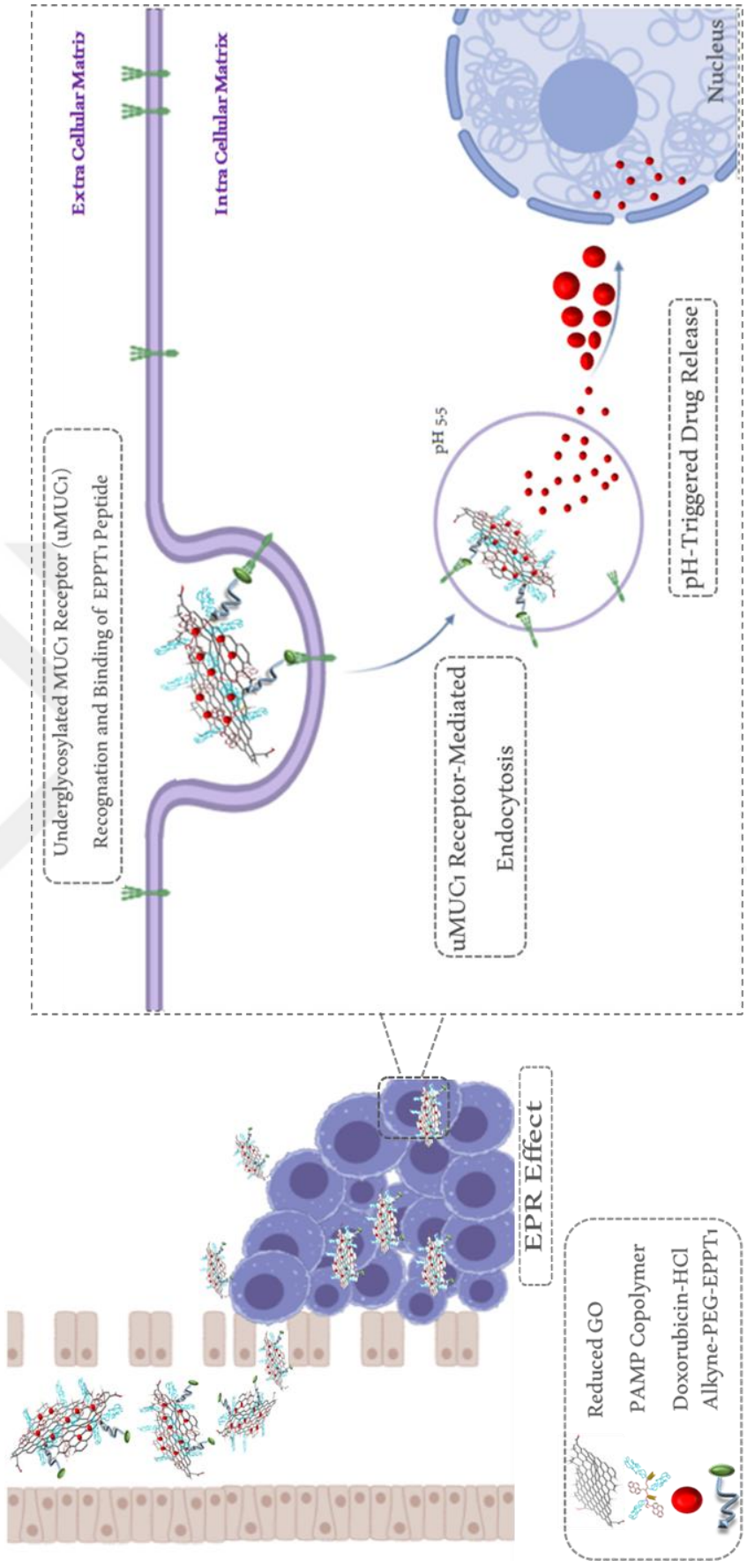


Figure 1.3: Schematic representation of the hypothesis of the project

CHAPTER 2

2. BACKGROUND

2.1 Cancer

Cancer is one of the leading causes of death globally (***Figure 2.1***). According to the National Cancer Institute, In 2020, 1,806,590 new cancer cases and 606,520 cancer deaths are estimated in the United States the International Agency for Research on Cancer (IARC) as of late assessed that 7.6 million passings overall were because of malignant growth with 12.7 million new cases for every year been accounted for around the world [31]. World health organization declared that in Turkey 24.4 % of the 91,655 women new cases is has been diagnosed as breast cancer and 118,882 number of man was also diagnosed as cancer in 2018. As Our world in data's research, the prevalence of breast cancer shows the highest prevalence globally; The estimated numbers are 17 million had breast cancer in 2017, 10 million had prostate cancer; and 9 million had colon & rectum cancer (***Figure 2.2***).

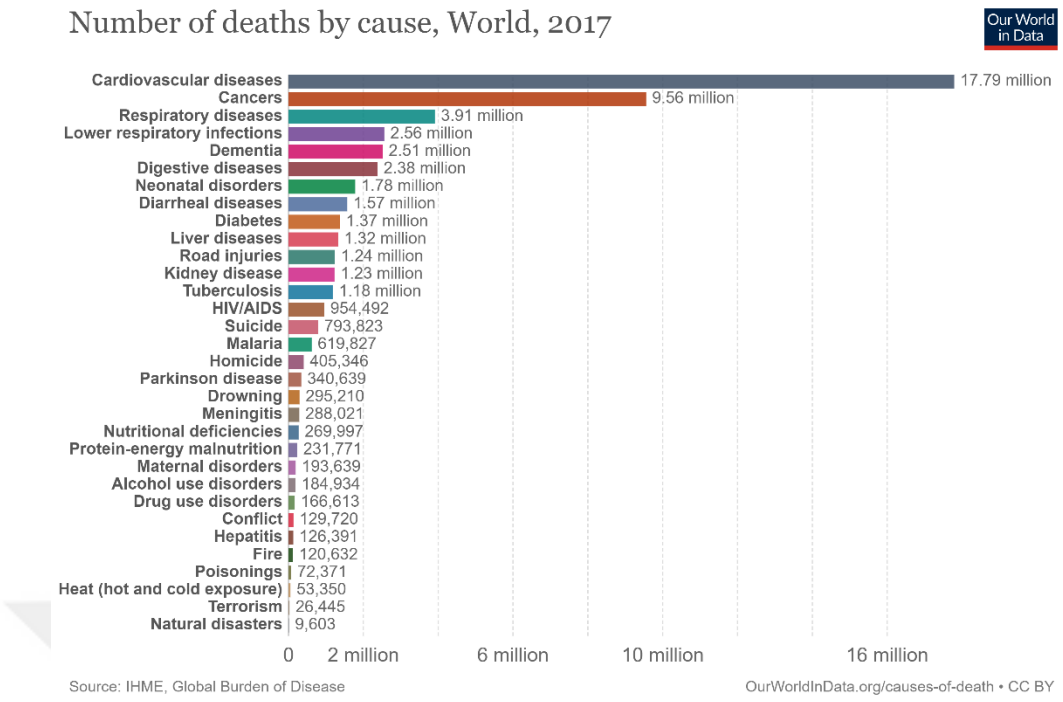


Figure 2.1: Numbers of the deaths by cause, World, 2017. IHME, Global Burden of Disease.

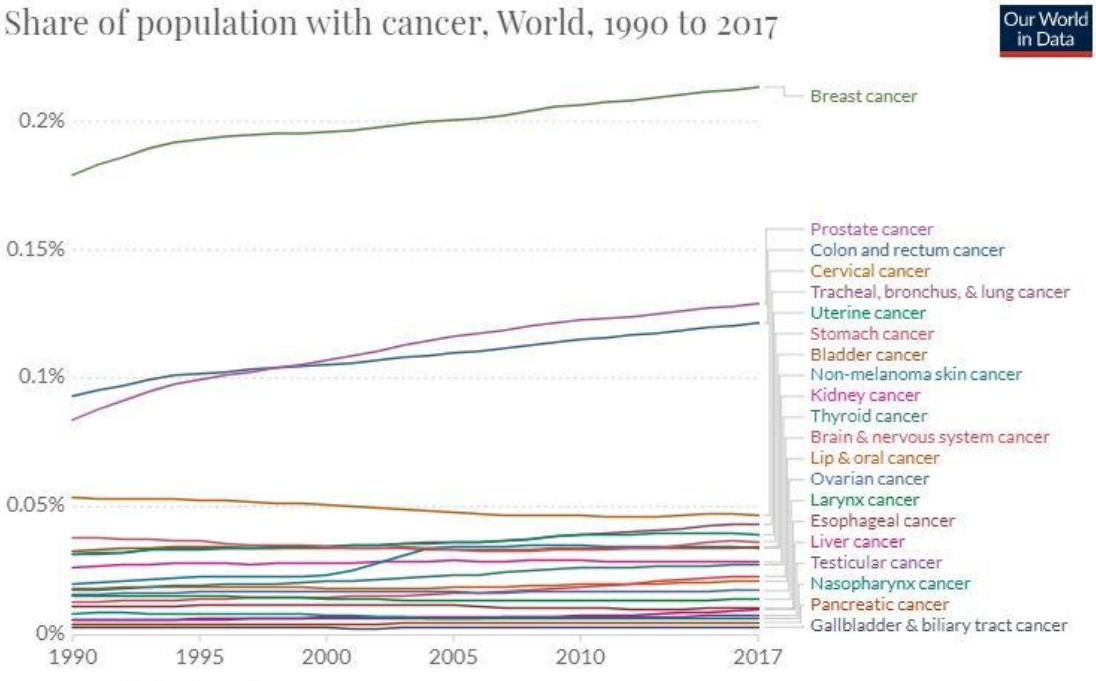


Figure 2.2: The distribution of cancer types worldwide from 1990 to 2017. IHME, Global Burden of Disease.

Cancer may be a multigenic and multicellular illness that can emerge from all cell sorts and organs with a multi-factorial etiology. Hanahan and Weinberg [32] have recognized six cancer cell phenotypes of the disease: limitless proliferation ability on cells, environmental independence for growth, avoidance of apoptosis, angiogenesis, invasion, and metastasis to distinctive parts of the body. The reason for the death of the individuals is uncontrolled cell growth and metastatic spread on the body [33]. The previous decade has seen an extensive advancement towards the medication and comprehension of the prior suggested signs of disease and allied to progress in early identification and the different medication modalities, numerous tumors have become healable [34].

2.2 Cancer Treatment Options

2.2.1 Radiotherapy

Three main approaches in cancer treatment are surgical, irritation by radiation, and chemotherapy. The breast cancer patients who survived radiation therapy increased from 29% in 2000 to 54% in 2016 in the US.

Radiation can be given as a curative primary cure as well as being used as a supportive cure to comfort patients from their indications lead to cancer. Additionally, radiation therapy can be implemented as a combinational strategy with other treatments such as surgery, chemotherapy, or immunotherapy. If it has been used before surgery, that treatment is used for shrinking the big tumor. On the other hand, after the surgery generally, radiotherapy is used the destroy remaining very small-sized tumors [35]. Recently, radiotherapy is also taken a part in molecular targeted therapy which is designing the enhance the therapeutic effectiveness of treatment [36]. Reilly and his colleagues Human Epidermal Growth Factor Receptor-2 (HER-2) receptor-targeted gold-nanoparticles (AuNP) was designed and evaluate its cytotoxicity and DNA damage capability. Iv-Vivo experiments demonstrated that X-radiation and AuNP combination caused 46% more regression on MDA-MB-361 cancer cells. There are also novel treatment options such as a nanoparticle which generates the radiation stimulated cancer cell damage for breast cancer[37]. It was designed to overcome the challenge of cancer

radiotherapy is that ionizing radiation damages both tumors and healthy tissues. These nanoparticles are obtained from high Z elements (such as gold and platinum) that efficiently absorb ionizing radiation that has been explored to increase the therapeutic efficiency of X-ray radiation therapy[38].

2.2.2 Surgery

Surgery is generally implemented against cancer by removing, debulking tumors and, alleviate cancer symptoms. Surgery often requires cuts through skin, muscles, and sometimes bone. After surgery, these cuts can be painful and take some time to recover from. Conversely, in emerging therapies, the diseased area can be healed or destroyed in the body without the need for surgery. For instance, drug carriers allow the drug or method to increase their effectiveness. The thesis aim is about developing and enhancing the ability of drug carriers for breast cancer.

Malignant growth on breast cancer for a long time, this sickness has been grouped by histopathologic standards, known as the tumor, node, and metastasis (TNM) staging system. Clinical measures incorporate immunohistochemical markers, for example, the estrogen receptor (ER), the progesterone receptor (PR), and the human epidermal development factor receptor 2 (HER2) are routinely utilized in symptomatic labs to give a grouping of bosom malignant growth and to help decide the ideal methodology for treatment [39]. According to the MayoClinic literature, the surgery for breast cancer classify in the aspect of the procedure such as mastectomy to remove the entire breast, lumpectomy to remove a portion of the breast tissue and remove nearby lymph nodes.

2.2.3 Chemotherapy

Cancer treatment approaches have been chosen depends on the tumor type and stage of cancer. Localized and metastasized cancer has generally implemented chemotherapy which can be used one or in combination with other forms of therapy [40]. Conventional chemotherapy has some limitations in terms of limited aqueous solubility of drugs, lack of selectivity and, multidrug resistance[41]. No matter the therapeutics produced from

natural or synthetic resources toxicity issue has always occurred because of the hydrophobic structure and dosage form of them [42]. Docetaxel (Taxotere) and doxorubicin (Adriamycin) are considered both of the most active chemotherapeutic agents for metastatic breast cancer patients. Dox which is an anthracycline cytostatic antibiotic is used as a chemotherapy drug in the treatment of a variety of cancer types very effectively. It causes DNA damage by the inhibition of topoisomerase II and consequently, leads to the inhibition of the process of duplication and transcription of mRNA and causes cell death. Without any prevention of the interaction with healthy tissue, there are side effects of this drug including myelosuppression, neutropenia, leukopenia, hand-foot syndrome, and drug-induced heart failure[43]. In the market, the most commonly used form is liposomal Dox forms which have still researching to eliminate the side effects of the Dox molecule. Another DDS formulations for Dox carrying are promising nanocarriers such as graphene-based designs.

2.2.4 Controlled Drug Delivery System

Controlled drug delivery systems (CDDS) come with a technological advantage. These systems have been designed for the cargo with the best targeting ability through the tumor side. They have some advantages such as provides longer shelf life for the beginning, both hydrophilic and hydrophobic substances can be incorporated into the formula. Additionally, they are able to administrate through oral, nasal, parental, intraocular, etc. The circulation time of the drug is vital for the highest yield. The controlled drug delivery system can be synthesized optimal size and surface characteristics that increase the circulation time on blood. Furthermore, nanoparticles provide the chance to sustain or stimuli drug release at a specific site by chemical characteristics [44]. Targeting chemotherapeutics by the CDDS ultimately decreases the side effects on the normal cells. Most cancer chemotherapeutics are administered either orally or intravenously to achieve systemic distribution for effective treatment. However, due to lack of selectivity these drugs cause significant damage to rapidly proliferating normal cells. The major objective of focusing on treatments is to target chemotherapeutics to cancer cells which eventually diminish the side effects. Nanoparticles are targeted either passively or actively to specific sites[45]. Accumulation of nanoparticles in tumor tissues relies upon

size, surface character, circulation half-life of the nanoparticles, and the degree of angiogenesis of the tumor [46].

2.2.4.1 Passive Accumulation In Tumor

The size of nanoparticles and conduct of tumor tissue vasculature assumes a critical job in passive targeting [47]. Solid tumors comprise of tumor parenchyma and stroma, which in turn comprise of vasculature and other supporting cells. Munn and his collages have clarified that because of the escalating metabolic needs of growing tumor cells, pre-existing blood vessels are consist of the angiogenic pressure and cause to the generation of new capillaries to the tumor in a progress called angiogenesis [48]. Formed new tumor capillaries are placed anomalous and showed terrible structural changes. Normal tissue vasculatures are placed by tight endothelial cells where ensure the prevention of entry of nanoparticles. On the other hand tumor tissue which consists of leaky vascularization cause gaps as large as 100 to 780 nm between endothelial cells (***Figure 2.3***). These gaps and abnormal vascular structure lead to increased permeability and retention (EPR) effect and allow the accumulation of nanoparticles in the tumor side [47, 48].

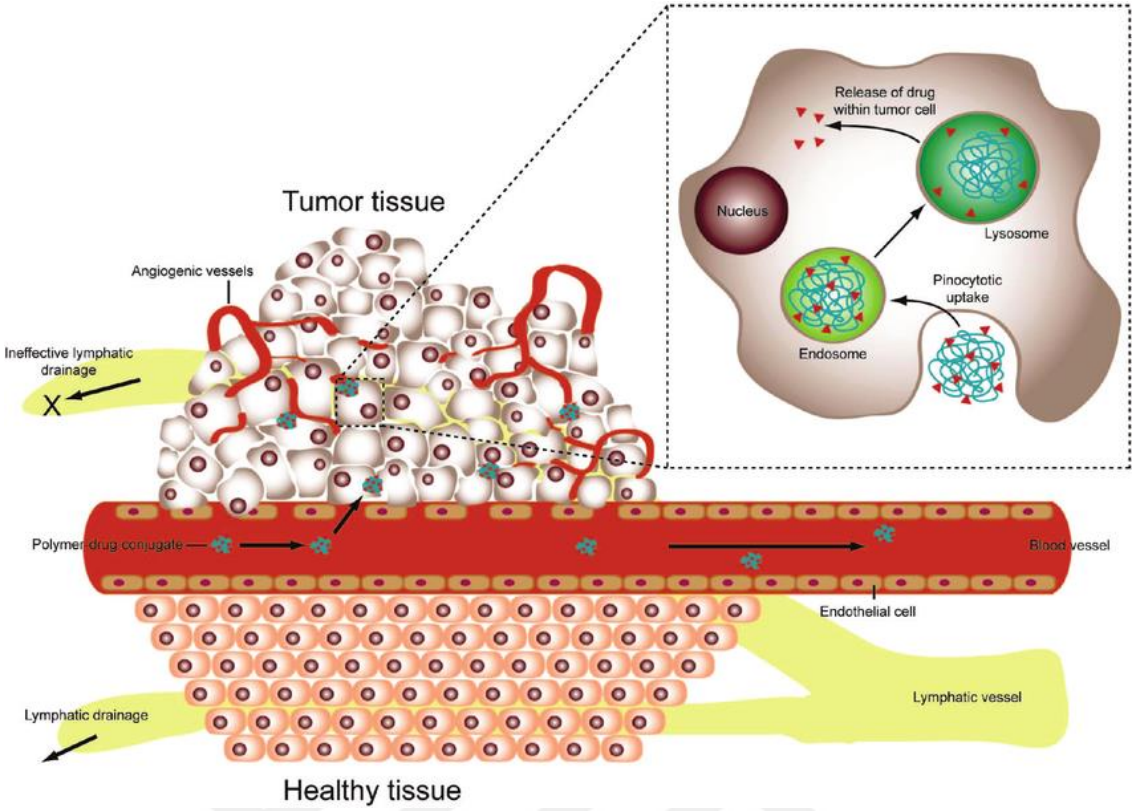


Figure 2.3: EPR effect representation [49].

Interstitial fluid pressure is responsible for their drug distribution on tumor tissue. Size, morphology, circulation half-life, and the degree of angiogenesis of tumor is the important factors for the accumulation of nanoparticles [50, 51] Polymeric nanoparticles, nanocrystals, liposomes, micelles, inorganic nanoparticles, and dendrimers, etc. are the most favorable systems for the drug delivery system that achieves passive targeting [41].

2.2.4.2 Active Accumulation In Tumor

Cancerous cells differ from healthy cells in terms of receptors that have overexpressed to reach more nutrition for their hypermetabolism [52]. By molecular recognition with receptors on tumor cells can be used as a tool for addressing and cargo the therapeutics with a suitable ligand [53]. With the help of passive targeting charging positively nanoparticles increase the cellular uptake ability by endocytosis however charged particles are recognized and cleared more easily than neutral particles[54]. Because of the less circulation time, there should be another modification to enhance targeting ability

such as coating nanoparticles (NP) with hydrophilic agents called poly(ethylene glycol) (PEG) which is generally used as enhancing circulation time and decrease the toxicity [55]. Active targeting strategy which comes through the systemic toxicity and enhances the therapeutic efficacy is implemented by the targeting ligands such as antibodies and non-antibodies ligands include proteins such as peptides, transferrins, vitamins, and aptamers to raise the selectivity by the different types of nanoparticles through the cancer tissue [56]. Targeting ligand should be chosen depends on the nanoparticle structure which is synthesized by the different materials as shown in ***Figure 2.4***.

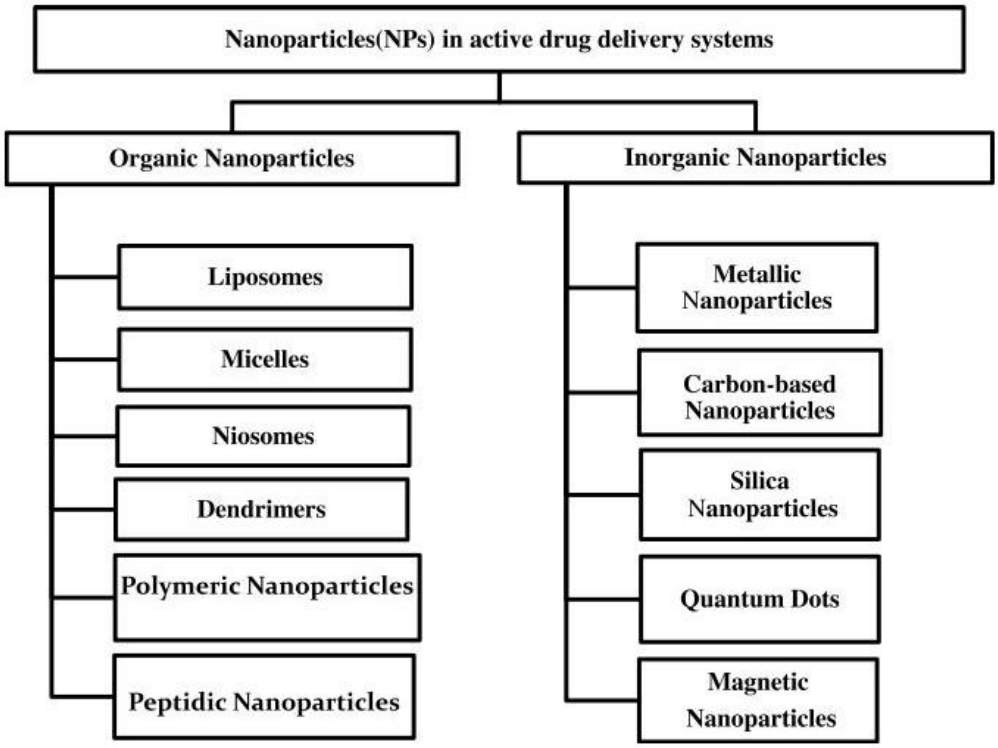


Figure 2.4: Types of nanoparticles used in targeted drug delivery [56].

2.2.5 Targeted Drug Delivery System

Before the recognized targeting ligand, Paul Ehrlich suggests the term ‘’ magic bullet’’ which is used to specify the best package is target and cargo the intended place in the body and then active targeting idea was asserted [57].

Conjugation of targeting a molecule with the overexpressed receptor in the tumor side leads to effective binding to cells through endosome (***Figure 2.5***). Nanoparticles with the active targeting ability can pass by the drug efflux pump caused by the high intracellular concentration [58]. There are lots of active targeting agents such as antibody-targeted nanocarriers, aptamer-targeted nanocarriers, folate- targeting nanocarriers by folate receptor, transferrin-targeted nanocarriers by transferrin receptor, and peptides which are also mentioned in this thesis a lot.

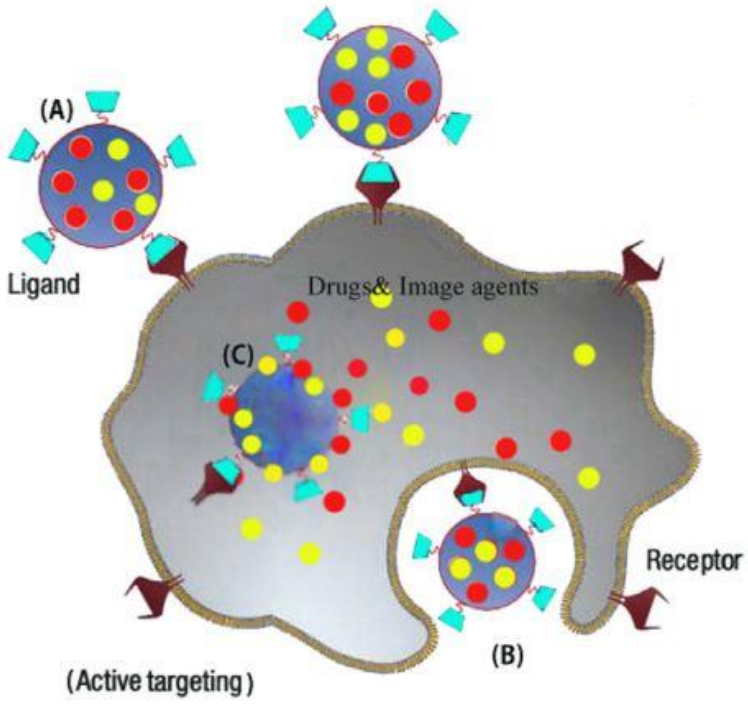


Figure 2.5: Schematic representation of active targeting mechanisms by which nanocarriers can deliver drugs& image agents to the target cells. (A) Ligands on the surface of the nanoparticles attach to a special receptor on the target cells; (B) Starting internalization of the nanoparticle–receptor complex by receptor-mediated endocytosis and vesicular transport through the endosomes; (C) Internalize into the cell and release its cargo into the target cell [56].

Underglycolyzed Mucin-1 (uMUC1) overexpression on breast cancer cells is a highly distinctive feature even in the case of triple-negative type. It was known that overexpression of the MUC1 receptor is a marker for the specific immunologic response of type triple-negative breast cancer which is a highly aggressive type of cancer. Muc1 is used as an identifier for the malignancy of in such tumors such as breast, ovarian, colon,

lung, gastric, pancreatic, and prostate cancers[59]. Although cancer and health cells include the same amino acid sequence, the adjunctive glycosylation patterns occur on these tumors [60]. MUC1 has been used as a targeting property by antibodies, vaccine therapies, and aptamers [61]. For example, in order to research triple-negative breast cancer cell imaging and treatment, PLGA and PVA were used to obtain charged nanoparticle to get interaction between radioactive aptamer which is able to target the MUC1 receptor by Carmo and his collages [62]. uMUC1 overexpression is effective for targeting imaging demand too. In the aspect of high affinity and selectivity for the receptor, peptides that are labeled with fluorescent molecules have chosen for that purpose. For instance synthetic, designed peptide EPPT1 that the sequences are YCAREPPTRTFAYWG was used to the target immunodominant region of uMUC1 receptor by Moore and her collages. Their research demonstrated that FITCY labeled EPPT1 targeted CLIO nanoparticles are highly efficient for early detection of the tumor, staining, and imaging of returned tumor tissue and, investigating the therapeutic efficiency [30].

2.2.5.1 Peptides as Targeting Ligands

Although peptides are the small sections of the proteins, their function is effective as much as its total protein thanks to the application of molecular design technology specifically after the discovery of hormones. Thus, new drugs are established depend on peptide [63]. Within the revelation of tumor-related peptides, phage-display peptide libraries incredibly contributed to recognizing compelling arrangements as ligands [64]. In expansion, the synthesis and modification of peptides were made simpler and less difficult with propels in chemical, solid-phase synthesis, and chemical ligation innovations [65]. After the *in-vitro* and *in-vivo* tests, peptide stability is challenging for that issue incorporating unnatural amino acids such as D-amino acids or cyclic structures that are able to avoid the degradation of peptide [66]. ***Table 1*** summarize peptides for DDS and molecular imaging [67]**.**

Table 1: Peptide Ligands for Nanoparticle-DDS and Imaging [67].

Peptide ligand	Target receptor	Target cancer cells	Carrier	Drug/imaging modality	Refs.
Octreotide	SSTR2	Breast	Liposome	Cantharidin/—	47)
Octreotide	SSTR2	Lung	Liposome	DOX/fluorescence	48)
Octreotide	SSTR2	Glioblastoma	Liposome	—/dual imaging (PET/MRI)	49)
RGD	$\alpha_v\beta_3$ integrin	Melanoma	Liposome	DOX/fluorescence	56)
cyclic RGD	$\alpha_v\beta_3$ integrin	Melanoma, breast, colon	Liposome	Matrine/—	57)
cyclic RGD	$\alpha_v\beta_3$ integrin	Colon	Liposome	DOX/fluorescence	58)
cyclic RGD	$\alpha_v\beta_3$ integrin	Glioblastoma	QD	—/dual imaging (PET/NIR fluorescenxce)	65)
ATN-161	$\alpha_5\beta_5$ integrin	Breast	Liposome	DOX/fluorescence	67)
T7	TFR	Ovarian	Liposome	PTX/fluorescence	80)
T7/TAT	TFR	Glioma	Liposome	DOX/NIR fluorescenxce	81)
T7/TAT	TFR	Lung	Liposome	PTX/NIR fluorescenxce	82)
KCCYSL	HER2	Breast	Liposome	DOX/—	91)
LTVSPWY	HER2	Ovarian	Magnetic nanoparticle	—/MRI	93)
AHNP	HER2	Breast	Liposome	DOX/—	95)
LHRL	LHRH receptor	Lung	Polymer, dendrimer, liposome	PTX/NIR fluorescenxce	101)
NGR	Aminopeptidase N	Fibrosarcoma	Liposome	siRNA and DOX/—	103)
NGR	Aminopeptidase N	Fibrosarcoma	Micelle	DTX/fluorescence	104)
NGR/heat activatable CPP	Aminopeptidase N	Fibrosarcoma	Liposome	DOX/fluorescence	105)
NGR	Aminopeptidase N	Glioma	QD	—/fluorescence	106)

The use of small peptide for targeting uMUC is getting more attention because of superior properties over antibodies [30]. A synthetic peptide EPPT1 (YCAREPPTRTFAYWG) exhibited significant binding affinity (K_d:20 μM) for the uMUC1-derived peptide PDTRP with the β strand type conformation as the active binding site. It was developed from CDR3 Vh region of the monoclonal antibody (ASM2) that was raised against human epithelial cells[30]. An early example in the literature that uses EPPT1 as a targeting agent is about EPPT1 peptide-based nanoparticles with the imaging probes for in-vivo magnetic resonance imaging (MRI) and fluorescence optical imaging. For instance, Zhao demonstrated that reduced MN-EPPT accumulation in the tumor size at the in-vivo experiment demonstrates that the adopted 5-FU therapy effected the aggression of cancer [30]. Additionally, On colonic tumors, there is higher signal intensity comes from P-(EPPT1)-IR783 which is the fluorescently labeled polymeric agent exhibit selectivity on human CRC tissue in-vitro and LS174T tumor-bearing mice. This conjugation is able to improve colonoscopic procedures by its higher selectivity [68]. As an example of EPPT1 targeted drug delivery, Stanton refers to his thesis that, EPPT1 motie with HPMA copolymeric nanoparticle results superiority on free dox on killing ability on pancreatic cells [69]. Later, EPPT1 targeted star-shaped ideal artificial vector has also developed and shown the potential of EPPT targeting for effective gene delivery [70]. As far as our knowledge, this study is the only example that uses EPPT1 targeted graphene-based drug delivery system to deliver chemotherapeutic agents selectively into the cell.

2.3 Graphene-Based Targeted Drug Delivery System

Graphene and its derivatives have been used for biomedical applications for the last decade [71-73]. Because of its unique physicochemical properties, it is able to be a demanding nanomaterial for the DDS design. In literature, targeted drug delivery systems are designed with graphene derivatives such as fluorene, carbon nanotubes, graphene oxide, reduced graphene oxide, nanographene oxide, graphene quantum dots[74-77]. Therapeutics, genes, siRNA, peptides are delivered to the targeted part of the body by the DDS that is made of graphene derivatives [78,79].

Gong and her colleagues investigated that various copolymers with GO conjugation with a lot of peptide contributions on the stimuli-responsive system indicate high drug loading efficiency and high biocompatibility [80].

Therapeutic carrier GO derivates are able to be more cytotoxic than just drugs with high biocompatibility of targeted carrier. Shuang Han and his colleagues have represented the GO-MIP-DOX molecule which is selectively binding to the receptors and pH-responsive drug release behavior. Synthesized molecularly imprinted polymer (MIP) contribution is caused by higher cytotoxicity on tumor cells than healthy one that indicates that promising material for the targeting delivery system with the ability to target CA125 molecules [81]. At physiological media (pH 7.4) is only 2.9% at increased pH 6.0 28% and acidic pH 4.5 is 54% within 50h. The reason why drug release triggers the pH change is that the lower pH value decreases the π-π the interaction between the aromatic groups on the GO and hydrophobic therapeutics Doxorubicin.

Iannazzo and his colleagues designed the targeted DDS is called GQD-PEG-BFG@Pyr-RF with PEG linker and the targeting ability comes from the targeting feature riboflavin (RF) by π–π interaction by pyrene groups with the graphene quantum dots (GQD) [82]. Targeting ability, water-solubility, biocompatibility, and fluorescence structure allow the molecule applicable DDS for the *in-vivo* experiments. An anticancer drug benzofuran structure (BFG) which is poorly soluble in water and bearing the targeting ligand riboflavin (RF) with graphene-based carriers showed enhanced drug cell-drug interaction which causes cytotoxicity on HEp-2 and HT-29 cell lines. GQD-PEG-BFG@Pyr-RF, compared to the free BFG indicates more effective cytotoxicity which is demonstrated with IC_{50} values as 114.5 vs. 153.7 μg/ mL, respectively.

Graphene-based nanoparticles are in targeting DDS literature is widely take apart. A much more similar example with the thesis is targeting graphene oxides are generally consist of hyaluronic acid which allows NGO nanoparticle goes into the cell via HA receptor-mediated endocytosis [83]. Jung et al. demonstrated that Epirubicin/NGO–HA was clarified by the lysotracker and confocal microscopy image which is an effective accumulation on cancer cells because of the receptor-mediated endocytosis. Not only targeting efficiency on overexpressed HA receptors also pH dependency on epirubicin loading and releasing is effective for the decrease of the side effects and enhanced cancer cell killing ability [84].

The nature of the cancer tissue and cells is acidic which is a tool for the drug-releasing specifically on cancer tissue by itself. Chowdhury et al. worked with amphiphilic copolymer with graphene comprises dual therapeutic release behavior either the acidic environment or via biodegradation of disulfide bonds [85]. Hepatocellular carcinoma-targeted therapy and imaging were investigated via DOX-GO with cyclic RGD-modified chitosan nanohybrid able to carry DOX (1.0 mg mg^{-1}) and again pH-responsive release [86].

In literature there are also lots of GO-based DDS examples such as the temperature stimulated [87], magnetic field stimulation [88], ultrasound stimulated [89], light stimulated [90], electric filed stimulated [91] drug-releasing as external stimulation necessity.

CHAPTER 3

3. EXPERIMENTAL SECTION

3.1. Materials

3.1.1. Chemicals and Reagents

Materials: Methyl methacrylate (MMA, Sigma-Aldrich, 99%), poly(ethylene glycol) methacrylate 500 Da (PEGMA, Sigma-Aldrich), poly(ethylene glycol) methacrylate 2000 Da (PEGMA, Sigma-Aldrich), 1-pyrenemethyl methacrylate (PMA, Sigma-Aldrich, 99%), N, N,N',N'",N"-pentamethyldiethylenetriamine (PMDETA, Sigma-Aldrich, 99%) were passed through a basic alumina column to remove inhibitor prior to use. Copper (I) bromide (CuBr, Sigma-Aldrich, 98%), ethyl 2-Bromo-2-methyl propionate (EiBr, Sigma-Aldrich, 98%) and graphene oxide (GO, Sigma-Aldrich, 4 mg/mL, dispersion in H2O), 3-Azido-1-propanol (96% Sigma-Alrich), methacryloyl chloride (Sigma-Aldrich), triethylamine (J.T. Baker), Methacryloyl chloride, doxorubicin-HCl (Sigma-Aldrich), propargyl alcohol, EPPT1 peptide (NH2-YCAREPPTRTFAYWG-CONH2) (Metabion), were used without further purification. Triton X-100 (Biomatik, 5% water), sodium chloride anhydrous (NaCl, Wisent Bioproducts, 99%), phosphate buffer solution (PBS, Multicell, Wisent Inc.), poly-L-lysine , Dulbecco's Modified Eagle's Medium (DMEM, Multicell, Wisent Inc.), Fetal bovine serum advanced, heat-inactivated (FBS, Capricorn Scientific GmbH), L-glutamine, 200 mM solution (29.23 mg/mL in 0.85% NaCl, Multicell, Wisent Inc.), penicillin-streptomycin solution (10,000 U/mL, Multicell, Wisent Inc.) Trypsin EDTA (0.25% trypsin in HBSS, Multicell, Wisent Inc.) trypan blue solution, (0.4%, Sigma) used as received. All other reagents were purchased from Sigma-Aldrich and used as received without further purification.

Instrumentation: ^{1}H (500 MHz) spectra were recorded in $CDCl_3$ with $Si(CH_3)_4$ as internal standard, using an Agilent VNMRS 500 MHz instrument. The particle size and zeta potential of rGO-PEG derivatives were determined in distilled water by dynamic

light scattering (DLS) using Malvern Zetasizer Nano ZSP. UV-Vis absorption measurements were recorded using the SpectraMax i3 spectrophotometer. SpectraMax® i3, Molecular Devices LLC plate scanners were used for spectroscopic analysis of 96 well plates. Fourier transform infrared (FTIR) spectra were recorded on an Agilent Technologies Cary 630 FTIR instrument, which is equipped with attenuated total reflectance (ATR), over the range 4000-400 cm^{-1}. Renishaw inVia Raman microscope was used for Renishaw inVia Raman spectroscopy analysis at 785 nm and K-alpha X-ray Photoelectron Spectrometer (XPS) System Thermo Scientific™ was used for XPS analysis. Particles that were dispersed in water applied on Formvar coated grid by drop-casting and transmission electron microscope (TEM) scans were recorded by JEM 1220, JEOL instrument. Thermogravimetric analyses (TGA) were done by using TGA 8000, Perkin Elmer instrument, under the N_2 atmosphere with a 10 °C per minute heating rate, between 30-800 °C. Zeiss LSM 800 NLO Multi-Photon and Confocal Microscope were used for fluorescent imaging.

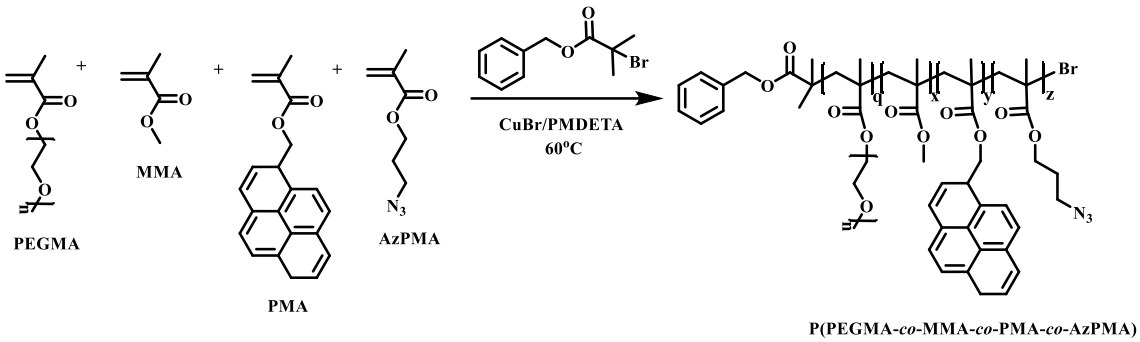
3.2. Methods

3.2.1. Synthesis of PEG Containing poly[(ethylene glycol methacrylate)-*co*-(methyl methacrylate)-*co*-(1-pyrene methacrylate)-*co*-(3-azido propyl methacrylate) Graft Copolymer (P(PEGMA-*co*-AzPMA-*co*-MMA-*co*-PMA)); *PAMP*

Multiple pyrene, azide, and PEG containing graft copolymer was synthesized as described in our previous publication [92]. Required monomers such as azide functional monomer (AzPMA), pyrene functional monomer (PMA), and benzyl functional initiator that allows the composition calculation using ^1H NMR was synthesized prior to the copolymerization.

Briefly, PEGMA (500 or 2000 g/mol) with different weight ratios MMA, AzPMA, and PMA and toluene as a solvent was added into the 10 mL glass reactor, followed by the addition of the ligand PMDETA and catalyst Cu(I)Br **(*Scheme 3.1*).** Finally, by the addition of the benzyl functional ATRP initiator, the reaction mixture is immediately frozen in the liquid nitrogen to make the reactor inert from the atmosphere. After 3 cycles of FPT (freeze-pump-thaw), the reaction mixture was put into an oil bath at 60 ^0C for 3 hours**.** After the removal of catalysts through the basic aluminum oxide, the concentrated

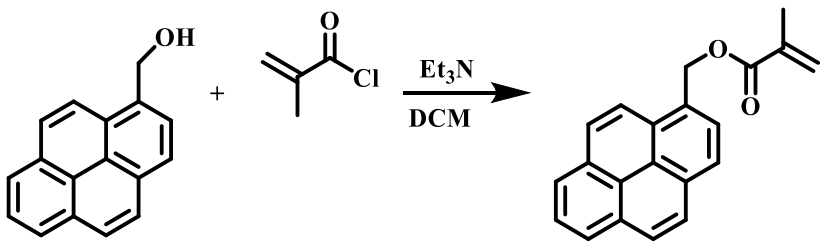
reaction mixture in THF was precipitated with cold diethyl ether. The product was characterized by ^{1}H NMR spectroscopy.



Scheme 3.1: Controlled copolymerization of PEGMA, PMA, MMA, and AzPMA monomers

3.2.1.1. Synthesis of 1-Pyrenemethyl Methacrylate Monomer; PMA

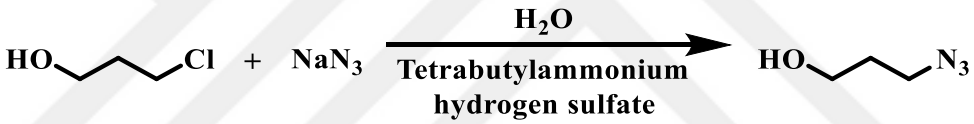
3 g (0.13 mole) 1-pyrenemethanol and 5.4 mL (0.39 mole) triethylamine was dissolved with 30 mL DCM in a round bottom flask. 1.89 mL (0.195 mole) methacryloyl chloride in 10 mL DCM was added to the reaction mixture dropwise at the nitrogen atmosphere (***Scheme 3.2***). At the same time, the reaction mixture was cooling by an ice bath to avoid extra heating. The following day, the precipitated solid was filtered and extracted two times with a 10% HCl solution and once with distilled water. The mixture which was dried with sodium sulfate and evaporated on the rotary evaporator was purified by reverse precipitation with methanol. The product was characterized by ^{1}H NMR spectroscopy.



Scheme 3.2: Synthesis of the 1-pyrenemethyl methacrylate

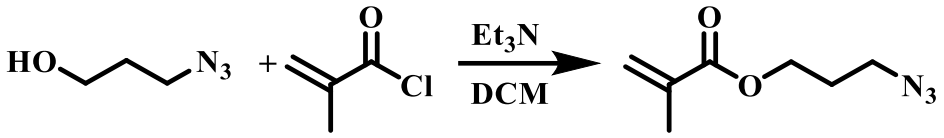
3.2.1.2. Synthesis of Azido-1-Propyl Methyl Methacrylate Monomer; AzPMA

Firstly, in order to obtain 3-azido-1-propanol, 10 mL (0.12 mole) 3-choloro-1-propanol, and 11.55 g (0.24 mole) sodium azide were mixed together in water in a round bottom flask (***Scheme 3.3***). As a phase transfer catalyst 0.365g (1.10^{-3} mole) tetrabutylammonium hydrogen sulfate (TBAHS) was added to the reaction flask in 15 mL water. The reaction was allowed to proceed at 80^0 C for 24 hours. At the end of the specific time, the unreacted sodium azide and salts were filtered off and the reaction mixture was extracted 3 times with diethyl ether, dried with sodium sulfate, and the solvent was removed on the rotary evaporator at high vacuum. The reaction mixture was vacuum distilled and obtained 9.1 g product as a clear liquid in a 75% yield. Product characterization was performed by ^{1}H NMR spectroscopy.



Scheme 3.3: Synthesis of 3-azido-1-propanol

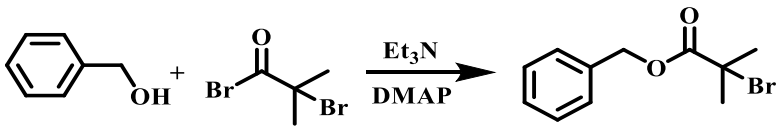
Secondly, to obtain AzPMA monomer, 9.27 mL (0.16 mole) acryloyl chloride which was dissolved in 15 mL DCM was added dropwise over 8g (0.08 mole) 3-azido-1-propanol that is in 85 mL DCM and 22.06 mL (0.18 mole) triethylamine dissolved in 22 mL DCM at the same time reaction mixture was cooled with an ice bath to avoid extra heating (***Scheme 3.4***)**.** The reaction was stirred for 2 hours in an ice bath then stirred at room temperature overnight. The following day, the precipitated solid was filtered and extracted 2 times with a 10% HCl solution and once with distilled water. The mixture, which was dried with sodium sulfate and evaporated on a rotary evaporator, was purified by vacuum distillation with the addition of hydroquinone. The product was characterized by ^{1}H NMR spectroscopy.



Scheme 3.4: Synthesis of azido-1-propyl methyl methacrylate (AzPMA)

3.2.1.3. Synthesis of Benzyl Group Containing Initiator (2-bromo-2-methyl propionate)

2.87 mL (0.028 mole) benzyl alcohol in 30 mL DCM, 7.73 mL (0.033 mole) triethylamine, and 0.34 g (0.0028 mole) DMAP were dissolved in a round bottom flask in 30 mL DCM and placed in an ice bath. 4.12 mL (0.033 mole) α-bromo is butyryl bromide diluted with 10 mL DCM was added dropwise to the stirred flask under nitrogen atmosphere (***Scheme 3.5***). The reaction was stirred for 2 hours in an ice bath then at room temperature reaction was stirred. The following day, the precipitated solid was filtered and extracted 2 times with a 10% HCl solution and once with distilled water. The mixture, which was dried with sodium sulfate and evaporated on a rotary evaporator, was purified by column chromatography with 1:9 ethyl acetate: hexane mobile phase. The obtained pure liquid product was characterized by ^{1}H NMR spectroscopy.



Scheme 3.5*:* Synthesis of benzyl group-containing initiator

3.2.2. PAMP Coating on Reduced Graphene Oxide and *in situ* Reductions of Graphene Oxide; PAMP-rGO

It was aimed to coat the graphene plates with the obtained PEG containing copolymers consist of pyrene groups that contain π bonds and reduced them while coating at the same

time. In the published article Demirel *et al.* [92] was mentioned the optimization of that step in detail. In brief, GO solution (4 mg/ mL) was obtained with the GO/copolymer: 1/10 (g/ g) coating ratio by reducing agent hydrazine. The solvent system was regulated to H_2O: DMF/ 2:1 (mL/ mL). In the beginning, the reaction mixture was stride at room temperature for 2 hours. Later on, the reaction was proceeded at 80^oC for 20 hours following the addition of the hydrazine hydrate with a ratio of 1 µL for 1 mg GO [93]. Following steps for the purification, in order to remove the uncoated copolymer, DMF, and hydrazine after coating, the plates were dispersed and washed several times in water and then acetone which is the good solvents for the copolymer. The reaction mixture was centrifuged at 14,000 rpm for 15 minutes, the supernatant was discharged. PEG functional copolymer and GO surface π- π interaction between the pyrene group on copolymer and the centrifuged precipitate were obtained as PEG functional copolymer coated graphene plates (***Figure 3.1***). By using the thermal behavior of the copolymer and rGO that have been already investigated, % of the copolymer coating efficiency on rGO plates was calculated.

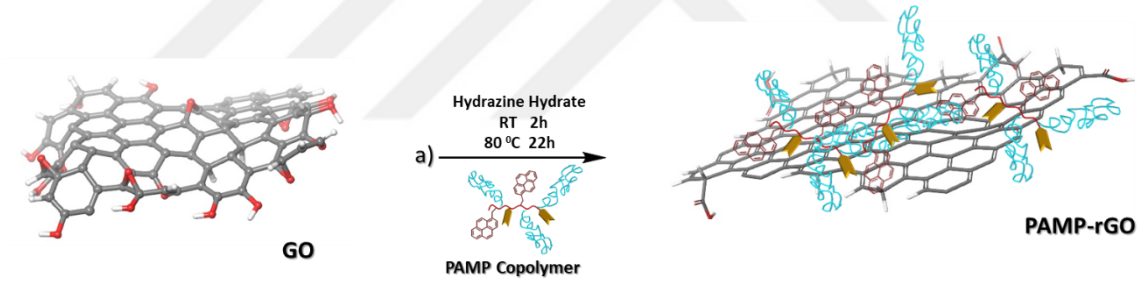


Figure 3.1: Schematic representation of PAMP coating and *in-situ* reduction to rGO.

3.2.3. Preparation of EPPT1 Targeting, PAMP Coated Nano platform by Cupper Catalyzed Azide-Alkyne Click Reaction; PAMP-rGO-EPPT1

Alkyne-PEG-EPPT1 polymer was conjugated to azide functionality of the PAMP coated rGO (PAMP-rGO) surface using $CuSO_4$/Sodium ascorbate catalyst system in PBS at pH:8. (***Figure 3.3***). Two azide groups on PAMP copolymer are targeted to click reaction with previously functionalized EPPT1 peptide with an alkyne group. 8 mg (1.178×10^{-7} mol) $(P_{15}A_{10}MP)_{2000}$-rGO was weighted and calculated to target the two alkyne groups on it, Alkyne-PEG-EPPT1 (2.36×10^{-7} mole) with the proportional of the amount with

azide group on PAMP which is coated with known coating efficiency on rGO. 8 mg $(P_{15}A_{10}MP)_{2000}$-rGO was dispersed into 7 ml pH: 8 PBS which is containing. Firstly 1.178×10^{-7} mol of $CuSO_4$ catalyst and 2.36×10^{-7} mol sodium ascorbate was added. Subsequently, 3 times freeze-pump-thaw (FPT) was practiced to the reactor to obtain the best yield from CuAAC. After that reactor put on 35 ^{O}C overnight. The $(P_{15}A_{10}MP)_{2000}$-rGO-EPPT1 composition was re-dispersed 3 times with pH:8 PBS solution and centrifuged to remove nonparticipating PAMP-rGO and unbonded Alkyne-PEG-EPPT1 was distracted from the reaction mixture. To get rid of extra ions that come from PBS salts, washed with approximate pH: 8 dd-water two times then drug-loaded particles were frizzed by liquid nitrogen and dried in a lyophilizer overnight.

By using the upper phase concentration of the reaction mixture unbonded peptide group which is able specifically detected by Ellman's Assay [94]. The amount of conjugated EPPT1 peptide was calculated using Ellman`s reagent which reacts to the SH group of the peptide and forms the 2-nitro-5-thiobenzoate (TNB^-) ion which is soluble in water and has a visible light absorption to make a quantitative calculation of the unreacted peptide amount.

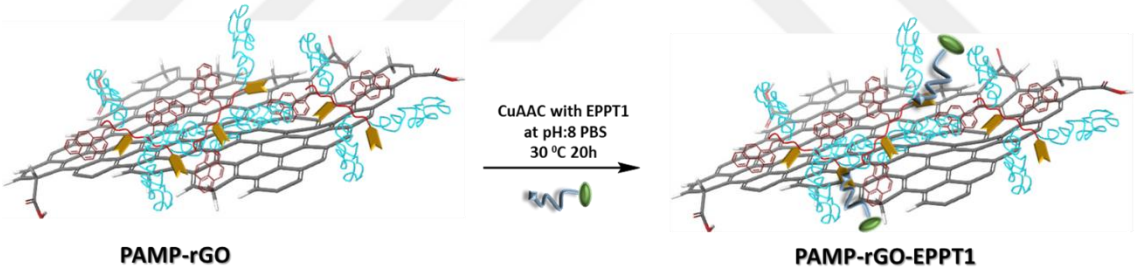


Figure 3.2: Schematic representation of EPPT1 peptide conjugation on the PAMP-rGO surface

3.2.4. Capping Remaining Azide Groups with Propargyl Alcohol; PMP-rGO-EPPT1

The remaining azide group after EPPT1 peptide conjugation either left as it is or was capped with an excess of propargyl alcohol to obtain a nonionic group containing a coated surface (***Figure 3.3***). 10 equivalent of propargyl alcohol compared to the remaining azide

group was added into an aqueous dispersion of PAMP-rGO-EPPT1 in the presence of $CuSO_4$ /sodium ascorbate same procedure was followed with the previous reaction. at 30^{o}C for 20h. The PMP-rGO-EPPT1 composition was washed with PBS solution and then dd-water and finally centrifuged to remove nonparticipating PAMP-rGO-EPPT1 and unbonded propargyl alcohol was distracted from the reaction mixture and then they were frizzed by liquid nitrogen and dried in a lyophilizer overnight.

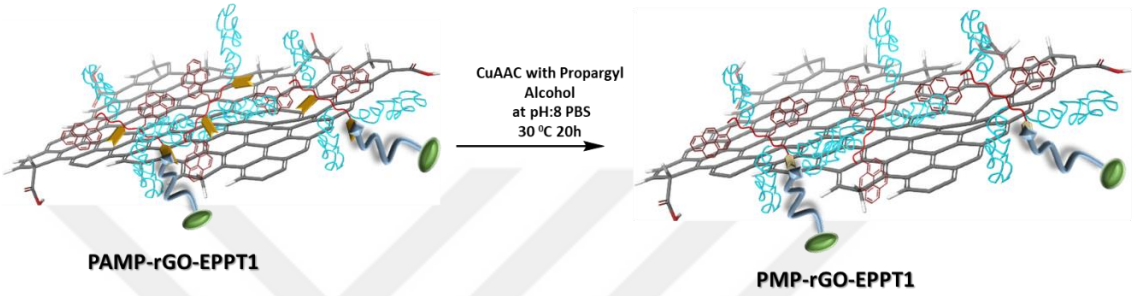
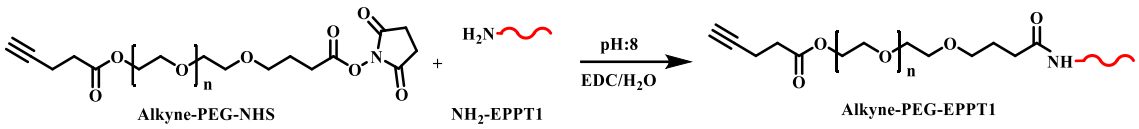


Figure 3.3: Schematic representation of capping remaining azide groups on PAMP-rGO-EPPT1.

2.3.1.1 Synthesis of Alkyne-PEG-EPPT1

The EPPT1 peptide (Sequence: *YCAREPPTRTFAYWG*) to be used as the targeting agent was synthesized by the Metabion. 10 mg (5.5×10^{-6} mol) NH_2-EPPT1 and 18.16 mg (6.05×10^{-6} mol) alkyne-PEG-NHS was reacted in the presence of 0.6 mg (5.5×10^{-6} mol) N-hydroxy succinimide (NHS) and 0.6 mg (5.5×10^{-6} mole) N-(3-dimethylaminopropyl)-N′-ethyl carbodiimide hydrochloride (EDC) in pH:8 PBS solution at 37 ^{0}C for overnight (***Scheme 3.6***). After the specified time, the reaction mixture was transferred to a dialysis membrane MWCO of 1 kDa and dialyzed against pH:8 PBS solution which followed with distilled water to remove the reaction by-products and remaining salts, respectively. The reaction solution obtained after dialysis was dried in a lyophilizer with a 58.63 % yield. The white solid obtained was characterized by ^{1}H NMR and Ellman's Assay.



Scheme 3.6: Synthesis of alkyne-EPPT1-PEG

3.2.5. Drug Loading on EPPT1 Targeted PAMP Coated rGO Nanoplatforms; PAMP-rGO-EPPT1-Dox and PMP-rGO-EPPT1-Dox

Doxorubicin-HCl was loaded on PAMP-rGO-EPPT1 or PMP-rGO-EPPT1 surface through π- π stacking, H-bonding, and electrostatic interactions have arrived with exceptionally high loading efficiency which is up to 95 %. Therapeutic loading was implemented by adding 10 mg Dox into 10 mg PAMP-rGO-EPPT1 or PMP-rGO-EPPT1 targeted nanoplatforms, was dispersed in 10 mL 10% DMSO containing pH:8 PBS solution by ultrasonication and stirred overnight at 35 ^{0}C in dark conditions (***Figure 3.4***). The reaction mixture was centrifuged at 14,000 rpm for 15 minutes, the supernatant was discharged and collected to measure unloaded drugs. PAMP-rGO-EPPT1-Dox or PMP-rGO-EPPT1-Dox composition was re-dispersed 3 times with pH:8 PBS solution and 1 time with double distilled water to get rid of the ions followed by centrifuging. Then, PAMP-rGO-EPPT1-Dox or PMP-rGO-EPPT1-Dox solution was freeze-dried overnight.

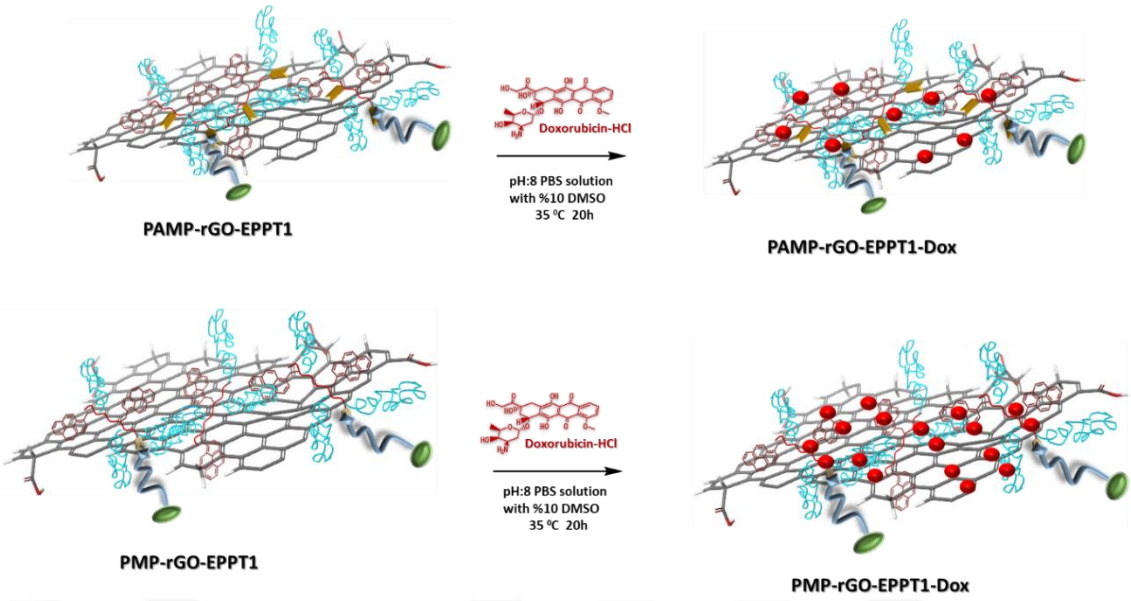


Figure 3.4: Symbolic representations of drug loading on PAMP-rGO-EPPT1 and PMP-rGO-EPPT1

UV-visible spectroscopy analysis of the initial supernatant of the Dox loading solutions was performed at 484 nm to indirectly calculate the drug loading efficiencies (LEs) and drug loading capacities (LCs) of the carriers by measuring the concentration of free DOX in the supernatant. Drug loading efficiencies (LEs) and drug loading capacities (LCs) were indirectly determined by measuring the concentration of free Dox in the upper phase (***Equation 3.1***).

$$\text{LE (wt\%)} = \frac{\text{Weight of loaded drug}}{\text{Weight of drug in feed}} \times 100$$

$$\text{LC (wt\%)} = \frac{\text{Weight of loaded drug}}{(\text{Weight of loaded drug} + \text{Weight of Nanocarrier})} \times 100$$

Equation 3.1: Calculation of LE and LC

3.2.6. Drug Loading on PAMP Coated rGO Followed by Conjugation of EPPT1 Peptide; PAMP-rGO-Dox-EPPT1

Investigation of the effect of the EPPT1 peptide conjugation order on drug release profile has been studied. For those experiments besides PAMP-rGO-EPPT1-Dox and PMP-rGO-EPPT1-Dox compositions, PAMP-rGO-Dox-EPPT1 and PMP-GO-Dox-EPPT1 have been also synthesized by the following route. Drug loading on graphene derivates by the adsorption on the surface through π-π stacking, H-bonding, and electrostatic interactions has arrived with exceptionally high loading efficiency which is up to 95 %. The step which is the PEGylation step via π-π interaction between copolymer and GO is the part for enhancing biocompatibility and solubility of the graphene oxide nano platform. The increased solubility and wide surface that is comprised of π-π bond allow the Doxorubicin (Dox) to load on its surface with a remarkably high loading efficiency up to 98%. Secondly, EPPT1 peptide conjugation on PAMP-rGO compositions provides to the nano platform targeting ability specifically overexpressed uMUC receptors on breast cancer cells (***Figure 3.5***).

Briefly, therapeutic loading was implemented by adding 10 mg Dox into 10 mg $(P_{15}A_{10}MP)_{2000}$-rGO nano-platform, was dispersed in 10 mL 10% DMSO containing pH:8 PBS solution by ultrasonication and stirred overnight at 35 ^{0}C in dark conditions. Secondly, 7 mg (1.178×10^{-7} mol) $(P_{15}A_{10}MP)_{2000}$-rGO-Dox was weighted and calculated the two alkyne groups, Alkyne-PEG-EPPT1 (2.36×10^{-7} mol) with the proportional of the amount with azide group on PAMP which is coated with known coating efficiency on rGO. 7 mg $(P_{15}A_{10}MP)_{2000}$-rGO-Dox was dispersed into 6ml pH: 8 PBS which is containing 10% DMSO in it. Firstly 1.178×10^{-7} mol of $CuSO_4$ catalyst and 2.36×10^{-7} mol Sodium ascorbate was added. Subsequently, 3 times Freeze-Pump-Thaw (FPT) was practiced to the reactor to obtain the best yield from CuAAC. After that reactor put on 35 ^{O}C overnight. The PAMP-rGO-Dox-EPPT1 composition was re-dispersed 3 times with pH:8 PBS solution and centrifuged to remove nonparticipating PAMP-rGO-Dox and unbonded Alkyne-PEG-EPPT1 was distracted from the reaction mixture. To get rid of extra ions that come from PBS salts, washed with pH: 8 dd-water two times then drug-loaded particles were frizzed by liquid nitrogen and dried in a lyophilizer overnight. For the remaining azides capped composition which is called PMP-rGO-Dox-EPPT1 were

obtained by the "click" reaction with the propargyl alcohol with the same procedure as described above.

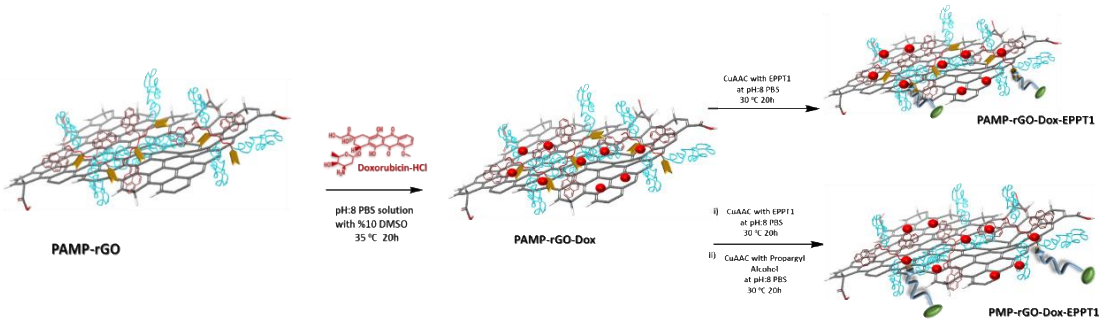


Figure 3.5: Symbolic representation of the order of drug loading and EPPT1 peptide conjugation on PAMP-rGO to obtain PAMP-rGO-Dox-EPPT1 and PMP-rGO-Dox-EPPT1

3.2.7. In-Vitro Drug Release Study

The presence of π bonds on hydrophilic Doxorubicin-HCl leads to non-covalent bonding with pi bonds inside the large surface of rGO. The release of Dox from targeted and/or non-targeted PEGylated (500/2000 g/mol) carrier (PAMP-rGO) was assessed in PBS buffer (pH:5.5 and pH:7.4) by dialysis with MWCO of 3.5kD dialysis membrane. 1 mg drug-containing component was placed in a 250 ml flask that contained the chosen pH PBS buffer 110 mL volume. At regular time intervals, 200 µL samples from the flask were withdrawn for analysis 3 samples from each component to investigate the amount of releasing Dox through the dialysis bag into the PBS environment. Volume replenishment was performed using withdrawn samples after getting absorbance from 483 nm. The concentrations of Dox in the release media were determined by UV–Vis spectrophotometry as described above. Each experiment was repeated 3 times. Percentage of the released drug was calculated as described in (***Equation 3.2***);

$$\text{Drug Release \%} = \frac{(\text{Abs. of Released DOX} - \text{Abs. of blank PBS solution}) \times \text{Mw}_{\text{Doxorubicin-HCl}}}{\text{Volume of PBS solution inside the flask} \times \varepsilon \times l \times (\text{The initial amount of DOX in a dialysis bag}) \times 100}$$

Equation 3.2: Calculation of % Drug Release

3.2.7.1. Cell Viability Analysis

The effect of targeted, non-targeted Dox loaded and just carriers were measured by MTS ([3-(4,5-dimethylthiazol-2-yl)-5-(3-carboxymethoxyphenyl)-2-(4-sulfophenyl)-2H-tetrazolium]) (CellTiter 96® AQueous One Solution Cell Proliferation Assay (MTS), Promega Corporation) and Resazurin (Alamar Blue) Assay. They are used to examine the % cell viability diversity of both cancer and healthy cell lines with a wide range variety of nanocarriers.

3.2.7.1.1. MTS Assay

Cells were seeded in the 96-well culture plates at a seeding density of 1×10^4 cells/cm^2 with full growth medium (10% FBS, 1% penicillin-streptomycin, 1% NEMAAM, and 1% L-glutamine containing DMEM medium 0.45% (w/v) glucose) and incubated overnight to allow the cells to attach. The treatment drug with different concentrations (2.5, 5,7.5 and, 10 μg/mL) was added to the culture plates with 200 μL DMEM containing 0.45% (w/v) glucose. After 24h incubation, the cells were washed from nanocarrier particles that are not able to interact with cells with PBS. After washing steps, cells were incubated with 1% MTS reagent containing FBS free medium for 3 hours and from UV absorption (λ_{abs}= 490nm) data cell viability calculated with respect to untreated controls by the following equation (***Equation 3.3***).

$$\text{Cell Viability \%} = \frac{\text{Test wel -Negative Control}}{\text{Positive Control-Negative Control}} \times 100,$$

Equation 3.3: Calculation of Cell Viability % from Absorbance.

3.2.7.1.2. Resazurin (Alamar Blue) Assay

Resazurin assay was practiced as a secondary cell viability analysis which is more convenient for disposing of the contribution of Doxorubicin on absorbance in terms of the maximum absorption peak that clashed at the 485 nm. Resazurin assay is also known

as Alamar Blue assay is low-priced, handling in the homogeneous system, fluorescence-based, and more sensitive than tetrazolium assays such as MTS assay [95]. 4 mg of Resazurin was dissolved in sterilized 10 ml PBS solution as 10X stock. The same procedure was followed with the MTS assay in terms of cell amount and drug concentration. The black ground 96-well plate was specifically used for the getting best fluorescence value. After the treatment with drugs and compositions, washed with PBS two times and added 1X Resazurin containing 200 μL DMEM without FBS and incubated 3 hours to obtain the resorufin which is caused by the reduction that is proportional to the cell viability of the resazurin. Then the value of fluorescence λ: 550-590 nm was recorded and cell viability was calculated as regards ***Equation 3.3*.**

3.2.7.1.3. Statistical Analysis

Two-way Analysis of variance (ANOVA) with Tukey post comparison test was done to determine the significant difference among the groups by GraphPad Prism software (version 8.02; GraphPad Software Inc.). Assigned symbols to concentration levels were used to report comparison results between different compounds at the same concentrations and same time points. Statistical significances are indicated in the figures as $p < 0.033$ (*), $p < 0.002$ (**), and $p < 0.001$ (***).

3.2.7.2. Cellular Uptake Studies

3.2.7.2.1. Confocal Microscopy Analysis (Qualitative)

In order to compare cellular uptake of targeted and/or non-targeted drug-loaded PEGylated rGO derivatives 25 $\times 10^3$ MDA-MB-231, and MCF-7 cells were seeded into glass-bottom 24 well-plate in 1 mL full growth medium and incubated for 24 hours at 37 °C in a humidified 5% CO_2 atmosphere. After 24 hours of cells that had already adherent on the plate were washed two times with PBS to remove the medium. Finally, determined concentrations μg/mL of drug-loaded nanocarriers were applied to cells with 10% FBS

containing DMEM. After 0.5 and 4 hours of treatment wells were triple washed with PBS, 1μL Hoechst dye (Thermo Scientific) containing medium were applied and incubated for 15 minutes for nuclei staining and the images were collected, then analyzed by Zeiss Zen software.

3.2.7.2.2. Flow Cytometry (FACS) Analysis

Flow cytometry was used to determine the intake rates of targeted and non-targeted Dox loaded GO-based nanocarriers. The analysis was carried out without further staining using the fluorescence feature of the Dox molecule currently on the structure. 3×10^5 MCF-7 cells are planted in a 6-well plate with 3 mL of FBS containing DMEM incubated for 12 hours to attach to the well surface. Compositions determined after incubation time equivalent to 100 μg/ mL in 500 μL. After 4 hours, the materials were drawn from the wells and washed 3 times with PBS, and removed from the surface by the addition of Trypsin/ EDTA. Then, cells were washed with %2 FBS containing PBS, again disperse in this solution, passed through a cell strainer, transferred to analysis tubes Flow Cytometry (BD Influx ™ Cell Sorter BD Biosciences). In the system where 50.000 interactions were analyzed, Dox was stimulated at 488 nm and its emission was read at 550 nm. The data obtained using the correct scatter channel (Forward Scatter Chanel (FSC)) and the side scatters channel (Side Scatter Channel (SSC)) were plotted.

CHAPTER 4

4. RESULTS

4.1. Preparation of EPPT1 Targeting, Drug Loaded, and PAMP Copolymer Coated rGO-based Nano platform

The present work specifically comprised further modifications of the efficiently PEGylated, biocompatible, and uMUC1 receptor-targeted therapeutic loaded nano-platform and investigations of anticancer activities based on the tuned chemical ***Figure 4.1***. Experimental analysis has been done for each step to obtain the best targeted drug-loaded GO-based nanoplatforms. Starting from the synthesis of PAMP copolymer which is tuned to investigate the effect of monomers on drug release profile and coating and reduction at the same time with GO was an effective way in the aspect of abundant pi bonds. Azide group presence led the system to make covalent bonding with target groups. Each step was proffered by the various experimental results for the characterizations in the results section.

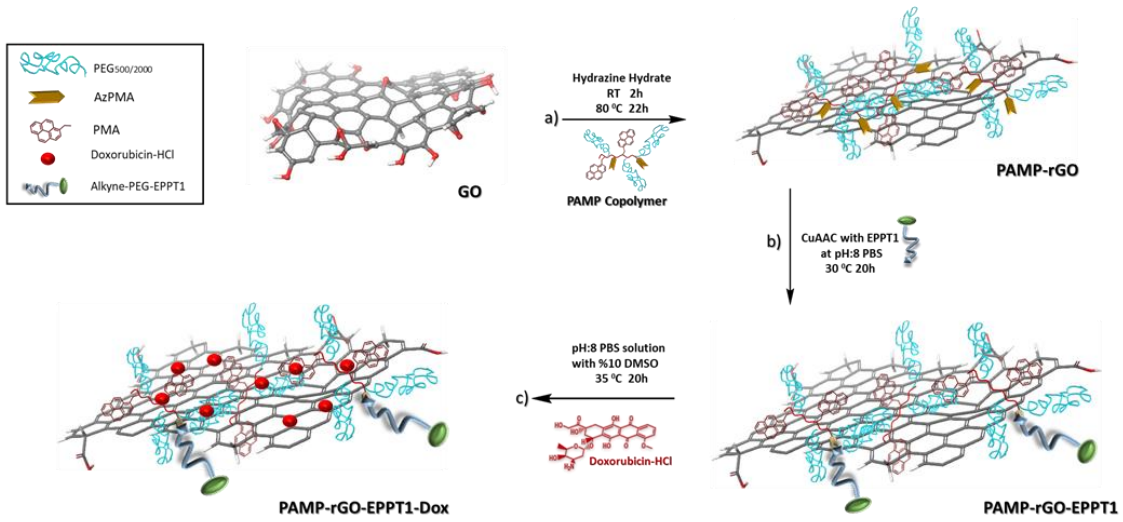


Figure 4.1: Schematic representation of EPPT1 targeting, drug-loaded PAMP coated rGO nanoplatforms

4.2. Synthesis and Characterizations of PAMP Copolymer

The first step to obtaining a coated rGO surface is to synthesize the functional PAMP copolymer using the described monomers. Among these monomers, while PEGMA with different molecular weight (500 g/mol and 2000g/mol) and methyl methacrylate (MMA) are commercially available, pyrene methacrylate (PMA) (***Figure 4.2b)*** and azido propyl methacrylate (AzPMA) (***Figure 4.2c)*** were synthesized as described in the Methods section. An initiator that allows calculation of copolymer composition and molecular weight using the ^{1}H NMR spectrum was also synthesized (***Figure 4.2a***). Novel copolymer P(PEGMA-co-AzPMA-co-MMA-co-PMA) (PAMP) that contains PEG brushes, azide, and pyrene groups with different compositions were synthesized via Atom Transfer Radical Polymerization (ATRP) (***Figure 4.2d)***. Monomers were copolymerized with different feeding ratios to tune the desired copolymer composition via controlled-radical polymerization. Molecular weights and copolymer composition were calculated using ^{1}H NMR spectroscopy. The total molecular weight of the copolymers was prepared with less than 50000 g/ mol. The reason why it was aimed to prepare the polymers under this molecular weight is they can be discarded by the renal secretion at the end and will not cause toxic effects, besides, branched structures prolong the circulation time in the blood and it is also known to reduce the hydrodynamic volume.

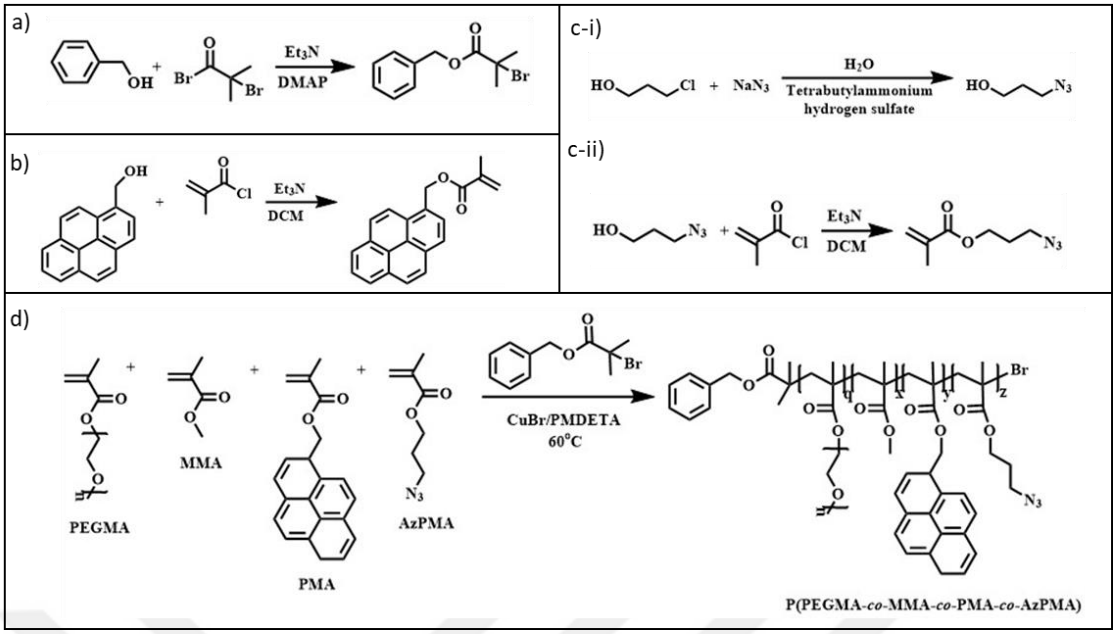


Figure 4.2: Chemical reactions of a) the initiator, b) PMA, c) AzPMA, and d) ATRP copolymerization of monomers.

Obtained copolymers for this study were summarized in ***Table 4.1*** including the molecular weight of the PEGMA brushes (500 and 2000 g /mol), the number of PEG brushes (PEGMA), the number of azide group (AzPMA), and the number of pyrene group (PMA). The copolymers were then called with their abbreviations, depending on the number of monomers contained in the copolymer and the coating product. P symbolize PEGMA copolymer, A is AzPMA, M is MMA and, the last P is PMA monomer. These copolymers were used for the coating process and the effect of summarized parameters on morphological characteristics, drug release profile at different pH, and biocompatibility have been examined and compared.

Table 4.1: Features of PAMP Copolymers.

	Copolymer Code	Temp. (^{0}C)	Time (h)	M_{nNMR} (g/mol)	DPn	#of PEGMA	#of MMA	#of PMA	#of AzPMA
PEG$_{2000}$	$(P_{12}A_5MP)_{2000}$	60	3	28337	39.8	12.12	19.22	3.67	4.79
	$(P_{25}A_{17}MP)_{2000}$	60	3	61483	108.56	24.74	56.52	10.72	16.58
	$(P_{15}A_{10}MP)_{2000}$	60	5	35517	46.63	14.49	10.64	11.96	9.54
PEG$_{500}$	$(P_{26}A_{16}MP)_{500}$	60	3	20352	64.67	25.89	11.85	10.74	16.17
	$(P_{17}A_9MP)_{500}$	60	3	15434	59.37	16.47	23.54	9.99	9.37

*Monomers/PMDETA/CuBr/Initiator:100/1/1/1

4.3. The PAMP Copolymer Coating and *in-situ* Reduction of Graphene Oxide *in-situ*: PAMP-rGO and Its Characterization

PAMP copolymer coating also called PEGylation was performed via π-π stacking on GO which is water-soluble graphene derivatives. Initial PAMP and GO interaction decrease the chance of stacking of the GO layer during reduction which is the process that took place in-situ during PEGylation to obtain a more defect-free surface of graphene. The reduction of GO to rGO was performed using hydrazine hydrate as a reducing agent at 80^{O}C while PAMP coating is under progress. Unbonded copolymers and hydrazine were removed by washing DMF and water before freeze-dried.

The amount of percent copolymer on the graphene surface was calculated as coating efficiency using thermal gravimetric analysis (TGA) [92]. The typical TGA curves of samples between 30 to 800 ^{0}C heated 10 ^{0}C/min under nitrogen atmosphere. Weight loss associated with PAMP copolymer degradation was used to calculate the copolymer coating efficiency on the graphene surface by considering the weight lost the contribution of rGO within the same temperature range (200-550 ^{0}C). PEGylation and simultaneously reduction of GO to rGO were confirmed by TGA results. As shown in ***Figure 4.3*** between 200-550^0 C the mass reduction of rGO was calculated as 8.549 % that was used as blank for analysis of each composition. Simply, PEGylation was calculated by extracting the 8.549% which is the amount of the rGO from the mass reduction PAMP-rGO compounds between 200-550^0 C. As can be seen in ***Figure 4.3***, PAMP-rGO compositions consist of

more than 60 weight percentage PAMP copolymer and the remaining percentage has been assumed that it is rGO **(*Table 4.2*).** The results also showed that the copolymer composition does not have a significant effect on coating efficiency.

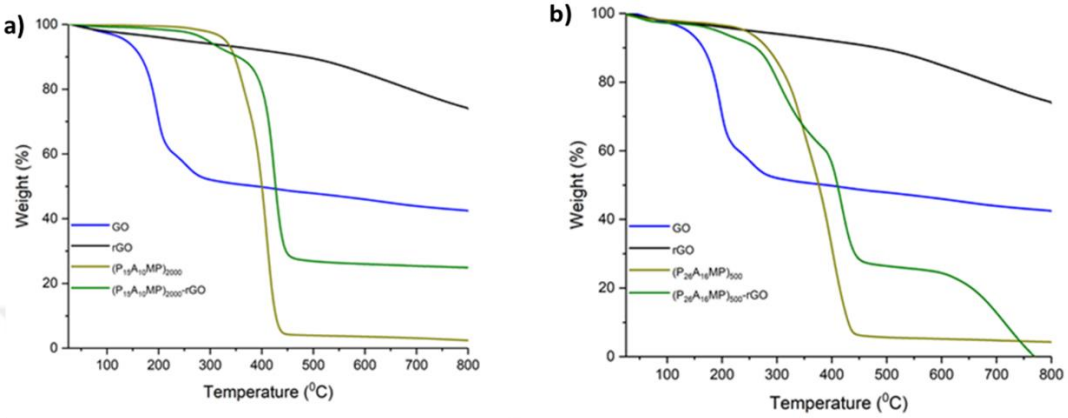


Figure 4.3 TGA curves of **a)** GO, rGO, $(P_{15}A_{10}MP)_{2000}$, $(P_{15}A_{10}MP)_{2000}$-rGO, and **b)** GO, rGO, $(P_{26}A_{16}MP)_{500}$, $(P_{26}A_{16}MP)_{500}$-rGO compositions.

Table 4.2 Abbreviations of the PAMP copolymer coated rGO carriers and their coating efficiency.

	Abbreviations of PAMP-rGO	**Coating Efficiency (mass %)**
PEG_{2000}	$(P_{9}AMP)_{2000}$-rGO	65.475 %
	$(P_{12}A_{5}MP)_{2000}$-rGO	61.087 %
	$(P_{25}A_{17}MP)_{2000}$-rGO	61.774 %
	$(P_{15}A_{10}MP)_{2000}$-rGO	63.647 %
PEG_{500}	$(P_{19}AMP)_{500}$-rGO	64.708 %
	$(P_{26}A_{16}MP)_{500}$-rGO	60.295 %
	$(P_{17}A_{9}MP)_{500}$-rGO	59.867 %
	$(P_{23}A_{12}MP)_{500}$-rGO	61.774 %

The presence of PAMP copolymer on rGO was also confirmed through AFM imaging. The data represented in ***Figure 4.4*** showed that plain GO surface demonstrates planar and thick folded layers. Increasing thickness indicated a successful accumulation of copolymer on the rGO surface after coating and reduction of GO. AFM images also demonstrate with the TGA result that copolymer coating on reduced graphene oxide surface successfully.

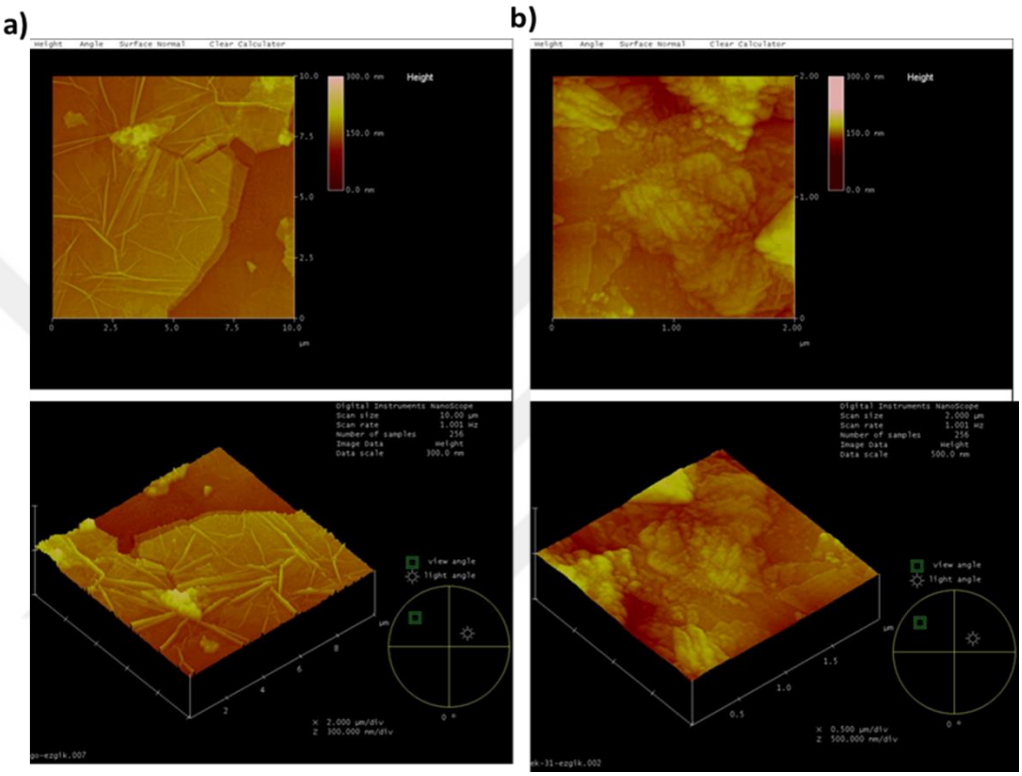


Figure 4.4 AFM analysis of **a)** GO and **b)** PAMP-rGO

4.4. Conjugation of EPPT1 Peptide on PAMP-rGO or PAMP-rGO-Dox Nano platform: (PAMP-rGO-EPPT1)

EPPT1 peptide containing the PEG chain was first synthesized to conjugate groups on the surface of PAMP-rGO through a highly efficient ”click” reaction using azide groups on the surface. N-terminus of the peptide used to conjugate to NHS active ester side of the *alpha*-alkyne-*omega* NHS terminated telechelic PEG (Alkyne-PEG-NHS) polymer chain with the molecular weight of 3.5 kDa which is longer than the used PEG brushes in the coated copolymer to promote the ligand cell surface interaction. EPPT1 conjugation

on telechelic PEG was performed through EDC/NHS coupling reaction in an aqueous environment at pH:8. (***Figure 4.5***). The excess amount of alkyne-PEG-NHS was detracted by the dialysis method to obtain pure Alkyne-PEG-EPPT1 conjugate.

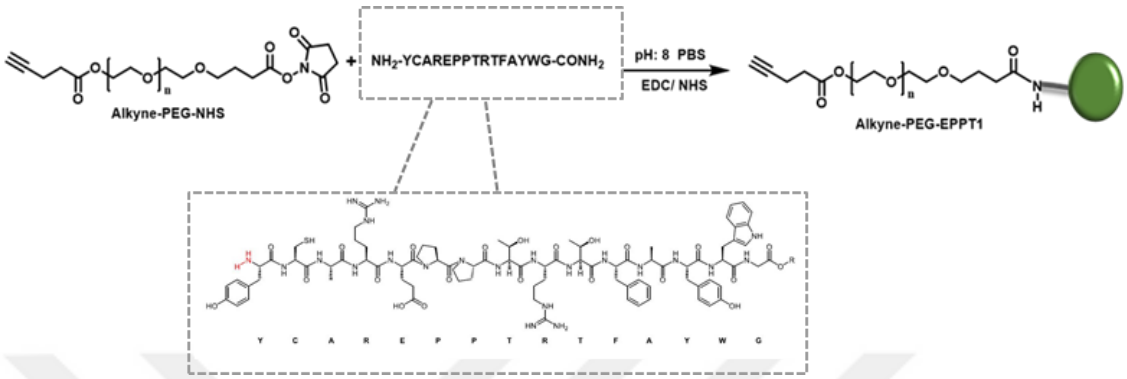


Figure 4.5: Schematic illustration of EPPT1 peptide conjugation

The reaction efficiency was calculated by ^{1}H NMR. As shown in ***Figure 4.6,*** the characteristic peaks of Alkyne-PEG-NHS and EPPT1 peptide itself can be clearly seen in the spectrum of Alkyne-PEG-EPPT1 conjugate. The backbone protons of PEG chains have been seen from 3.25 to 4.00 ppm at the Alkyne-PEG-EPPT1 spectrum. While alkyne proton at 2.03 ppm is still visible at the spectrum of Alkyne-PEG-EPPT1, characteristic signals of NHS protons at 2.96 ppm were disappeared indication the conjugation of EPPT1. Moreover, the signals of aromatic groups of the amino acid were clearly detected between 6.60 and 7.25 ppm at the Alkyne-PEG-EPPT1 spectrum and these signals were used to calculate the conjugation efficiency of the peptide as 83.84%.

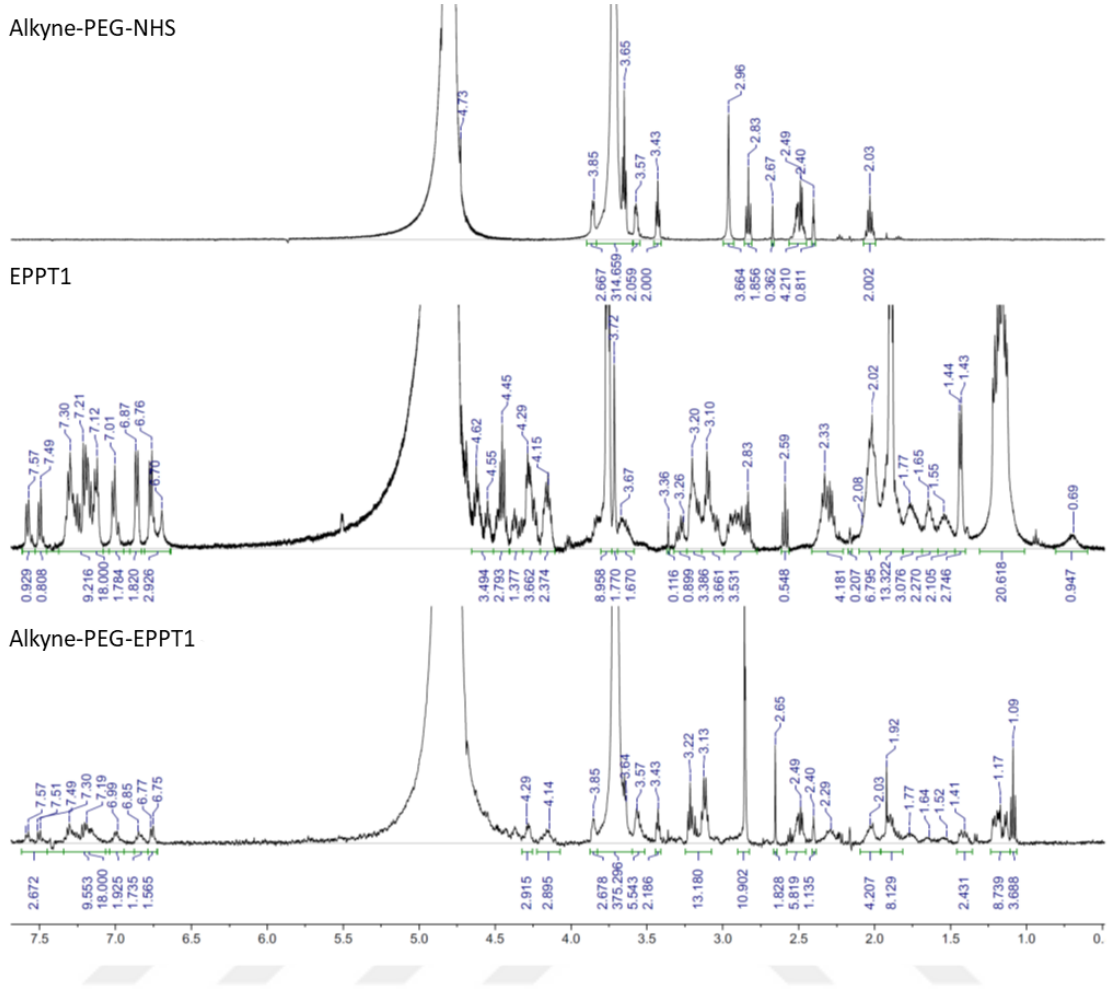


Figure 4.6: ^{1}H NMR spectrum of a) Alkyne-PEG-NHS, b) EPPT1 and, c) Alkyne-PEG-EPPT1

The obtained Alkyne-PEG-EPPT1 was grafted on azide functional surface of PAMP-rGO via copper-catalyzed azide-alkyne click reaction (CuAAC). The efficiency of covalent conjugation with peptide was evaluated by looking for the peptide concentration in the upper phase of the reaction mixture. Since EPPT1 peptide consists of cysteine amino acid with -SH group, Ellman`s assay was able to use to determine the peptide concentration. The peptide concentration can be calculated by considering the additional absorbance of the 2-nitro-5-thiobenzoate (TNB) which is formed from 5,5'-dithiobis-(2-nitrobenzoic acid (DTNB) with the presence of -SH group once the molar absorptivity coefficient is calculated using the calibration curve that is generated in ***Figure 4.7***. Calculations are shown that PEG-EPPT1 conjugate was successfully grafted to the surface of different PAMP-rGO compositions with high reaction yield (**Table 4.3)**.

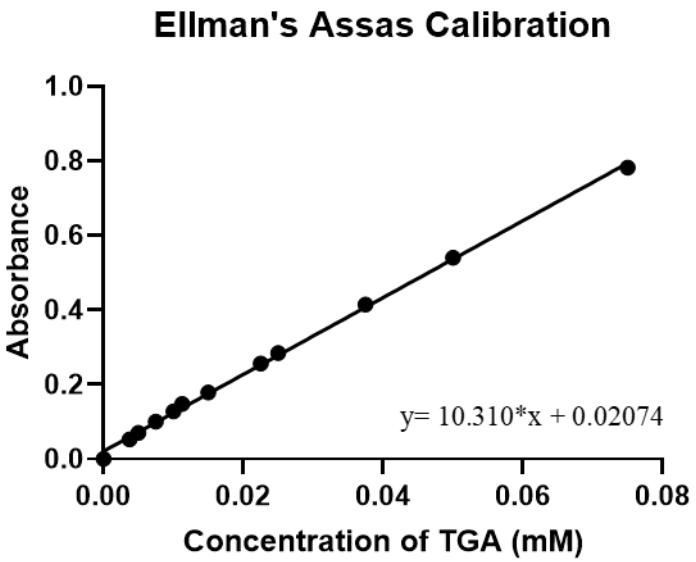


Figure 4.7: Calibration curve for the Ellman's Assay

Table 4.3 showed that regardless of coated copolymer composition, peptide conjugation took place with high reaction yield, and only less than 1% (weight) peptide did not react and stay in the upper mixture. Even though "click" reactions are highly efficient reactions, the almost quantitative reaction yield at the surface indicates that there is a possibility to have peptide-graphene interaction which is well known in the literature [96].

Table 4.3: Ellman's Assay analysis for EPPT1 conjugation

Compound	Upper Phase Conc.	Initial Conc.	% Click
$(P_{15}A_{10}MP)_{2000}$-rGO-EPPT1	2.97E-08	6.60E-05	99.95
$(P_{15}MP)_{2000}$-rGO-EPPT1	3.08E-08	6.70E-05	99.95
$(P_{26}A_{16}MP)_{500}$-rGO-EPPT1	1.08E-07	8.30E-05	99.87
$(P_{26}MP)_{500}$-rGO-EPPT1	3.73E-08	8.40E-05	99.96

AzPMA group on PAMP copolymer makes PAMP-rGO functional for covalent bonding with the desired property. Coming sections include the investigation of ionic groups comes from the azide group either effect or not the drug release rate. Therefore, to be able to investigate the effect of the azide groups on cytotoxicity, cellular uptake, and drug

release profile at the physiological and acidic environment, unused azide groups in the copolymer either left as it is or capped with propargyl alcohol. It can easily follow by copolymer abbreviations which shows monomer "A" if there is an azide group in the structure (represented as PAMP and PMP, respectively). FTIR analysis was a sufficient analysis to observe whether all azide group capped or not. As it is shown in ***Figure 4.8***, the FTIR spectra of AzPMA characteristic broad R-N=N^+=N^- stretching band at 2100 cm^{-1} [1] can be clearly seen on $P_{23}A_{12}MP_{500}$ and $P_{23}A_{12}MP_{500}$-rGO compounds. Whereas the absence of the N=N=N stretching band indicates that the remaining azide was successfully capped as seen in $(P_{26}MP)_{500}$-EPPT1 compound.

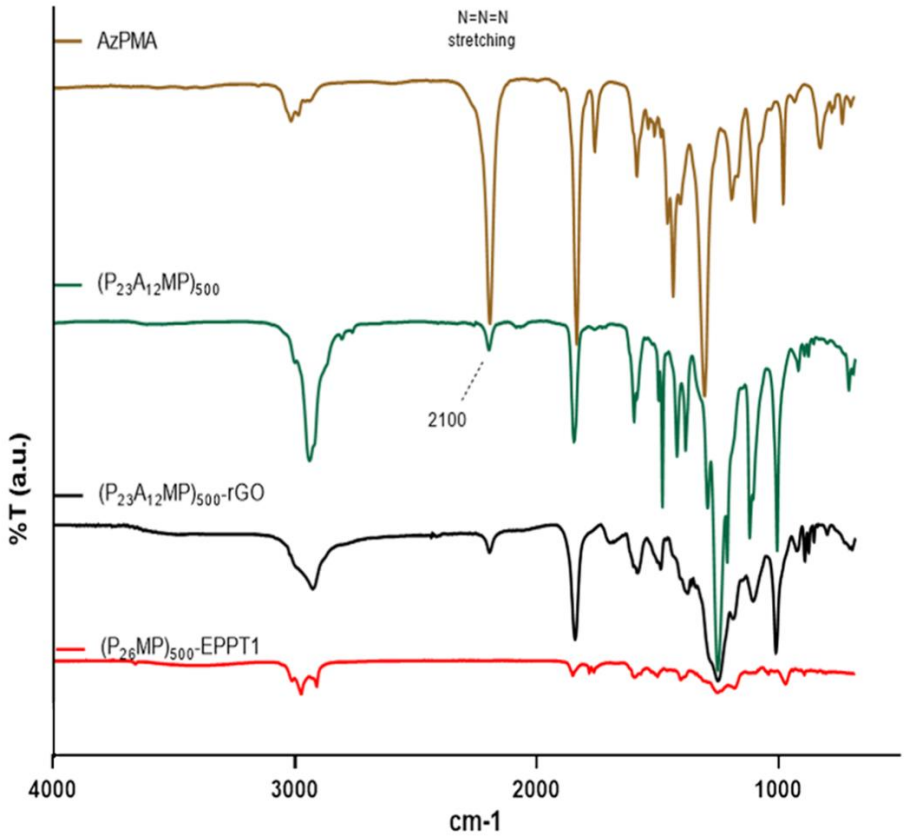


Figure 4.8: FTIR spectrum of a) AzPMA, b) $PAMP_{500}$, c) $PAMP_{500}$-rGO, d) PMP_{500}-EPPT1

4.5. Drug Loading on EPPT1 Targeted PAMP Coated rGO Nanoplatforms: PAMP-rGO-EPPT1-Dox and PMP-rGO-EPPT1-Dox

As a therapeutic doxorubicin-HCl was loaded onto PAMP-rGO-EPPT1 or PMP-rGO-EPPT1 via π-π stacking and hydrophobic interactions through cyclic structure and functional groups. Performing a therapeutic effect with high loading efficiency is compulsory for vehicles. Accordingly, drug-loading of copolymer coated and peptide conjugated rGO nanoplatforms was achieved with a range of 92 wt% to 98 wt% drug loading efficiency.

Drug loading order was also investigated in terms of the morphological difference, the effect of drug release profile and cell viability, and cellular uptake edibility on cancer cells distinctly. For instance, if PAMP-rGO composition would be loaded with Dox before EPPT1 conjugation, Dox was put before the EPPT1 on the naming as PAMP-rGO-Dox-EPPT1. The reason why we should have researched the order is from the synthetic point of view, PAMP-rGO-Dox-EPPT1 not only has difficulty with the determination of exact Dox concentration but also has some concerns about Dox contribution to optical quantification of EPPT1 peptide in the supernatant solution because of the possibility of the Dox release during peptide conjugation. On the other hand, PAMP-rGO-EPPT1-Dox is the most feasible way for the aspect of measuring the stable covalently bonded EPPT1 peptide and measure the exact drug loading efficiency.

Regardless of the order of Dox loading, the loaded amount of Dox was calculated using the calibration curve that was used to calculate the molar absorptivity coefficient (ε) as 4924 M^{-1} with the linear slope method with 99.66% reliability ***(Figure 4.9).*** By using Lambert-Beer Law with a calculated molar absorptivity coefficient, the amount of Dox loaded or released was determined by measuring the max absorption of a solution of interest at 483 nm.

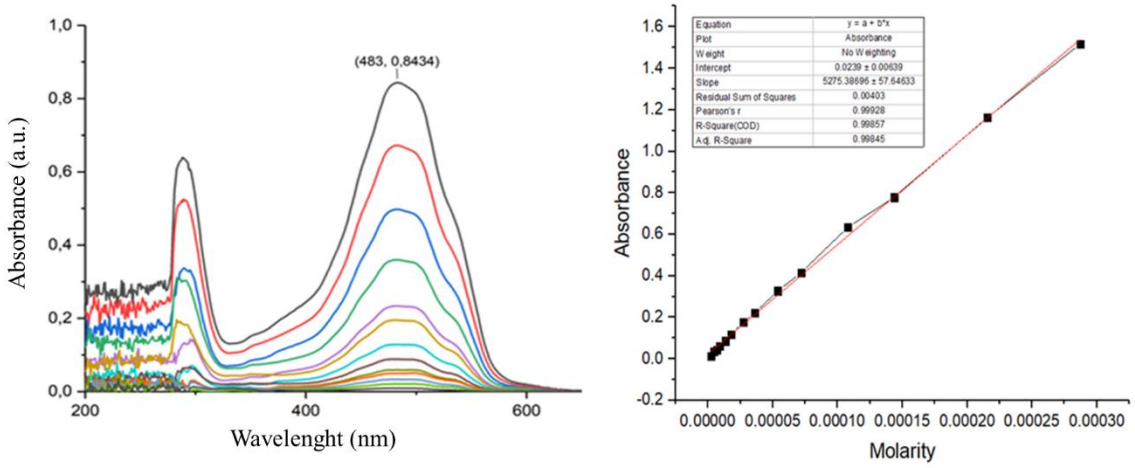


Figure 4.9 a) UV-Visible full-spectrum scanning **b)** Absorption calibration curve through different concentration of Dox-HCl

The effect of the temperature is represented in ***Figure 4.10***. Drug loading efficiency (LE) reached to 98.86% at 35 ^{o}C at pH8 10% DMSO containing PBS solution. Besides, at 19 ^{o}C LE reached only 74.8% at the same conditions.

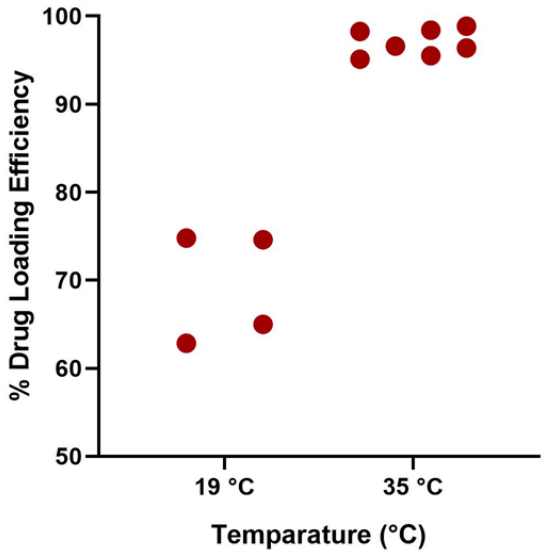
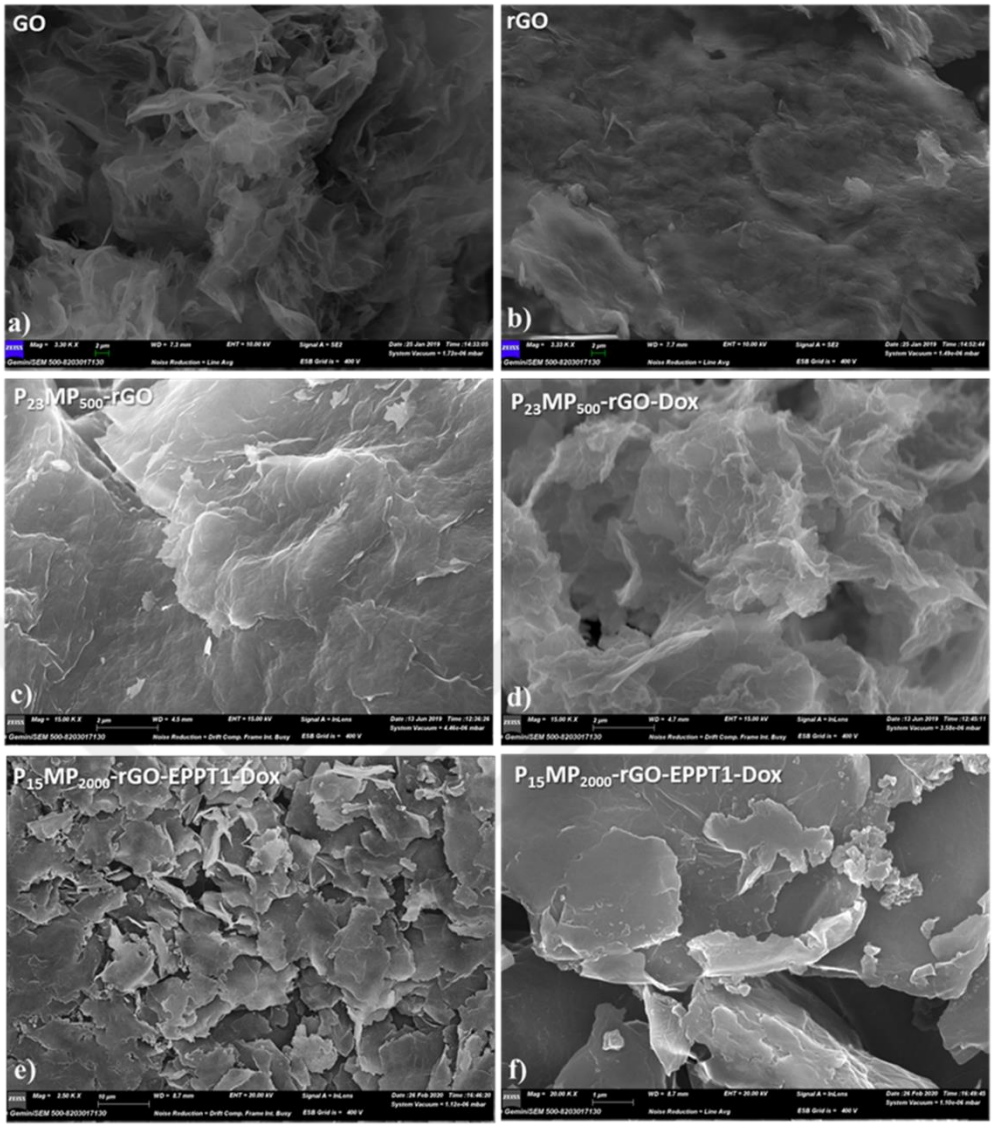


Figure 4.10 Drug loading efficiency (LE) chances depend on temperature.

Drug loaded, targeted carrier (PAMP-rGO-EPPT1-Dox), and it's all precursor including the one synthesized for comparison were investigated to obtain further proof for drug loading. ***Figure 4.11*** shows the SEM micrograph of PAMP-rGO-Dox, PAMP-rGO-EPPT1-Dox, and their precursor's indication of the morphological change through surface modifications (***Figure 4.11a-f*****).** Furthermore, EDX data represented in ***Figure 4.11*****g** exhibited how elemental mapping of the carrier in each step has changed. Before the reduction of GO consist of some functional group such as carboxyl, hydroxyl, and epoxy groups, those are contributing to the oxygen percentages (37.97%). As a control, GO in aqueous solution was reduced to rGO by using hydrazine without any copolymer in the system. This process caused an appreciable decrease in the percentage of oxygen (11.28%), while a noticeable amount of N was detected as a result of trapping hydrazine between the insoluble, stacked graphene layers which is not a concern for copolymer coated graphene layer with enhancing solubility and dispersibility. While $(P_{15}A_{10}MP)_{2000}$-rGO exhibited 1.37% of nitrogen content, the Dox loaded version of it exhibited 2.09% of nitrogen indicating the Dox presence in the carrier. Despite there is only one nitrogen in one Dox molecule, it should be noted that the total mass of the Doxorubicin-HCl molecules in PAMP-rGO-EPPT1-Dox carrier is more than 45% (w/w). At the last step, successful conjugation of EPPT1 even further increased the nitrogen percentage (2.94%) owing to the amino groups of the amino acids.



g)

Compund Name	C %	O %	N %
GO	59.51	37.97	0.59
rGO	85.99	11.28	2.60
Doxorubicin-HCl	57.37	33.25	5.06
$(P_{15}A_{10}MP)_{2000}$-rGO	68.88	29.72	1.37
$(P_{15}A_{10}MP)_{2000}$-rGO-Dox	66.26	31.46	2.09
$(P_{15}A_{10}MP)_{2000}$-rGO-EPPT1-Dox	64.07	32.99	2.94

Figure 4.11: SEM images of **a)** GO, **b)** rGO, **c)** $P_{23}MP_{500}$-rGO, **d)** $P_{23}MP_{500}$-rGO-Dox, **e)** $P_{15}MP_{2000}$-rGO-EPPT1-Dox with low magnification, **f)** $P_{15}MP_{2000}$-rGO-EPPT1-Dox with high magnification and, **g)** SEM-EDX analysis of some compositions

TEM samples are prepared by the dropping of grids with a low concentration on water and dried under the vacuum at microcopy. Thus, lots of layers overlapped as it is obviously shown on TEM images (***Figure 4.12***). The images support the presence of the EPPT1 peptide on the PAMP coated rGO surface through morphological change on the pictures (***Figure 4.12b and d).*** PAMP-rGO-Dox and PAMP-rGO-EPPT1-Dox show similar morphological view with the black dots comes from dominantly the reprecipitation of Dox molecules during sample preparation (***Figure 4.12a and b).***

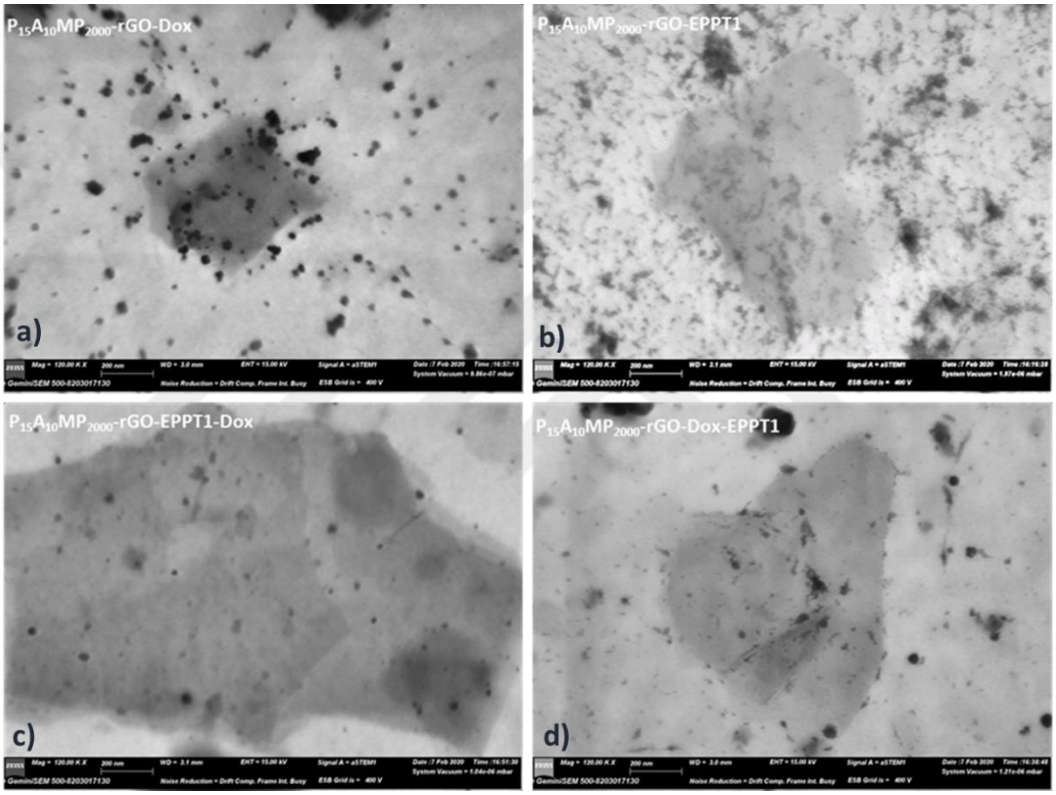


Figure 4.12: TEM images of **a)** $(P_{15}A_{10}MP)_{2000}$-rGO-Dox, **b)** $(P_{15}A_{10}MP)_{2000}$-rGO-EPPT1, **c)** $(P_{15}A_{10}MP)_{2000}$-rGO-EPPT1-Dox and, **d) (**$P_{15}A_{10}MP)_{2000}$-rGO-Dox-EPPT1

Dox loading was also confirmed by the TGA thermograms (***Figure 4.13***). Dox displays characteristic degradation range itself. Even though the presence of the Dox was clearly showed through its characteristic degradation range. The exact mass of Dox presence on the carrier was not able to calculate from TGA. Because the derivative which arises from the Dox is seen between 200-430 ^{o}C is overlap with the degradation of the rGO. Moreover, thermally decomposition of PAMP-rGO-Dox-EPPT1 showed an extra decay in the range of 460 °C to 485 °C which indicated the additional EPPT1 molecule on the

compound (***Figure 4.13***). Although this decay is only 1.34%, it can be interpreted as the contribution of functional groups on the peptide. This situation in in-vitro experiments will be explained and proved in detail.

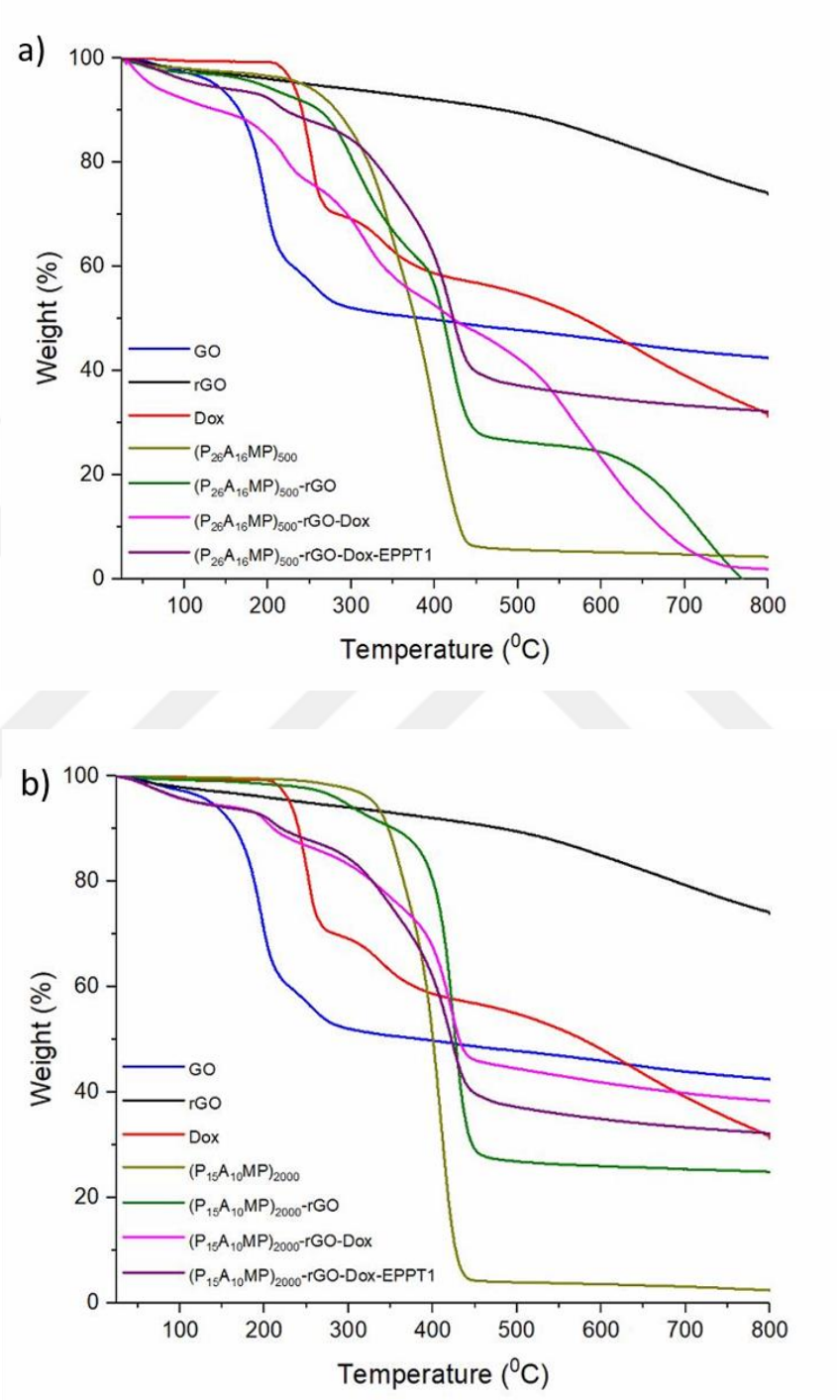


Figure 4.13 TGA curves of **a)** GO, rGO, Dox, $(P_{26}A_{16}MP)_{500}$, $(P_{26}A_{16}MP)_{500}$-rGO, and $(P_{26}A_{16}MP)_{500}$-rGO-Dox, $(P_{26}A_{16}MP)_{500}$-rGO-Dox-EPPT1 **b)** GO, rGO, Dox, $(P_{15}A_{10}MP)_{2000}$, $(P_{15}A_{10}MP)_{2000}$-rGO, $(P_{15}A_{10}MP)_{2000}$-rGO-Dox, $(P_{15}A_{10}MP)_{2000}$-rGO-Dox-EPPT1 compounds.

The characteristics shifts in D and G bands for each stage are shown in ***Figure 4.14***. GO commonly displays characteristic D and G bands, which indicates the change of electronic configuration on the carbon lattice. D band is associated with sp^3 hybridization of carbon atoms and the G band originates from sp^2 carbon atoms vibrations on the plane. The reduction of GO to rGO changes the degree of in-plane defects and functionalities on the surface resulting change in the ratio of D and G band intensity [97]. GO showed D and G bands at 1319 cm^{-1} and 1586 cm^{-1}, respectively and the G band is shifted to 1588 cm^{-1} once GO was reduced to rGO causing a slight decrease in I_D/I_G ratio from 1.31 to 1.29. After PAMP coating and simultaneous reduction D band shifted downward to 1313 cm^{-1} and the G band shifted upward to 1596 cm^{-1} and resulted in a narrower G band. The decreased I_D/I_G ratio increased once GO was coated and simultaneously reduced, which indicates the interaction between the copolymer and the graphene surface. Since Dox loaded increases this interaction even further decrease in I_D/I_G ratio was observed even more significant from 1.25 to 1.05 after Dox loading on the PAMP-rGO surface.

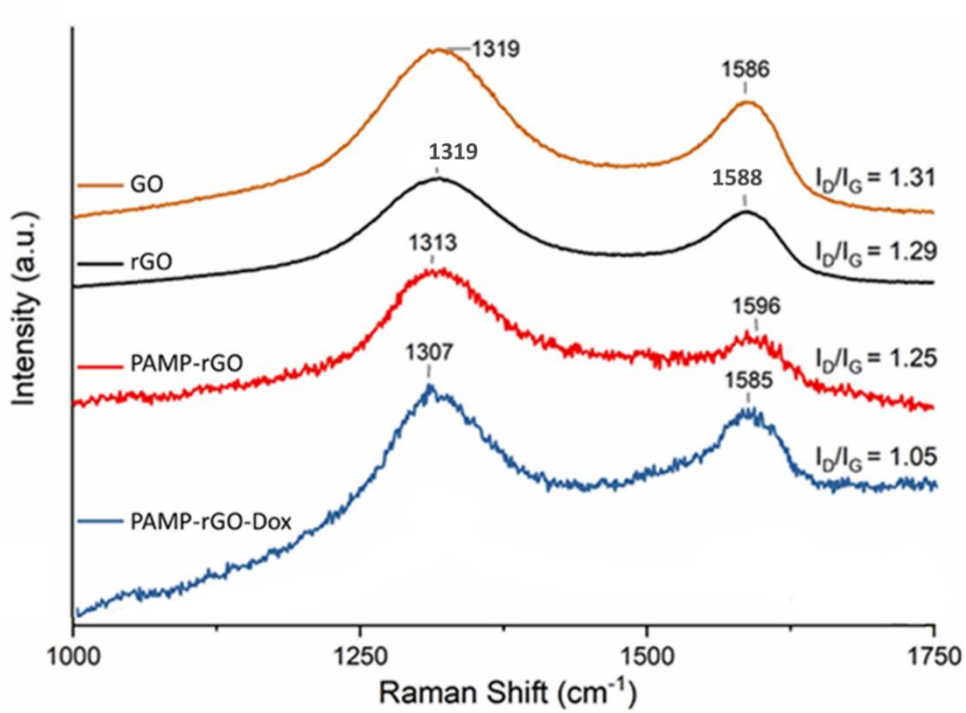


Figure 4.14: Raman spectra of a) GO, b) rGO, c) PAMP-rGO, d) PAMP-rGO-Dox compounds.

Additionally, DLS measurements were performed not only to get size information but also to measure the surface charge of the carriers (***Figure 4.15***). Overall measurement of the compositions from DLS shows that PEG with 200 g/mol molecular weight containing PAMP copolymer coated compositions are smaller-sized and more stable in water, PBS and, medium conditions. Negatively charged PEG containing copolymer coating and peptide conjugated composition PAMP-rGO-EPPT1 which is called empty nanocarriers shows fewer surface charges around -30 Mv. Doxorubicin-HCl is the hydrophilic salt form of the Doxorubicin molecule that was measured 0 Mv itself. Therefore, the increment of the surface charge after the Dox loading was another prove to be effective drug loading.

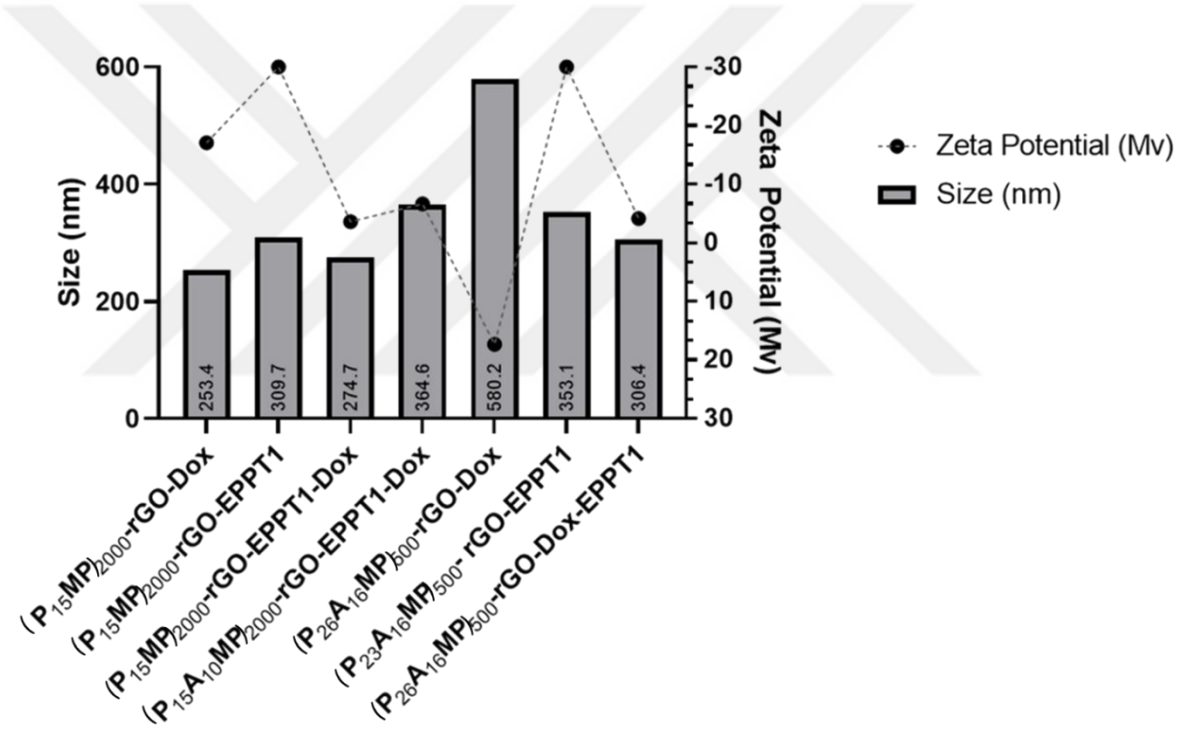


Figure 4.15: DLS and Zeta analysis of carriers.

4.6. The Effect of Copolymer Features in Drug Release Profile at Physiological and Acidic Environment

4.6.1. Investigation of the Effect of Azide Groups and PEG Brush Length of Copolymer on Drug Release Profile

To show whether the presence of azide groups has an influence on Dox release; Dox was loaded on the PAMP coated rGO and intentionally all azide groups were capped with propargyl alcohol to obtain PMP coated rGO.. As it can be seen in ***Figure 4.18a-b***, the increase in drug release percentage is higher for the rGO that is coated with shorter PEG containing copolymer than the longer PEG containing copolymer indicating the PEG density at the surface also effect the rate of the release.

Similarly, azide groups in the copolymer were mainly aimed to use for further functionalization, they can also act as an accelerator of drug release. Our results supported this thought as presented in ***Figure 4.16.*** While 16 azide groups bearing $(P_{26}A_{16}MP)_{500}$-rGO-Dox nanocarrier released 36% of the Dox, $(P_{26}MP)_{500}$-rGO-Dox which is all azide capped analog of it only reached the 23% drug release rate after 48h at the pH value of 5.5 (***Figure 4.16b)*** indicating the clear contribution of the azide group on release. Similarly, $(P_{15}A_{10}MP)_{2000}$ and $(P_{15}MP)_{2000}$ coated rGO nanocarrier released 35% and 26% of the Dox, respectively under the same conditions (***Figure 4.16a*****).** Statistical analysis also indicate that as the time passed by there is an increasement of the % drug release rate between $(P_{15}MP)_{2000}$-rGO-Dox and $(P_{15}A_{10}MP)_{2000}$-rGO-Dox. The increase in drug release percentage is higher for the rGO that is coated with shorter PEG containing copolymer than the longer PEG containing copolymer indicating the PEG density at the surface also effect the rate of the release. Moreover, the quantity of the drug release differences between azide containing and capped compositions decreases once the number of azide group decreases in the structure ***(Figure 4.16 a and b).***

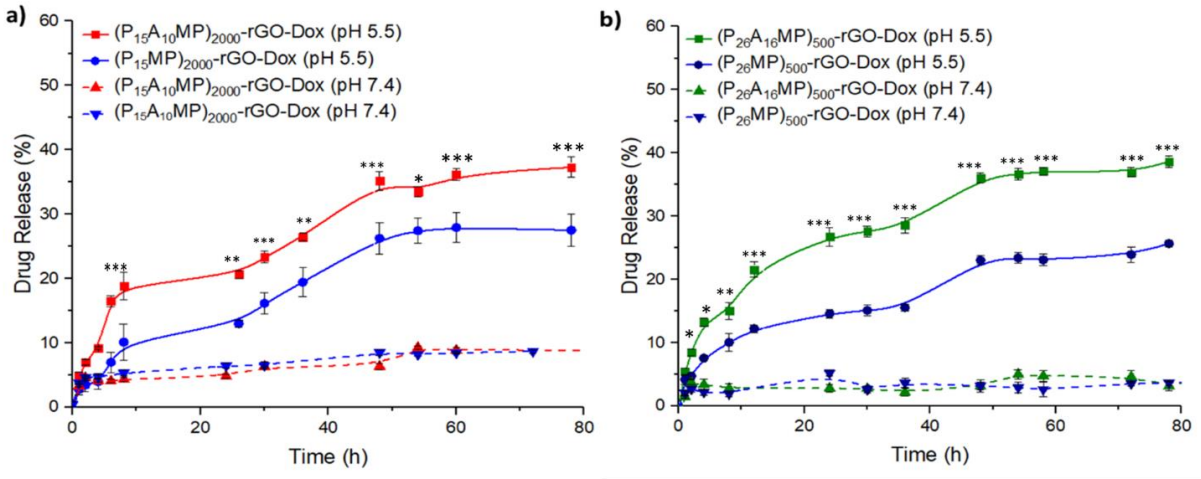


Figure 4.16 *In-vitro drug release profile of* ***a)*** *$(P_{15}A_{10}MP)_{2000}$-rGO-Dox, $(P_{15}MP)_{2000}$-rGO-Dox* ***b)*** *$(P_{26}A_{16}MP)_{500}$-rGO-Dox, $(P_{26}MP)_{500}$-rGO-Dox at pH 5.5 and 7.4.* Statistical difference between different compounds at pH 5.5 and each time points were significant at the 0.05 level where * denotes $p \leq 0.05$, ** denotes $p \leq 0.001$, and *** denotes $p \leq 0.001$.

As it can be seen in ***Figure 4.17***, a shorter (500 g/mol) PEG containing carrier is faster (5%) for initially 24 h than the similar analogous that has a longer (2000 g/mol) brush length. While shorter brush containing $(P_{26}A_{16}MP)_{500}$-rGO-Dox reached up to 36.05%, longer brush containing $(P_{25}A_{17}MP)_{2000}$-rGO-Dox reached up to 28.9% at the end of the 48 h. Once the drug release profile of $(P_{25}A_{17}MP)_{2000}$-rGO-Dox was compared with $(P_{15}A_{10}MP)_{2000}$-rGO-Dox, results show that $(P_{15}A_{10}MP)_{2000}$-rGO-Dox which has less number of brush showed an accelerated profile even though it has fewer azide groups (azide group increases the release rate) indicating the release rate affected by the density of the PEG content **(*Figure 4.17*).**

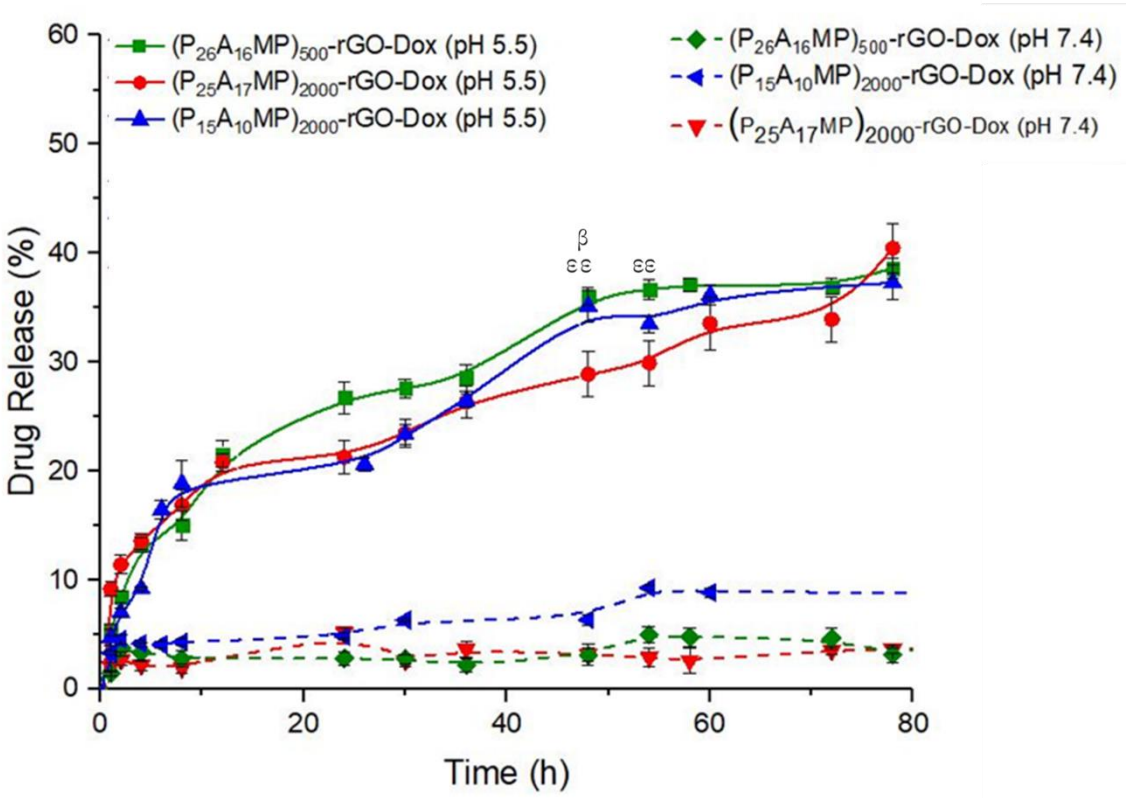


Figure 4.17: In- vitro drug release profiles of the $(P_{26}A_{16}MP)_{500}$-rGO-Dox, $(P_{25}A_{17}MP)_{2000}$-rGO-Dox, and $(P_{15}A_{10}MP)_{2000}$-rGO-Dox at pH 5.5 and 7.4. Statistical difference between different compounds at each time points were significant at the 0.033level where one symbol denotes p≤0.05, two symbols denote p≤0.01, and three symbols denotes p≤0.001. Symbols are assigned as; *(ε) $(P_{26}A_{16}MP)_{500}$-rGO-Dox vs $(P_{25}A_{17}MP)_{2000}$-rGO-Dox, (β) $(P_{25}A_{17}MP)_{2000}$-rGO-Dox vs $(P_{15}A_{10}MP)_{2000}$-rGO-Dox and, (Δ) $(P_{25}A_{17}MP)_{2000}$-rGO-Dox vs $(P_{15}A_{10}MP)_{2000}$-rGO-Dox.*

4.6.2. Investigation of the Effect of Presence and Order of EPPT1 Peptide Conjugation on Drug Release

Investigation of the effect of the presence of peptide at the surface, peptide conjugated and non-conjugated analogous were compared ***(Figure 4.18).*** Shows that the presence of the EPPT1 peptide at the surface of coated rGO decreases the drug release. While $(P_{15}A_{10}MP)_{2000}$-rGO-Dox carrier releases 35% of the loaded Dox at a pH of 5.5 within 48 h, $(P_{15}A_{10}MP)_{2000}$-rGO-Dox-EPPT1 carrier releases 28% of the Dox under the same conditions. Similarly, but slightly short PEG brush contribution, drug release of 37% of $(P_{26}A_{16}MP)_{500}$-rGO-Dox decreased to 27% when EPPT1 peptide was conjugated on the surface.

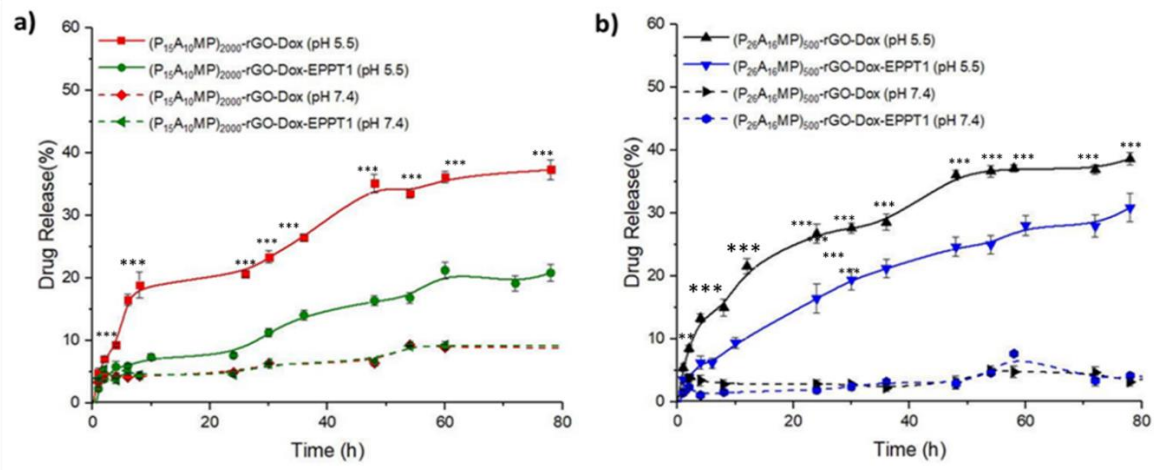


Figure 4.18: In-vitro drug release profiles of **a) (**$P_{15}A_{10}MP)_{2000}$-rGO-Dox, $(P_{15}A_{10}MP)_{2000}$-rGO-Dox-EPPT1 and **b)** $(P_{26}A_{16}MP)_{500}$-rGO-Dox, $(P_{26}A_{16}MP)_{500}$-rGO-Dox-EPPT1 at pH 5.5 and 7.4. Statistical difference between different compounds at pH 5.5 and each time points were significant at the 0.05 level where * denotes $p \leq 0.05$, ** denotes $p \leq 0.01$, and *** denotes $p \leq 0.001$.

The order of EPPT1 conjugation effect was determined by the following drug release experiments. ***Figure 4.19b*** showed that when Dox loading was performed as the last step after EPPT1 conjugation the release accelerated comparing the one EPPT1 conjugation was performed after Dox loading indicating the order of EPPT1 conjugation matters. However, this is not valid for azide capped composition and statistic analysis promotes that there is no significant difference (***Figure 4.19a***). In that situation the order of EPPT1 conjugation wasn`t significant for the initial 48 h and $(P_{15}MP)_{2000}$-rGO-Dox-EPPT1 accelerated slightly after 60 h.

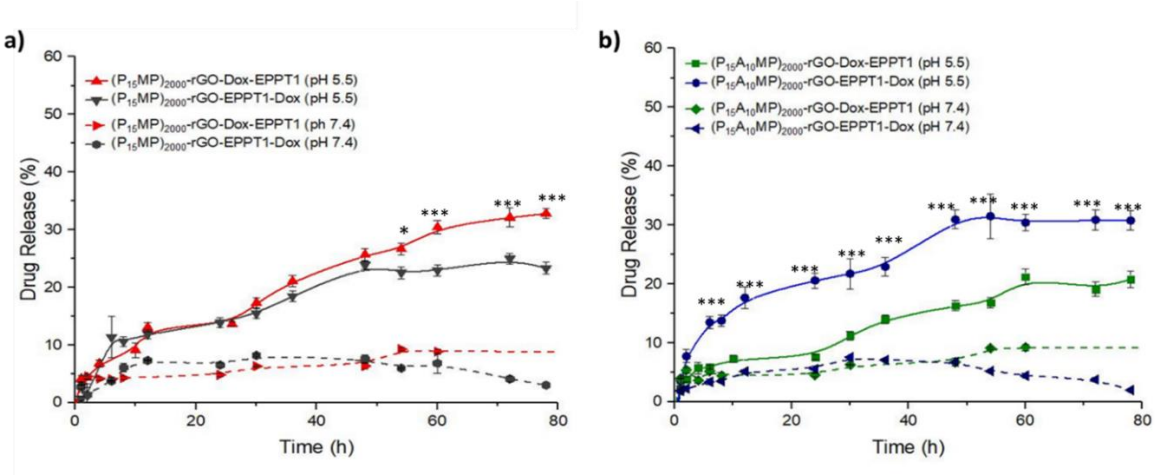


Figure 4.19: In-vitro drug release profiles of **a) (**$P_{15}MP)_{2000}$-rGO-Dox-EPPT1, $(P_{15}MP)_{2000}$-rGO-EPPT-Dox and **b)** $(P_{15}A_{10}MP)_{2000}$-rGO-Dox-EPPT1, $(P_{15}A_{10}MP)_{2000}$-rGO-EPPT1-Dox at pH 5.5 and 7.4. Statistical difference between different compounds at pH 5.5 and each time points were significant at the 0.05 level where * denotes $p \leq 0.05$, ** denotes $p \leq 0.01$ and, *** denotes $p \leq 0.001$.

Collectively, the presence of the azide group accelerated the release even though peptide conjugation decreases for longer PEG brush containing compositions (collectively summarized in ***Figure 4.20a***. Since decreasing PEG density increases the drug release along with azide groups, shorter PEG brush containing compositions do not always obey this trend. As it can be seen in ***Figure 4.20b,*** Dox release of $(P_{26}MP)_{500}$-rGO-EPPT1-Dox was faster than $(P_{26}A_{16}MP)_{500}$-rGO-EPPT1-Dox after 24 h.

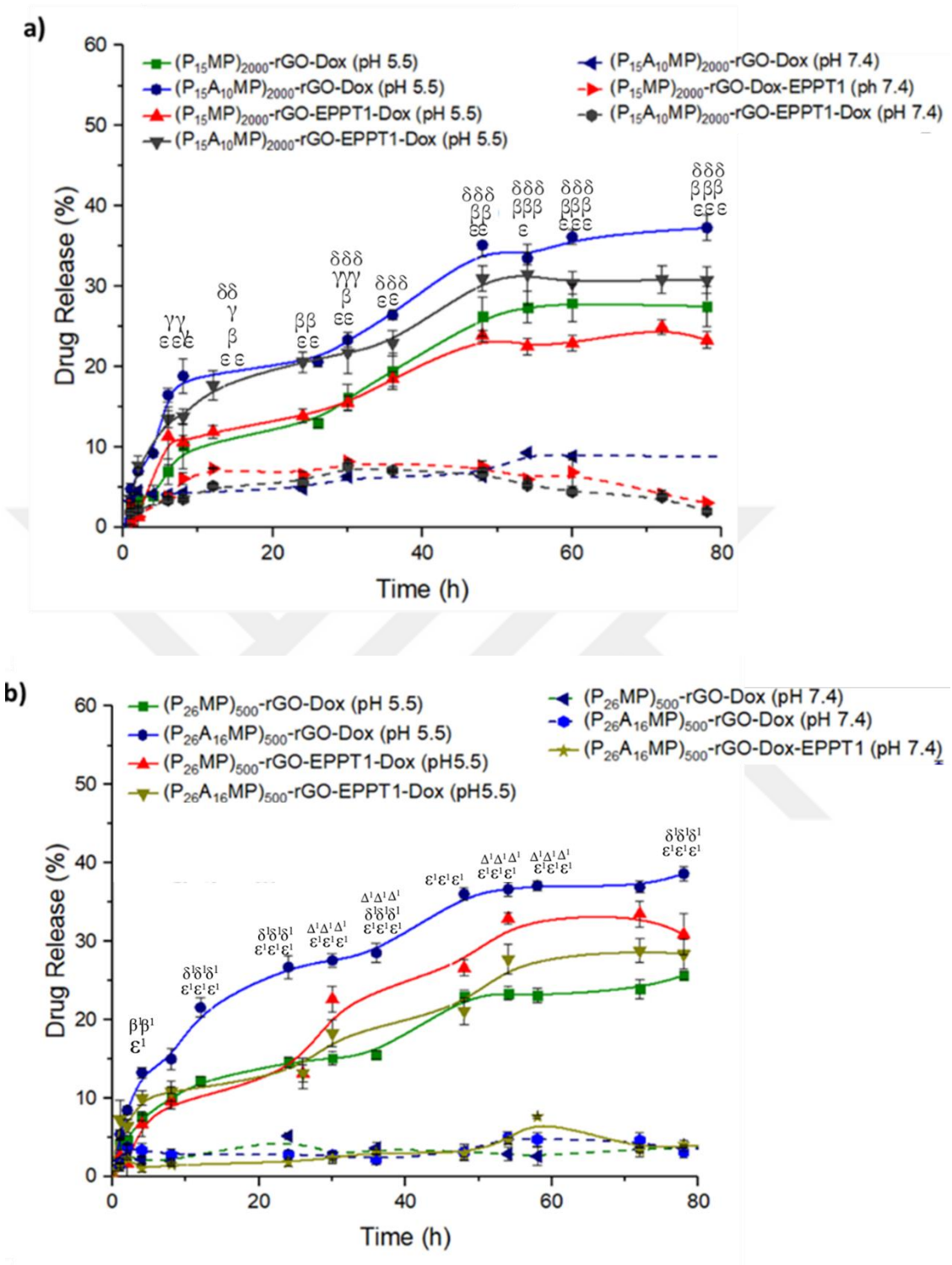


Figure 4.20*:* In-vitro drug release profiles of **a) (**$(P_{15}MP)_{2000}$-rGO-Dox, $(P_{15}A_{10}MP)_{2000}$-rGO-Dox, $(P_{15}MP)_{2000}$-rGO-EPPT1-Dox, $(P_{15}A_{10}MP)_{2000}$-rGO-EPPT1-Dox and **b)** $(P_{26}MP)_{500}$-rGO-Dox, $(P_{26}A_{16}MP)_{500}$-rGO-Dox, $(P_{26}MP)_{500}$-rGO-EPPT1-Dox, $(P_{26}A_{16}MP)_{500}$-rGO-EPPT1-Dox at pH 5.5 and 7.4. Statistical difference between different compounds at each time points were significant at the 0.05 level where one symbol denotes $p \leq 0.05$, two symbols denote $p \leq 0.01$, and three symbols denote $p \leq 0.001$. Symbols are assigned as; *(ε)* **(**$(P_{15}MP)_{2000}$-rGO-Dox vs $(P_{15}A_{10}MP)_{2000}$-rGO-Dox*, (β)* $(P_{15}MP)_{2000}$-rGO-EPPT1-Dox ve $(P_{15}A_{10}MP)_{2000}$-rGO-EPPT1-Dox *and, (Δ)*

($P_{15}MP)_{2000}$-rGO-Dox vs ($P_{15}MP)_{2000}$-rGO-EPPT1-Dox, *(γ)* **(**$P_{15}MP)_{2000}$-rGO-Dox vs ($P_{15}A_{10}MP)_{2000}$-rGO-EPPT1-Dox, *(δ)*($P_{15}A_{10}MP)_{2000}$-rGO-Dox vs ($P_{15}MP)_{2000}$-rGO-EPPT1-Dox, *(ε^1)* ($P_{26}MP)_{500}$-rGO-Dox vs ($P_{26}A_{16}MP)_{500}$-rGO-Dox, *(β^1)* ($P_{26}MP)_{500}$-rGO-EPPT1-Dox vs ($P_{26}A_{16}MP)_{500}$-rGO-EPPT1-Dox, *(Δ^1)* ($P_{26}MP)_{500}$-rGO-Dox vs, ($P_{26}MP)_{500}$-rGO-EPPT1-Dox, *(γ^1)* ($P_{26}MP)_{500}$-rGO-Dox vs ($P_{26}A_{16}MP)_{500}$-rGO-EPPT1-Dox and, *(δ^1)* ($P_{26}A_{16}MP)_{500}$-rGO-Dox vs ($P_{26}MP)_{500}$-rGO-EPPT1-Dox.

The results shown in ***Figure 4.21*****a** showed that the order of Dox loading did not change the rate of the drug release for azide groups containing composition. Statistical analysis also demonstrates that at each time points there are no statistical differences. On the other hand, azide capped version responded to the order of the Dox loading by slowing down the Dox release once Dox loading followed by EPPT1 conjugation (***Figure 4.21*****b**). It should be noted that ($P_{26}MP)_{500}$-rGO-EPPT1-Dox composition performed a very similar profile with ($P_{26}A_{16}MP)_{500}$-rGO-EPPT1-Dox (26% vs %30) showing that PEG density on the surface is competing with the azide groups contribution in drug release.

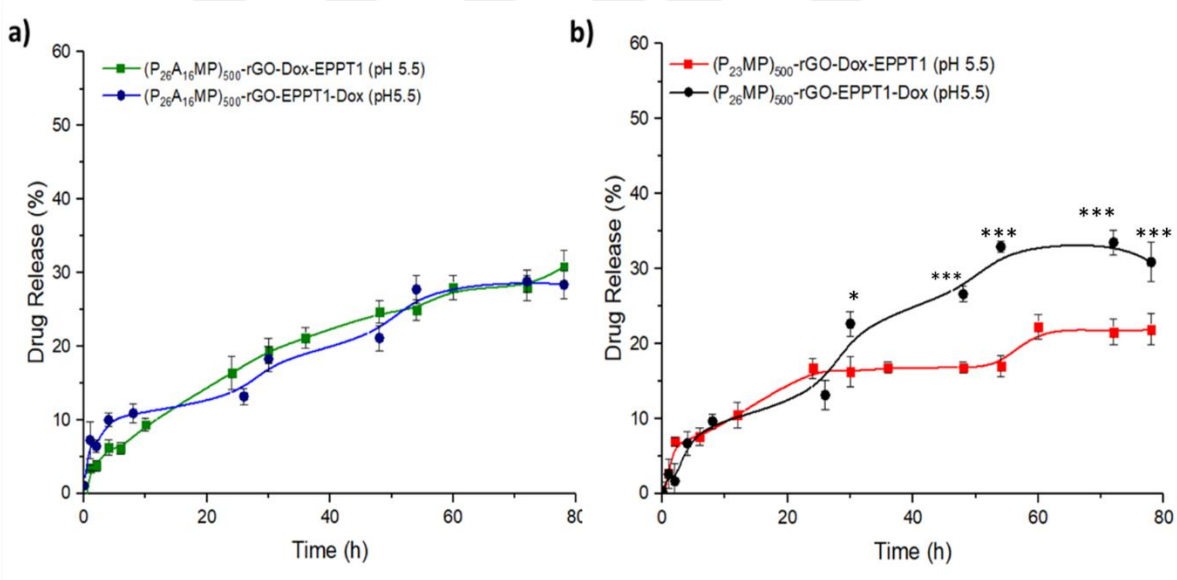


Figure 4.21: In-vitro drug release profiles of **a) (**$P_{26}A_{16}MP)_{500}$-rGO-Dox-EPPT1, ($P_{26}A_{16}MP)_{500}$-rGO-EPPT1-Dox and **b)** ($P_{23}MP)_{500}$-rGO-Dox-EPPT1, ($P_{26}MP)_{500}$-rGO-EPPT1-Dox at pH 5.5. Statistical difference between different compounds at each time points were significant at the 0.05 level where * denotes $p \leq 0.05$, ** denotes $p \leq 0.01$, and *** denotes $p \leq 0.001$.

4.7. Anticancer Activity of Targeted Nano platform

4.7.1. MTS Assay

MTS assay was first tried to get cell viability results from the targeted and nontargeted derivatives of $PAMP_{500}$ and $PAMP_{2000}$ compositions. NAD(P) H-dependent dehydrogenase enzymes in metabolically active cells can cause a reduction of the MTS tetrazolium compound and produce the colorful formazan product that is soluble in the cell culture medium. Since living cells can interact with the MTS tetrazolium compound and turn it into a colored formazan product, there will be a significant increase in color intensity, which can be easily measured by measuring absorbance at 490-500 nm. The cell viability of longer PEG brush containing carriers obtained by MTS assay was presented in ***Figure 4.22.*** The problem has shown that despite there is Dox with high concentration there is still 60% or higher cells are alive which is not possible in literature. The reason why there is that much high viability is the overlapping with the absorption of MTS tetrazolium solution and Dox, resazurin assay (Alamar blue assay) was also used to determine cell viability since the absorbance of generated resorufin is at a different region (Ex=530-570 nm, Em=590-620 nm) and does not overlap with the absorption of Dox.

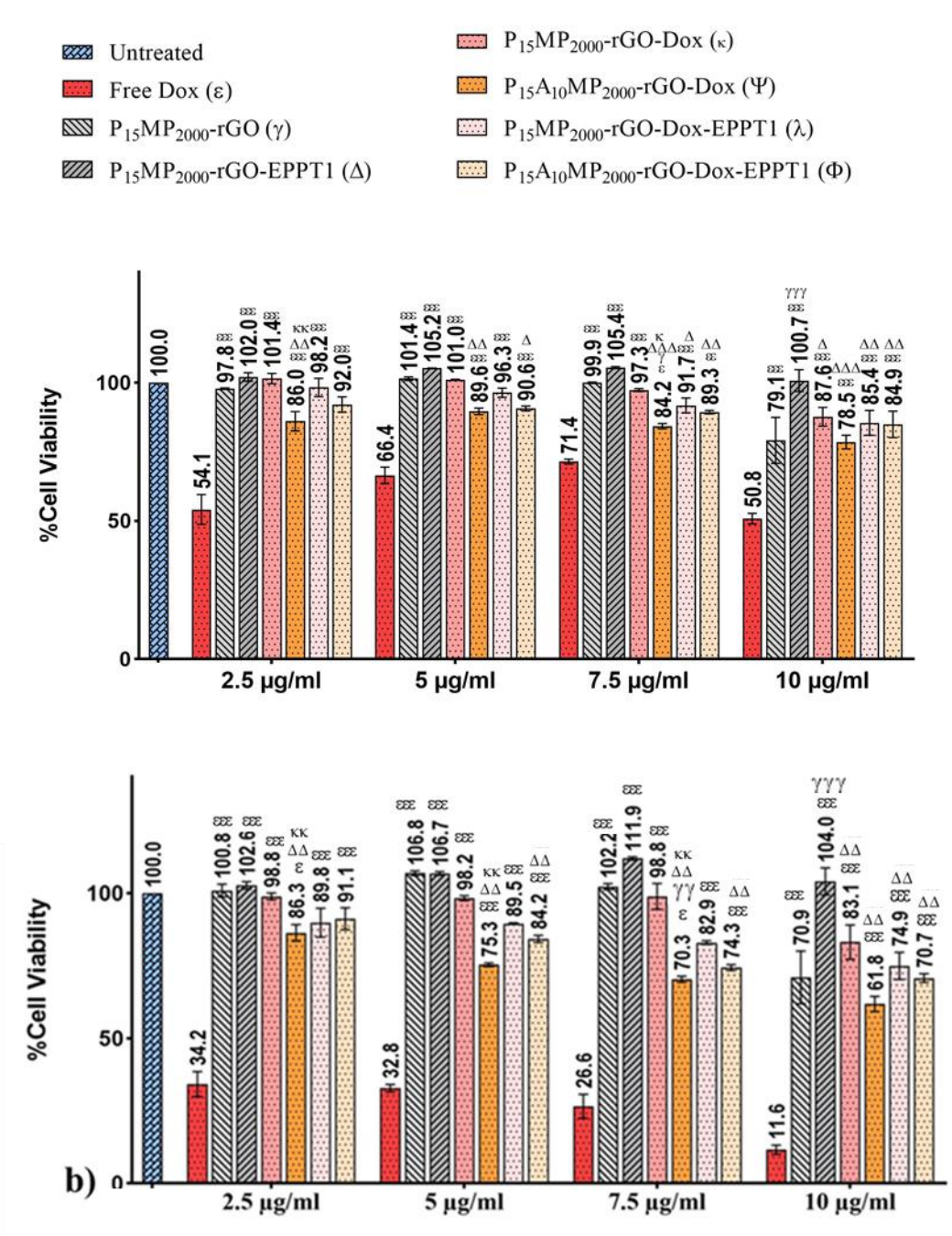


Figure 4.22 MTS assay analysis of $(P_{15}A_{10}MP)_{2000}$ derivatives on MDA-MB-231cancer cell line at **a)** 24h and **b)** 48h. Assigned symbols to concentration levels were used to report comparison results between different compounds at the same concentrations and same time points. Symbols that are assigned to each compound denote $p \leq 0.05$ for one symbol, $p \leq 0.01$ for two symbols, and $p \leq 0.001$ for three symbols.

4.7.2. Resazurin Assay

After 24 and 48h incubation with Dox and Dox carrying different compositions, results demonstrated that $PAMP_{2000}$ coated derivatives show a concentration and time-dependent cell viability profile at MCF-7 breast cancer cell line ***(Figure 4.23).*** The empty carriers ($(P_{15}A_{10}MP)_{2000}$-rGO-EPPT1 and $(P_{15}A_{10}MP)_{2000}$-rGO-EPPT1) did not show any reduction in cell viability, on the contrary, they showed the cell proliferation indicating the biocompatibility of the carrier [98] Dox amount in the Dox carrying targeted and non-targeted carriers were tunes as having the same amount such as 2.5, 5, 7.5, and 10 µg/µl. Accelerated release performance of azide containing non targeted azide containing $(P_{15}A_{10}MP)_{2000}$-rGO-Dox showed lower cell viability comparing the $(P_{15}MP)_{2000}$-rGO-Dox for 24 h by reflecting the release behavior. Azide group-containing $(P_{15}A_{10}MP)_{2000}$-rGO-Dox killed more cancer cells than analog that does not contain azide groups for all concentration values. Once EPPT1 conjugated on the carrier, as mentioned before it slows down the release, and the differences in cell viability were not clear for 24h time point ***(Figure 4.23a)*** As it was showed in the drug release profile data, EPPT1 targeted carrier with or without azide, release more Dox for 48h which starts showing time and dose-dependent release for 2.5, 5, and 7.5 µg/µl by killing almost 75% of the cancer cells ***(Figure 4.23b)***.

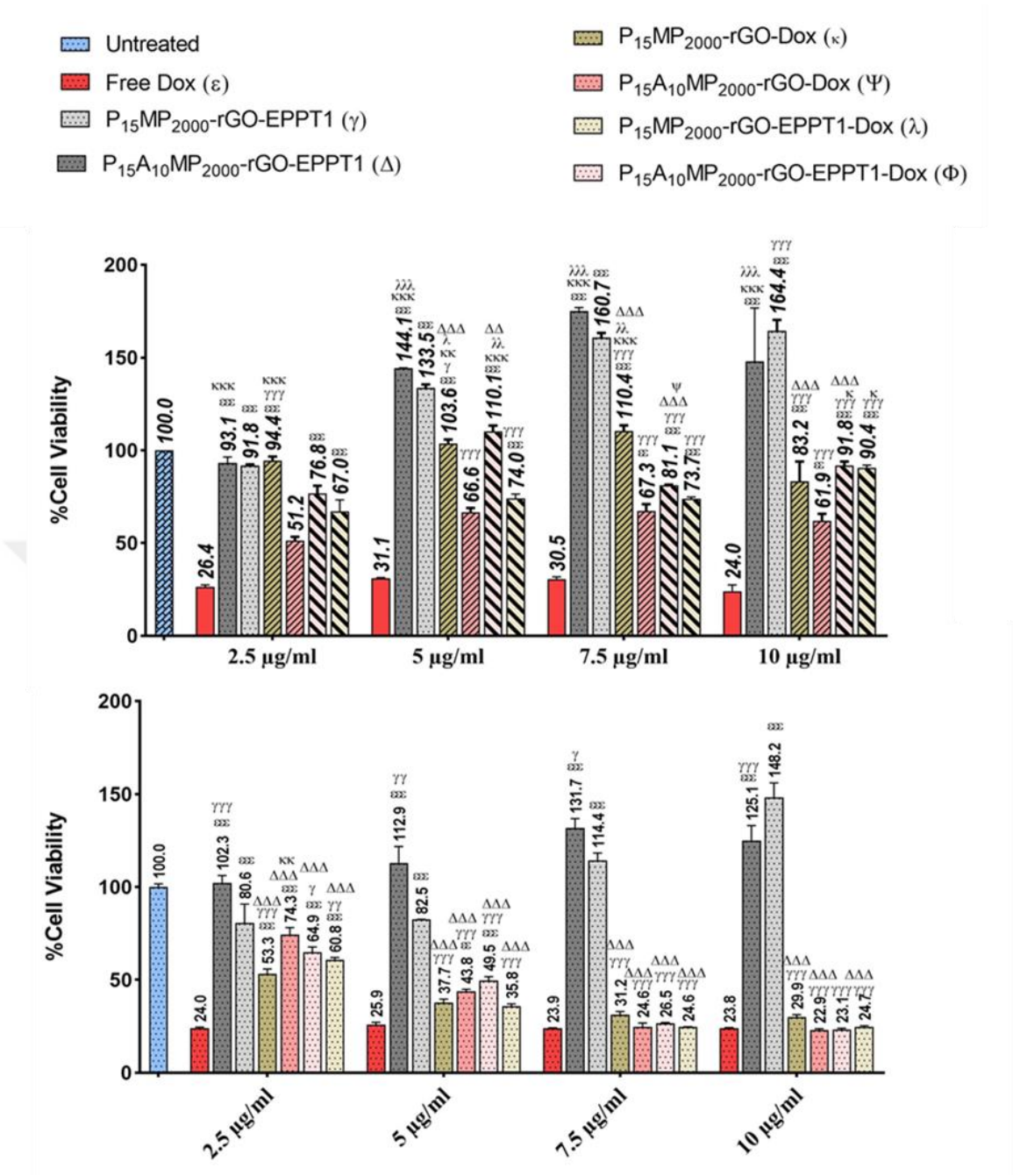


Figure 4.23: Resazurin assay analysis of $(P_{15}A_{10}MP)_{2000}$ derivatives on MCF-7 cancer cell line at **a)** 24h and **b)** 48h. Assigned symbols to concentration levels were used to report comparison results between different compounds at the same concentrations and same time points. Symbols that are assigned to each compound denote $p \leq 0.05$ for one symbol, $p \leq 0.01$ for two symbols, and $p \leq 0.001$ for three symbols.

Since PEG_{500} containing PAMP copolymer compositions are not able to effectively disperse in the water, reduction on the cell viability wasn't able to measure as clear as PEG_{2000} containing compositions however a trend that is proportional with drug release profile was able to observe. The empty carrier did not create significant cytotoxicity at any compositions (***Figure 4.24a-b)***. $(P_{26}A_{10}MP)_{500}$-rGO-Dox used to release more drugs than $(P_{26}MP)_{500}$-rGO-Dox within the same time frame which resulted in better anticancer activity by killing more cancer cells (≈60%), especially after 48 h incubation (***Figure 4.24b)***. Similarly, targeted nanocarrier with shorter PEG brush reflected the behavior that was obtained during drug release. The differences in the cell viability of the azide containing and non-containing targeted carrier became more visible for 48 h because $(P_{26}A_{16}MP)_{500}$-rGO-Dox-EPPT1 was faster than $(P_{26}MP)_{500}$-rGO-Dox-EPPT1 for this time point ***(Figure 4.24).***

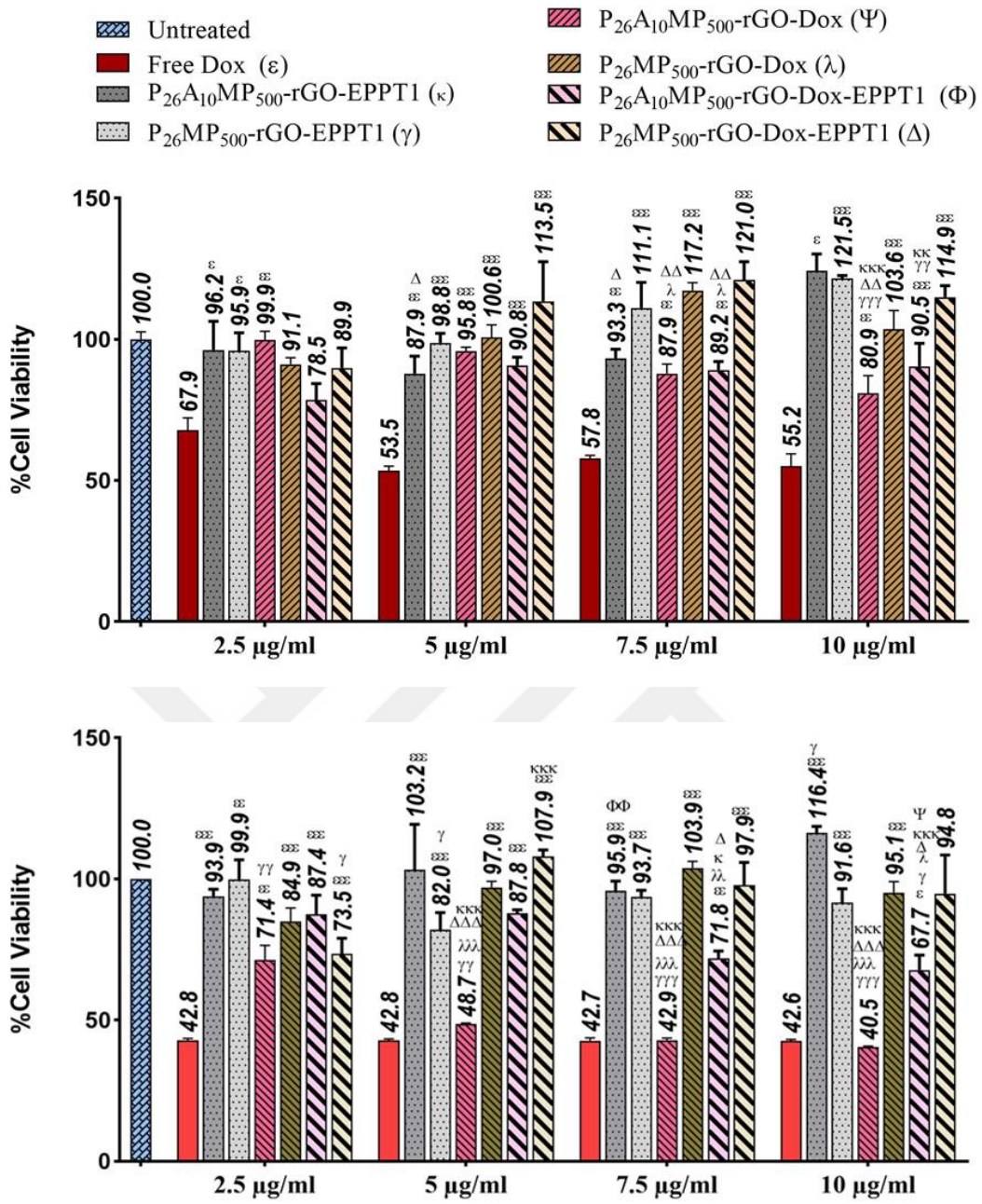


Figure 4.24: Resazurin assay analysis of $(P_{26}A_{10}MP)_{2000}$ derivatives on MCF-7 cell line at **a)** 24h and **b)** 48h. Assigned symbols to concentration levels were used to report comparison results between different compounds at the same concentrations and same time points. Symbols that are assigned to each compound denote $p \leq 0.05$ for one symbol, $p \leq 0.01$ for two symbols, and $p \leq 0.001$ for three symbols.

4.7.3. Investigation of Selective Cellular Entry of Biocompatible Targeted and Non-Targeted GO Based Nano platform.

It is expected that EPPT1 conjugated targeted nanocarrier can selectively accumulate into uMUC receptor overexpressed breast cancer cell lines such as MCF-7 and MDA-MB-231. Cellular uptake comparison of the targeted and non-targeted carrier was done on the MCF-7 cancer cell line using confocal microscopy imaging and flow cytometer analysis on MDA-MB-231.

4.7.3.1. Confocal Microscopy Imaging of Cellular Entry of Targeting Nanocarriers

The cellular uptake and intracellular localization of Dox, $(P_{15}MP)_{2000}$-rGO-Dox, and $(P_{15}MP)_{2000}$-rGO-EPPT1-Dox were initially investigated by confocal laser scanning microscopy. Since the important thing is having targeting agents on the carrier and the amount of Dox release is very similar for an early time point, these compositions were used for this study instead of the most effective one. Cellular entry was followed through Dox fluorescence intensity which represented as red in the picture where the nucleus was colored as blue using Heucst **(*Figure 4.25*)** Free Dox as a small drug molecule can pass the cell membrane through diffusion and accumulate into the nucleus over time that can be clearly seen in the first raw of the ***Figure 4.29***, especially in the merged picture. Once targeted $(P_{15}MP)_{2000}$-rGO-EPPT1-Dox and non-targeted $(P_{15}MP)_{2000}$-rGO-Dox compositions were compared, enhanced uptake of targeted composition was evidenced by increased fluorescence intensity of Dox in the cell.

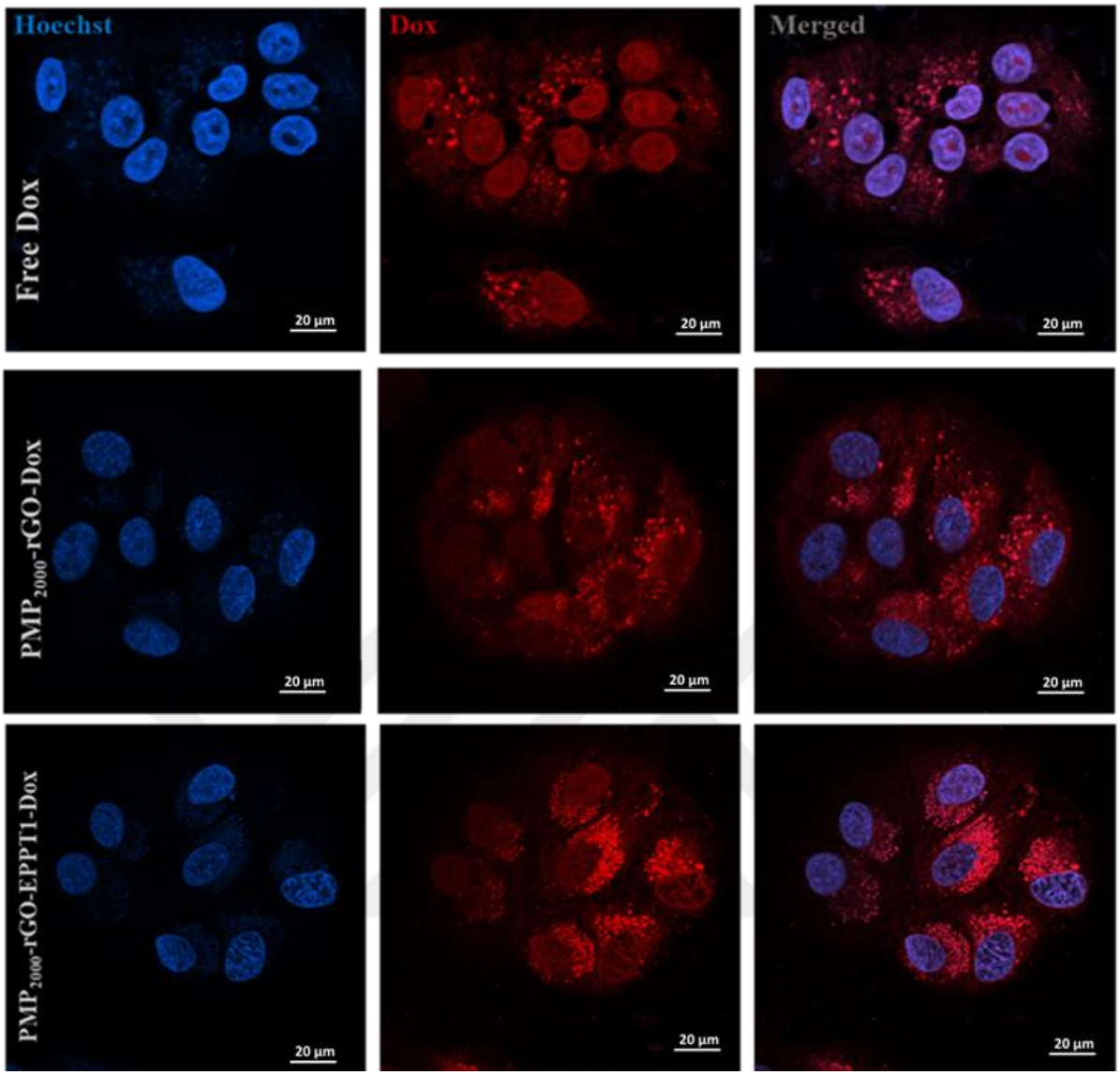


Figure 4.25: Cellular uptake analysis of $P_{15}MP_{2000}$-rGO-Dox and $P_{15}MP_{2000}$-rGO-EPPT1-Dox with MCF-7

4.7.3.2. Flow Cytometry Analysis of Cellular Entry of Targeted Nanocarrier

In addition to confocal microscopy imaging, flow cytometer analysis was also be done for quantitative analysis of cellular uptake. Similarly, counting was performed based on Dox intensity for free Dox, targeted ($(P_{15}MP)_{2000}$-rGO-EPPT1-Dox) and non-targeted ($(P_{15}MP)_{2000}$-rGO-Dox) nanocarriers. ***Figure 4.26*** shows that more number of the cell has Dox in case of free Dox sample and followed by the targeted rGO nanocarrier which clearly has more incidence than non-targeted versions based on carried Dox intensity. The untreated cell is used as a negative control. Results clearly supported the confocal

microscopy imaging experiment and showed that EPPT1 conjugated targeted drug-carrying nanoplatform has a better ability for cellular internalization.

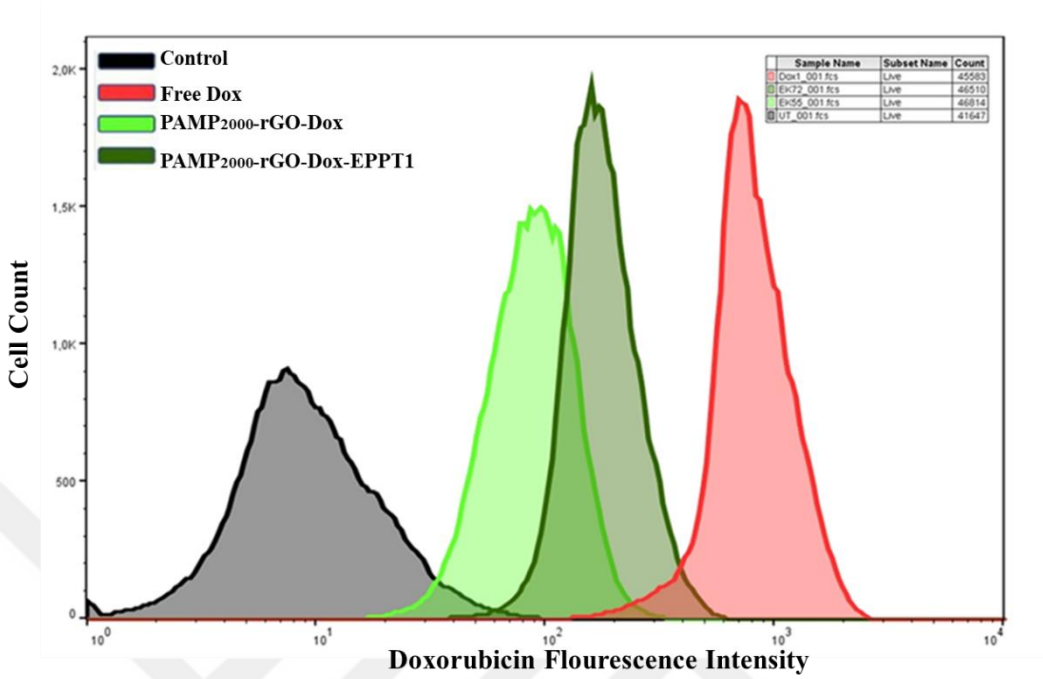


Figure 4.26: FACS analysis results of targeted $PAMP_{2000}$-rGO-Dox-EPPT1, non-targeted $PAMP_{2000}$-rGO-Dox nanoplatforms, and Free-Dox

CHAPTER 5

5. DISCUSSION

5.1. Synthesis and Characterization of Targeted Drug Carrier

The wide surface area of graphene oxide can be used for drug interaction however dose, shape, and time-dependent toxicity of graphene oxide needs to be addressed for a biocompatible drug carrier system. To address this concern; we have reported the efficient PEGylation method to improve biocompatibility and stability of graphene derivates. Multiple pyrene groups on copolymer P(PEGMA-*co*-MMA-*co*-PMA) were coated on rGO with the coating efficiency ranging between 58.8 % and 71.2 %. Instead of the more defected area and the more functional group-containing GO, simultaneous PEGylation and, reduction of the GO were performed to get efficiently PEGylated rGO nano platform which shows high hemocompatibility and low cytotoxicity. Two different PEG lengths (PEG 500 g/mol and PEG 2000 g/mol) were scanned to decide which is the best composition from the point of dispersibility and stability in aqueous systems. In-vitro studies such as MTS, LDH, and ROS, also demonstrate that longer PEG brush with the 2000 g/mol molecular weight and 80% PEG monomer content is the best composition which could be performed to the HEK-293T and MRC-5 cells with 150 μg/ mL concentration.

One of the tools the published method provides us was to obtain a functional PEGylated graphene surface using a functional copolymer by applying the same process[92]. As long as coated polymer has multiple pyrenes and PEGMA brushes, it can be expected that it will be coated on the graphene surface with enhanced biocompatibility. If this copolymer has another monomer including the desired functionality, the coated graphene surface with this copolymer will have the same functionality. By taking advantage of this method, azide functional monomer was included in pyrene and PEGMA containing monomer to obtain P(PEGMA-*co*-AzPMA-*co*-MMA-*co*-PMA) copolymer that can be further functionalized with targeting agent for cell-specific uptake. As Zhao and his collages demonstrate that PEGMA groups with a different molecular weight contribute to

biocompatibility[99]. However, biocompatibility might not be the only parameter that can be affected by the length of the PEGMA chain. Drug loading capacity and releasing profile might also be affected by the PEGMA chain length which is one of the parameters that is going to investigate in this study. Moreover, initially, the AzPMA monomer was just a tool for functionalization via CuAAC click reaction, but it was found that monomer charge transforming ability depends on the pH of the environment and contributes to the drug release of carriers. Novel copolymer with all these monomers contributes to features of the drug carrier such as drug loading and selectively release profile, targeting ability, and biocompatibility.

Due to the six-membered carbon ring structure, carbon nanomaterials have shown extraordinary ability in the drug delivery field for several years, which allows π-π interactions of drugs with aromatic rings and hydrophobic interactions [100]. This interaction has been effectively used between the multiple pyrene groups containing copolymer and GO surface which is a water-soluble derivate of graphene [92]. The study set the minimum requirements for the number of pyrene and PEG brushes to enhance biocompatibility. Moreover, it was paved the way for the functionalization of the surface of the rGO using the functional copolymer that could have been obtained just by the incorporation of a functional monomer in the copolymer structure. To obtain the desired functional copolymer, azide functional monomer was introduced to a copolymer structure that was already had the three monomers namely, PMA, PEGMA, and MMA with their responsibility in the copolymer structure. PMA monomer was used to enhance the interaction between copolymer and GO nanoplates. Zhang and coworkers indicated that ~55pN energy was required for picking up pyrene bearing PEG composition from GO were measured by TEM [101]. It shows that π-π is a strong interaction between the pyrene group and GO. PEGMA macromonomer is used as a water-soluble polymer chain to enhance solubility and biocompatibility of the coated surface. Different chain length allows us to tune the PEG content at the surface without increasing molecular weight of the copolymer. MMA monomer was used as a chain extender with a similar backbone structure with other monomers. A newly added AzPMA monomer was used for further functionalization through the “click” reaction.

By π-π stacking interaction with PAMP copolymer with the molecular weight are 500 and 2000 g/mol and reduced graphene oxide biocompatible PAMP-rGO was obtained with a better dispersibility characteristic in an aqueous environment. It is seen that PAMP-

rGO compositions consist of an averagely 60% copolymer by mass-based on TGA analysis. From AFM, SEM-EDX, and TEM results it is significantly observed that copolymers make a difference in the morphological structure of bare GO.

EPPT1 is a purchased peptide that is used as a targeting ligand against underglycosylated MUC1 (uMUC1) receptors overexpressed on the membrane surface of metastatic breast cancer cells [102]. The targeting delivery system was designed for the cargo the therapeutics with high yield through the breast cancer cells by receptor-mediated endosomal cell entrance mechanism. Delivery of therapeutic on the targeted region is crucial for minimizing the side effects on healthy tissue and treat the cancer region. Conjugation between azide groups on PAMP copolymer and Alkyne-PEG-EPPT1 molecule gives a targeting future to the carrier. Not only the absence of characteristic azide group at 2100 cm^{-1} in but also Ellman's assay results demonstrate the covalently bonding with a high yield around up to 98%. Even though "click" reactions are highly efficient reactions, the almost quantitative reaction yield at the surface indicates that there is a possibility to have peptide-graphene interaction which is well known in the literature [96]. It is important to mention that azide functionality in the copolymer was initially just a tool for further functionalization. However, preliminary data showed that its ionic structure might affect the drug release profile. It was thought that the effect of azide group on the carrier's activity needs to be investigated since it hasn`t been studied before in the literature. Therefore, to be able to investigate the effect of the azide groups on cytotoxicity, cellular uptake, and drug release profile at the physiological and acidic environment, unused azide groups in the copolymer either left as it is or capped with propargyl alcohol.

Dox is an ionic and hydrophobic molecule that is a widely used chemotherapy agent. The mechanism of the Dox was proposed is generally works through the DNA disrupting gene expression, generating reactive oxygen species [103]. Dox has been formed in a different DDS in literature, especially liposomal form the Doxil that has the FDA approval. In order to improve its therapeutic impact with efficacy and safety for cancer therapy, drug carrier design should be considered. Dox was loaded on the PAMP-rGO-EPPT1 as the final step of the targeted drug delivery system to obtain PAMP-rGO-EPPT1-Dox. Knowing the amount of the drug-loaded on the carrier is very important to tune the different components in a comparable way during the investigation of the drug release profile. When Dox loading was performed as the last step, the loaded Dox amount can be

easily calculated using the remaining Dox concentration in the supernatant which made this step more favorable for the study. However, it is also possible to load Dox right after PAMP coating to have non-targeted PAMP-rGO-Dox and follow with EPPT1 conjugation as the last step (PAMP-rGO-Dox-EPPT1). In this study, the effect of a different order of drug loading or peptide conjugation on the drug release profile was also investigated. Both drug loading order gives the therapeutics loading is able to reach 98% Dox loading yield on an empty carrier by non-covalent bonding and interactions. Calculated Dox loading efficiency results were clearly showed that the length of the PEG brush does not have an effect on loading efficiency. On the other hand, the temperature and pH of the solvent used in the drug loading reaction were the parameters that effected the loading efficiency.

The order of the drug loading on the carrier was investigated in terms of the effect on drug release profile and cell viability behavior. In addition to PAMP-rGO-EPPT1-Dox, PAMP-rGO nanocarrier was first loaded with Dox and then EPPT1 peptide conjugated to obtain PAMP-rGO-Dox-EPPT1. These compositions were investigated to understand the effect of the peptide conjugation order on the drug release profile and morphology of nanoplatforms. Regardless of Dox loading order whether before peptide conjugation or after peptide conjugation, high drug loading efficiency was obtained at 37ºC compared to room temperature because of the enhanced noncovalent interactions. This also indicates that the presence of the peptide at the graphene surface does not have an effect on drug loading. However, our results will show that it will have an effect on Dox release for some composition in which the amount of the EPPT1 by mass gets increase comparing to PEG. Morphological analysis is done by the AFM which allows an understanding of the additional layer on increased thickness.

Copolymer, EPPT1, and Dox addition on the rGO surface were additionally investigated through SEM imaging along with EDAX analysis. Furthermore, Raman spectroscopy is one of the specific characterization ways for the graphene derivative carrier and was used to confirm Dox loading, as well as different coating steps of the carriers. Besides the morphological change in every step that clearly indicates related modification, elemental mapping through EDAX gave further proof about Dox loading and peptide conjugation. The reduction of graphene removes the oxygen-containing groups from the surface, as a result, the atomic oxygen percentage in the rGO decreased to 11.28% from 37.97%. rGO showed N content as a result of hydrazine treatment for reduction. Since rGO surface

modification will take some further steps before obtaining the final product, the remaining hydrazine will be washed out from the system in each step and will not cause specific toxicity associated with it. The comparison of rGO and $(P_{15}A_{10}MP)_{2000}$-rGO also showed how N content getting a decrease in each step even though the conjugated component has the N on it. When Dox loading is achieved N content increase further by indicating Dox loading which has a single N per molecules. At the last step, successful conjugation of EPPT1 even further increased the nitrogen percentage owing to the amino groups of the amino acids.

The size of the drug carriers is an important parameter and measuring the size of the graphene-based drug delivery system has its challenge because of the graphene sheets.Overall DLS results indicate that nanocarriers are not equally measured but typically PEG with 2000 g/mol molecular weight containing PAMP copolymer coated compositions are more stable in water, PBS, and medium conditions. DLS measurements showed that final compositions that contain 2000 g/mol PEG brushes resulted in a smaller size than 500 g/mol PEG containing analogs. All final composition that has peptide and drug on the surface resulted in the size smaller than 350 nm which can be accepted as good enough for penetration and accumulation in tumor tissue through an enhanced permeability and retention (EPR) effect [104]. It should be also noted that the shape of the graphene might not allow the obtain best size information using DLS. Additionally, TEM was used as another imaging technique to visualize the functional graphene layers.

Surface charge of the carriers as important as their size and it is one of the important futures to have stable nanocarrier in the physiological condition. $(PMP)_{2000}$-rGO-EPPT1 shoed higher negative surface charge value with the contribution of both PEG chains and EPPT1 peptide. Non targeted drug-loaded $(PMP)_{2000}$-rGO-Dox composition exhibited less negative surface charge due to positively charged Dox. When final targeted compositions containing with and without azide group were measured, the results showed that negatively charged value decreases. This might be an indication of an interaction of peptide and Dox in terms of charge neutralization. A similar trend was observed for a shorter PEG chain containing compositions.

5.2 Drug release Profiles of Dox Loaded Targeted and non-targeted Nanocarriers

The synthesized carrier has components that might influence its performance. For instance, PEG brush length might affect the release rate even though it did not affect the drug loading capacity. Similarly, the presence of the EPPT1 peptide on the surface might serve as an additional coating layer or a component that changes the charge and lipophilicity of the surface. More importantly, the ionic azide group might affect the Dox release since Dox becomes positively charged in the acidic environment. Besides the existence of these components in the carrier, the order of how they exist might also affect the performance of the carrier. In this thesis, all these parameters and their synthetic order were investigated in terms of how they affect the release behavior of the rGO nanoplatform where all these components build on. Moreover, it was investigated that can any of these components be a tool to accelerate the drug release on rGO surface. Generally, all designed carriers showed pH-dependent release by accelerating at acidic pH.

Once the release profile of PAMP-rGO-Dox and PMP-rGO-Dox were compared, results clearly showed that existing of azide groups on the surface accelerates the Dox release since Dox becomes positive in the acidic environment. Dox mainly interacts with GO through π-π stacking and hydrogen bonding. In the proposed system GO was chemically reduced to rGO having a less functional group for hydrogen bonding. In the acidic environment, hydrogen bonds get weaken and the release of Dox gets accelerated. Dox release can take place more efficiently from the GO surface than the rGO surface because of the interaction type. Several examples in the literature that used rGO as a graphene-based platform yielded around %30 cumulative releases over time indicating that most of the Dox still retains on the graphene surface due to the relatively stronger π-π interaction [105,106] Some researcher used external stimuli to increase drug release from rGO surface such as laser radiation [107] and introducing small molecules on the surface that changes the hydrophilicity of the surface [108]. The quantity of the drug release differences between azide containing and capped compositions decreases once the number of azide group decreases in the structure. Data supported that azide groups can

be a tool for both functionalization and acceleration of the drug release without any external stimuli.

Before introducing the peptide into the scenario, the density of the PEG effect on drug release was investigated. The density of PEG on the rGO surface can be tune both PEG brush length and the number of the brushes. For example, a higher number of shorter brushes can create a similar effect with a lower number of longer brushes. Moreover, just the number of brushes with the same length might also affect the release rate since it changes the PEG density on the rGO surface. To be able to compare these, firstly, the copolymers coated on the rGO were selected with differed PEG length with a similar number of brushes including a similar number of azide groups. Although the drug release % difference is not significant, it raised the question of how the number of brushes for the same brush length containing copolymer might change the drug release. The results show that the composition which has less number of brush showed an accelerated profile even though it has fewer azide groups indicating the release rate affected by the density of the PEG content.

As the next step EPPT1 peptide was conjugated onto PAMP coated, Dox loaded rGO surface through azide groups via “click” chemistry. The peptide has a lipophilic structure with both hydrophilic and hydrophobic amino acids. Even though it is covalently conjugated to rGO surface, the pending side of the chain can also interact with rGO surface via suitable amino acid and act as an additional layer. The effect of the presence of peptide groups decreases the drug release rate. EPPT1 peptide acts as an additional layer on already loaded Dox on the rGO surface for this case. However, peptide conjugated surfaces most of the time can increase the H bonding interaction and allows Dox to be more readily available in the case of pH change [109]. Therefore, the order of EPPT1 conjugation (or order of Dox loading) needs to be investigated as the next step to find whether it affects the rate of the release. When Dox was loaded as the last step, the release was accelerated however if Dox was loaded before peptide conjugation there is no significant difference between azide containing or azide absence one. Collectively our results showed that when Dox loading was performed as the last step during preparation of the targeted rGO based carrier, the drug release profile gives the better release. As mentioned before, this might be because of the increased chance of Dox making H bonding with the modified rGO surface with the help of peptide on the surface. Moreover, the presence of the azide group accelerated the release even though peptide conjugation

decreases for longer PEG brush containing compositions. Besides, shorter PEG brush containing compositions do not always obey this trend. The order of EPPT1 peptide conjugation and Dox loading was further investigated for shorter PEG (500 g/mol) brush containing compositions. Azide capped version responded to the order of the Dox loading by slowing down the Dox release once Dox loading followed by EPPT1 conjugation.

5.3 In-Vitro Experiments

The results of detailed drug release studies showed that the targeted platform showed a better release profile if it is having azide groups and Dox loading is performed after EPPT1 conjugation for denser PEGylated surface which shows better biocompatibility based on our previously published study [92]. As the next step, best composition and their precursors as control (to understand its behavior better) were used as a drug carrier to investigate the anticancer activity on breast cancer cells such as the MCF-7 line which is progesterone receptor-positive (PR), estrogen receptor (ER) positive and human epidermal growth factor receptor 2 (HER2) negative and, MDA-MB-231 line as a triple-negative cell line. Additionally, MDA-MB-231 and MCF-7 epithelial cancer cell lines have known as they show intermediate MUC1 expression when they compared with investigated 12 different cell lines [110]. It was revealed by the immunocytochemistry result the overexpression of the MUC1 receptor is more present at MCF-7 than MDA-MB-231 breast cancer cell lines. Because of that MCF-7 was chosen for the rest of the in-vitro experiments owing to the targeting EPPT1 peptide.

First of all MTS assay was performed. Interestingly results showed that none of the carriers shows dose-dependent anticancer activities. Even at higher Dox concentrations for 48h, 60% of the cancer cells are still alive. Even though MTS assay is one of the commonly used assays and has examples used for Dox carrier graphene derivatives, the absorption of the formazan product and the absorption of Dox loaded on the rGO are overlapped and this overlap might create misinterpretation and cell viability can be measured higher than its actual value[99].

Thus, to determine the cytotoxicity and biocompatibility of the nanocarriers, free Dox, PAMP-rGO-EPPT1, PMP-rGO-EPPT1 empty carriers, PAMP/PMP-rGO-DOX non-targeted drug carriers and PAMP/PMP-rGO-EPPT1-Dox targeted drug carriers were

assessed in the cell viability experiments by Resazurin Assay at 24th and 48th hours of interaction with MCF-7 cancer cell line. Concentration and time-dependent toxicity were reflected by the reduction of cell viabilities when the Dox concentration in carriers was set to four different concentrations 2.5, 5, 7.5, and 10 μg/μl. $(P_{15}A_{10}MP)_{2000}$-rGO-EPPT1 and $(P_{15}A_{10}MP)_{2000}$-rGO-EPPT1 as the empty carriers are not cytotoxic by themselves. After 24h $(P_{15}A_{10}MP)_{2000}$-rGO-Dox administered MCF-7 cells showed lower cell viability comparing the $(P_{15}MP)_{2000}$-rGO-Dox because drug release accelerates in the presence of azide group. EPPT1 conjugation on the carrier slows down the release, and the differences in cell viability were not clear for 24h interaction between cells. EPPT1 targeted carrier with or without azide, released more Dox for 48h which starts showing time and dose-dependent release.

The dispersibility problem of the PEG_{500} containing PAMP copolymer coated compositions in the water did not allow to measure the cell viability as clear as PEG_{2000} containing compositions however a trend that is proportional to the drug release profile was able to observe. As same as the longer PEG brush containing copolymer compositions, $(P_{26}A_{10}MP)_{500}$-rGO-Dox used to release more drugs than $(P_{26}MP)_{500}$-rGO-Dox within the same time frame which resulted in better anticancer activity.

The $(P_{15}MP)_{2000}$-rGO-Dox-EPPT1 composition and its derivates have been chosen as a targeted and $(P_{15}MP)_{2000}$-rGO-Dox non-targeted composition for the final *in-vitro* studies to understand the cellular uptake ability. In regular cell culture practice, longer incubation time does not allow to observe selectivity of the targeting agent since it gets saturated over time and both conditions reach the max internalization. Once cells are incubated with targeted and non-targeted composition for a short period of time, the targeted composition will have a better chance to internalize and create a more therapeutic effect. To confirm the targeted ability of EPPT1 peptide Confocal images were used after 4 hours of incubation period and Dox intensity in the nucleus was observed as an indicator. As a result after 4 hours of interaction with cancer cells, higher fluorescence intensity was observed for targeted than non-targeted one at the nucleus,. It is declared that EPPT1 conjugation is able to recognize the uMUC1 receptors which are overexpressed at cancer cells and binding to the cellular membrane which causes the expected receptor-mediated endocytosis and higher cellular uptake ability. Qualitatively, it is observed by the confocal images, thus quantitatively by flow cytometry analysis established that EPPT1 containing drug carrier is able to enter the cellular membrane more than non-targeted one. EPPT1

containing composition was imaged with dark green and light green is non targeted one. It was shown that 4 hours of incubation non-targeted and targeted compositions with MCF-7 cancer cells resulted in Dox fluorescence on cells. FACS discriminates the cell depends on the Dox fluorescence of live and dead cells assuming that the targeted one will internalize more and will show higher intensity. Confocal images and FACS results promote the fact that targeted PAMP coated Dox loaded nanoparticle is selectively effective to the damage on cancer cells. As the latest research, Quagliarini and her collages also demonstrate that although there is some limitation comes from the GO, GO-based DDS is able to cargo free Dox through the nucleus by attaching to the membrane if CF-7 and MDA-MB-231 cells [111]. Collectively our results supported that the obtained system has already overcome the problems that come from GO by effective PEGylation and higher targeting ability by EPPT1 peptide with tunable drug release profile.

CHAPTER 6

6. CONCLUSIONS AND FUTURE WORK

For the efficient nanoparticle design and applications which are carrying materials to the next step for the scalable production, synthesis and characterization design should be consistent and well-defined chemical reactions. Our system contains novel PAMP copolymers that were synthesized by ATRP controlled polymerization which is used to regulate and fix the number of monomers or its ratio. Besides, the optimized drug loading step in moderate conditions with high loading efficiency is practical for commercially obtaining PAMP-coated biocompatible GO-based nanocarrier. Almost 96% of Dox therapeutics loading efficiency has been reached by pi-pi interaction between sp^2 hybridized carbon atoms on rGO. Additionally, overexpressed MUC1 receptor-mediated endosomal cellular uptake has been designed for effective therapeutics cargo through the cell nucleus. Morphological analysis of Dox loaded and empty GO-based carriers have been promoted by AFM, TEM, SEM, Raman spectroscopy, DLS, and Zeta analysis. All results demonstrated that optimization of the best targeted GO-based nanocarriers relevant to the EPPT1 conjugation order before or after the drug loading. The pH-dependent drug release property was investigated by drug release experiments. It was seen that at physiological pH 7.4 is only cause drug release up to %15 as it is desired to become effective DDS. Components like PEG brushes, ionic azide groups, and EPPT1 on the surface were investigated in terms of how they affect the drug release behavior of the carrier.

Azide functionality increased the drug release percentage because of the ionic charge exchange which prompts the Dox release from the rGO surface at both $PAMP_{500}$ and $PAMP_{2000}$ coated non targeted carriers. In the case of PAMP-rGO-EPPT1-Dox functionality is observed that the impact on the drug release caused by azide functionality has suppressed by EPPT1 peptide sterically at PEG_{500} and PEG_{2000} compositions. Additively, the suppression is observed higher on PEG_{2000} containing one than PEG_{500} containing one. Cellular uptake and cell viability results indicate that the EPPT1 conjugated targeted carrier is biocompatible and drug-carrying capacity is tunable. Those

results show that $(PAMP)_{2000}$-rGO-EPPT1-Dox can be effective for further treatment. As a future plan, this optimized rGO based carrier will be used as a dual drug delivery system by introducing gene delivery modality on it. Our result showed that ionic groups increase the drug release rate. Artificial vectors for gene delivery have a positive charge that might accelerate the drug release and tune to the required time for the effective knockdown of the gene.

CHAPTER 7

7. BIBLIOGRAPHY

[1] H. P. Boehm, A. Clauss, G. Fischer, and U. Hoffman, “Surface Properties of Extremely thin Graphite Lamellae,” in *Proceedings of the Fifth Conference on Carbon*, 1962.

[2] C. Lee, X. Wei, J. W. Kysar, and J. Hone, “Measurement of the elastic properties and intrinsic strength of monolayer graphene,” *Science (80-.).*, 2008.

[3] A. A. Balandin *et al.*, “Superior thermal conductivity of single-layer graphene,” *Nano Lett.*, 2008.

[4] A. Peigney, C. Laurent, E. Flahaut, R. R. Bacsa, and A. Rousset, “Specific surface area of carbon nanotubes and bundles of carbon nanotubes,” *Carbon N. Y.*, 2001.

[5] L. Staudenmaier, “Verfahren zur Darstellung der Graphitsäure,” *Berichte der Dtsch. Chem. Gesellschaft*, 1898.

[6] N. A. Savostianova *et al.*, “Third harmonic generation from graphene lying on different substrates: optical-phonon resonances and interference effects " Third harmonic generation in graphene and few-layer graphite films,” *Phys. Rev. B Phys. Rev. X Prog. Electromag. Res. Opt. EXPRESS*, 2013.

[7] Y. Si and E. T. Samulski, “Synthesis of water soluble graphene,” *Nano Lett.*, 2008.

[8] K. Yang, L. Feng, H. Hong, W. Cai, and Z. Liu, “Preparation and functionalization of graphene nanocomposites for biomedical applications,” *Nat. Protoc.*, vol. 8, no. 12, pp. 2392–2403, 2013.

[9] Z. Liu, J. T. Robinson, X. Sun, and H. Dai, “PEGylated nanographene oxide for delivery of water-insoluble cancer drugs,” *J. Am. Chem. Soc.*, vol. 130, no. 33, pp. 10876–10877, 2008.

[10] D. R. Dreyer, A. D. Todd, and C. W. Bielawski, “Harnessing the chemistry of graphene oxide,” *Chem. Soc. Rev.*, vol. 43, no. 15, pp. 5288–5301, 2014.

[11] J. Chen, B. Yao, C. Li, and G. Shi, “An improved Hummers method for eco-friendly synthesis of graphene oxide,” *Carbon N. Y.*, 2013.

[12] J. Liu, L. Cui, and D. Losic, “Graphene and graphene oxide as new nanocarriers for drug delivery applications,” *Acta Biomater.*, vol. 9, no. 12, pp. 9243–9257, 2013.

[13] J. Liu, W. Yang, L. Tao, D. Li, C. Boyer, and T. P. Davis, “Thermosensitive graphene nanocomposites formed using pyrene-terminal polymers made by RAFT polymerization,” *J. Polym. Sci. Part A Polym. Chem.*, 2010.

[14] J. Liu *et al.*, “Synthesis, characterization, and multilayer assembly of pH sensitive graphene-polymer nanocomposites,” *Langmuir*, vol. 26, no. 12, pp. 10068–10075, 2010.

[15] V. Palmieri, G. Perini, M. De Spirito, and M. Papi, “Graphene oxide touches blood:: In vivo interactions of bio-coronated 2D materials,” *Nanoscale Horizons*, vol. 4, no. 2, pp. 464–471, 2019.

[16] J. S. Suk, Q. Xu, N. Kim, J. Hanes, and L. M. Ensign, “PEGylation as a strategy for improving nanoparticle-based drug and gene delivery,” *Adv. Drug Deliv. Rev.*, vol. 99, pp. 28–51, 2016.

[17] A. L. Klibanov, K. Maruyama, V. P. Torchilin, and L. Huang, “Amphipathic polyethyleneglycols effectively prolong the circulation time of liposomes,” *FEBS Lett.*, 1990.

[18] A. N. Banerjee, “Graphene and its derivatives as biomedical materials: Future prospects and challenges,” *Interface Focus*, vol. 8, no. 3, 2018.

[19] K. Yang, S. Zhang, G. Zhang, X. Sun, S. T. Lee, and Z. Liu, “Graphene in mice: Ultrahigh in vivo tumor uptake and efficient photothermal therapy,” *Nano Lett.*, vol. 10, no. 9, pp. 3318–3323, 2010.

[20] Y. Li and L. Yang, “Driving forces for drug loading in drug carriers,” *J. Microencapsul.*, vol. 32, no. 3, pp. 255–272, 2015.

[21] H. Kobayashi, R. Watanabe, and P. L. Choyke, “Improving conventional enhanced permeability and retention (EPR) effects; What is the appropriate target?,” *Theranostics*. 2014.

[22] S. Patil, A. Sandberg, E. Heckert, W. Self, and S. Seal, “Protein adsorption and cellular uptake of cerium oxide nanoparticles as a function of zeta potential,” *Biomaterials*, 2007.

[23] B. Ustamehmetoğlu, I. Osken, M. E. Cinar, E. Sezer, E. Karaca, and T. Ozturk, “Synthesis and Characterization of Dithienothiophene, Bithiazole and Thiophene Containing Polymer,” *Electrochim. Acta*, vol. 227, pp. 435–446, 2017.

[24] W. Zhang, Z. Guo, D. Huang, Z. Liu, X. Guo, and H. Zhong, “Synergistic effect of chemo-photothermal therapy using PEGylated graphene oxide,” *Biomaterials*, vol. 32, no. 33, pp. 8555–8561, 2011.

[25] S. Wu *et al.*, “Adsorption properties of doxorubicin hydrochloride onto graphene oxide: Equilibrium, kinetic and thermodynamic studies,” *Materials (Basel).*, vol. 6, no. 5, pp. 2026–2042, 2013.

[26] X. Yang, X. Zhang, Z. Liu, Y. Ma, Y. Huang, and Y. Chen, “High-efficiency loading and controlled release of doxorubicin hydrochloride on graphene oxide,” *J. Phys. Chem. C*, vol. 112, no. 45, pp. 17554–17558, 2008.

[27] S. Wu *et al.*, “Adsorption properties of doxorubicin hydrochloride onto graphene oxide: Equilibrium, kinetic and thermodynamic studies,” *Materials (Basel).*, vol. 6, no. 5, pp. 2026–2042, 2013.

[28] Mohadeseh *et al.*, “Normalization of doxorubicin release from graphene oxide: New approach for optimization of effective parameters on drug loading,” *Biotechnol. Appl. Biochem.*, vol. 64, no. 3, pp. 433–442, 2017.

[29] T. Hyeon and V. Rotello, “Featuring an artistic representation of cellular endocytosis,” *Chem. Soc. Rev.*, 2012.

[30] A. Moore, Z. Medarova, A. Potthast, and G. Dai, “In Vivo Targeting of Underglycosylated MUC-1 Tumor Antigen Using a Multimodal Imaging Probe,” *Cancer Res.*, vol. 64, no. 5, pp. 1821–1827, 2004.

[31] R. Baskar, K. A. Lee, R. Yeo, and K. W. Yeoh, “Cancer and radiation therapy:

Current advances and future directions," *Int. J. Med. Sci.*, vol. 9, no. 3, pp. 193–199, 2012.

[32] D. Hanahan and R. A. Weinberg, "Hallmarks of cancer: The next generation," *Cell*. 2011.

[33] C. L. Chaffer and R. A. Weinberg, "A perspective on cancer cell metastasis," *Science*. 2011.

[34] L. A. Pollack, J. H. Rowland, C. Crammer, and M. Stefanek, "Introduction: Charting the landscape of cancer survivors' health-related outcomes and care," in *Cancer*, 2009.

[35] G. Delaney, S. Jacob, C. Featherstone, and M. Barton, "The role of radiotherapy in cancer treatment: Estimating optimal utilization from a review of evidence-based clinical guidelines," *Cancer*. 2005.

[36] S. Y. Hwang, S. Park, and Y. Kwon, "Recent therapeutic trends and promising targets in triple negative breast cancer," *Pharmacology and Therapeutics*. 2019.

[37] J. Deng, S. Xu, W. Hu, X. Xun, L. Zheng, and M. Su, "Tumor targeted, stealthy and degradable bismuth nanoparticles for enhanced X-ray radiation therapy of breast cancer," *Biomaterials*, vol. 154, pp. 24–33, 2018.

[38] Y. S. Yang, R. P. Carney, F. Stellacci, and D. J. Irvine, "Enhancing radiotherapy by lipid nanocapsule-mediated delivery of amphiphilic gold nanoparticles to intracellular membranes," *ACS Nano*, 2014.

[39] F. B. De Abreu, G. N. Schwartz, W. A. Wells, and G. J. Tsongalis, "Personalized therapy for breast cancer," *Clin. Genet.*, vol. 86, no. 1, pp. 62–67, 2014.

[40] M. M. Dale and H. P. Rang, "Rang & Dale's pharmacology. 6th ed," *(Edinburgh): Churchill Livingstone*. 2007.

[41] C. Moorthi, R. Manavalan, and K. Kathiresan, "Nanotherapeutics to overcome conventional cancer chemotherapy limitations," *J. Pharm. Pharm. Sci.*, vol. 14, no. 1, pp. 67–77, 2011.

[42] A. A. Stavrovskaya, "Cellular Mechanisms of Multidrug Resistance of Tumor Cells," *Biochemistry (Moscow)*. 2000.

[43] L. Harris *et al.*, “Liposome-encapsulated doxorubicin compared with conventional doxorubicin in a randomized multicenter trial as first-line therapy of metastatic breast carcinoma,” *Cancer*, 2002.

[44] K. Cho, X. Wang, S. Nie, Z. Chen, and D. M. Shin, “Therapeutic nanoparticles for drug delivery in cancer,” *Clinical Cancer Research*. 2008.

[45] T. M. Allen and P. R. Cullis, “Drug Delivery Systems: Entering the Mainstream,” *Science*. 2004.

[46] E. Pauwels, K. Kairemo, P. Erba, and K. Bergstrom, “Nanoparticles in Cancer,” *Curr. Radiopharm.*, 2010.

[47] D. Ghosh Dastidar, D. Ghosh, and G. Chakrabarti, “Tumour vasculature targeted anti-cancer therapy,” *Vessel Plus*, vol. 2020, 2020.

[48] R. K. Jain, “Delivery of molecular medicine to solid tumors: Lessons from in vivo imaging of gene expression and function,” in *Journal of Controlled Release*, 2001.

[49] M. E. Fox, F. C. Szoka, and J. M. J. Fréchet, “Soluble polymer carriers for the treatment of cancer: The importance of molecular architecture,” *Acc. Chem. Res.*, vol. 42, no. 8, pp. 1141–1151, 2009.

[50] L. Brannon-Peppas and J. O. Blanchette, “Nanoparticle and targeted systems for cancer therapy,” *Advanced Drug Delivery Reviews*. 2012.

[51] S. D. Nathanson and L. Nelson, “Interstitial fluid pressure in breast cancer, benign breast conditions, and breast parenchyma,” *Ann. Surg. Oncol.*, 1994.

[52] X. Y. Xiong, Y. C. Gong, Z. L. Li, Y. P. Li, and L. Guo, “Active targeting behaviors of biotinylated Pluronic/poly (lactic acid) nanoparticles in vitro through three-step biotin-avidin interaction,” *J. Biomater. Sci. Polym. Ed.*, 2011.

[53] P. Galvin *et al.*, “Nanoparticle-based drug delivery: Case studies for cancer and cardiovascular applications,” *Cellular and Molecular Life Sciences*. 2012.

[54] J. D. Byrne, T. Betancourt, and L. Brannon-Peppas, “Active targeting schemes for nanoparticle systems in cancer therapeutics,” *Advanced Drug Delivery Reviews*. 2008.

[55] M. Yu and J. Zheng, “Clearance Pathways and Tumor Targeting of Imaging Nanoparticles,” *ACS Nano*. 2015.

[56] F. Salahpour Anarjan, “Active targeting drug delivery nanocarriers: Ligands,” *Nano-Structures and Nano-Objects*, vol. 19, p. 100370, 2019.

[57] M. Bacac *et al.*, “A novel carcinoembryonic antigen T-cell bispecific antibody (CEA TCB) for the treatment of solid tumors,” *Clin. Cancer Res.*, 2016.

[58] X. Wu, J. Chen, M. Wu, and J. X. Zhao, “Aptamers: Active targeting ligands for cancer diagnosis and therapy,” *Theranostics*. 2015.

[59] S. B. Ho *et al.*, “Mucin Gene Expression in Normal, Preneoplastic, and Neoplastic Human Gastric Epithelium,” *Cancer Res.*, 1995.

[60] J. Taylor-Papadimitriou, J. Burchell, D. W. Miles, and M. Dalziel, “MUC1 and cancer,” *Biochimica et Biophysica Acta - Molecular Basis of Disease*. 1999.

[61] J. G. Walter, Ö. Kökpinar, K. Friehs, F. Stahl, and T. Scheper, “Systematic investigation of optimal aptamer immobilization for protein-microarray applications,” *Anal. Chem.*, 2008.

[62] F. S. Do Carmo *et al.*, “Anti-MUC1 nano-aptamers for triple-negative breast cancer imaging by single-photon emission computed tomography in inducted animals: Initial considerations,” *Int. J. Nanomedicine*, vol. 12, pp. 53–60, 2017.

[63] J. E. Smith, C. D. Medley, Z. Tang, D. Shangguan, C. Lofton, and W. Tan, “Aptamer-conjugated nanoparticles for the collection and detection of multiple cancer cells,” *Anal. Chem.*, 2007.

[64] C. J. Cheng and W. M. Saltzman, “Enhanced siRNA delivery into cells by exploiting the synergy between targeting ligands and cell-penetrating peptides,” *Biomaterials*, 2011.

[65] P. V. Paranjpe, Y. Chen, V. Kholodovych, W. Welsh, S. Stein, and P. J. Sinko, “Tumor-targeted bioconjugate based delivery of camptothecin: Design, synthesis and in vitro evaluation,” *J. Control. Release*, 2004.

[66] J. You, X. Li, F. De Cui, Y. Z. Du, H. Yuan, and F. Q. Hu, “Folate-conjugated polymer micelles for active targeting to cancer cells: Preparation, in vitro

evaluation of targeting ability and cytotoxicity," *Nanotechnology*, 2008.

[67] M. Hagimori, Y. Fuchigami, and S. Kawakami, "Stimuli-Responsive Systems of Therapeutics Peptide-Based Cancer-Targeted DDS and Molecular Imaging," vol. 65, no. 7, pp. 618–624, 2017.

[68] I. Kogan-Zviagin, Y. Shamay, A. Nissan, O. Sella-Tavor, M. Golan, and A. David, "Intra-colonic administration of a polymer-bound NIRF probe for improved colorectal cancer detection during colonoscopy," *J. Control. Release*, vol. 192, pp. 182–191, 2014.

[69] D. Aldoori, "Curriculum vitae Curriculum vitae Curriculum vitae Curriculum vitae," *Cv*, no. loker, pp. 28–30, 2008.

[70] Y. Y. Durmaz, Y. L. Lin, and M. E. H. Elsayed, "Development of degradable, pH-sensitive star vectors for enhancing the cytoplasmic delivery of nucleic acids," *Adv. Funct. Mater.*, vol. 23, no. 31, pp. 3885–3895, 2013.

[71] H. S. Kim, T. J. Oweida, and Y. G. Yingling, "Interfacial stability of graphene-based surfaces in water and organic solvents," *J. Mater. Sci.*, 2018.

[72] N. Ma *et al.*, "Folic acid-grafted bovine serum albumin decorated graphene oxide: An efficient drug carrier for targeted cancer therapy," *J. Colloid Interface Sci.*, 2017.

[73] M. Zamani, M. Rostami, M. Aghajanzadeh, H. Kheiri Manjili, K. Rostamizadeh, and H. Danafar, "Mesoporous titanium dioxide@ zinc oxide–graphene oxide nanocarriers for colon-specific drug delivery," *J. Mater. Sci.*, 2018.

[74] S. Ryon *et al.*, "Graphene-based materials for tissue engineering Graphical Abstract HHS Public Access," *Adv Drug Deliv Rev*, 2016.

[75] C. Genslein, P. Hausler, E.-M. Kirchner, R. Bierl, A. J. Baeumner, and T. Hirsch, "Detection of small molecules with surface plasmon resonance by synergistic plasmonic effects of nanostructured surfaces and graphene," in *Plasmonics in Biology and Medicine XIV*, 2017.

[76] D. Iannazzo *et al.*, "Synthesis and anti-HIV activity of carboxylated and drug-conjugated multi-walled carbon nanotubes," *Carbon N. Y.*, 2015.

[77] S. Singal, A. K. Srivastava, S. Dhakate, A. M. Biradar, and Rajesh, "Electroactive graphene-multi-walled carbon nanotube hybrid supported impedimetric immunosensor for the detection of human cardiac troponin-I," *RSC Adv.*, 2015.

[78] T. T. M. Thi, P. T. Dat, V. C. Minh, N. H. Tho, and N. X. Sang, "Physical Adsorption and Photocatalytic Activity of Titanium Dioxide Nanotube and Graphene Oxide Composite," *VNU J. Sci. Nat. Sci. Technol.*, 2018.

[79] P. N. Joshi, S. Kundu, S. K. Sanghi, and D. Sarkar, "Graphene Quantum Dots - From Emergence to Nanotheranostic Applications," in *Smart Drug Delivery System*, 2016.

[80] A. Manuscript, "Materials Chemistry B," 2020.

[81] S. Han, L. Su, M. Zhai, L. Ma, S. Liu, and Y. Teng, "A molecularly imprinted composite based on graphene oxide for targeted drug delivery to tumor cells," *J. Mater. Sci.*, vol. 54, no. 4, pp. 3331–3341, 2019.

[82] D. Iannazzo *et al.*, "A smart nanovector for cancer targeted drug delivery based on graphene quantum dots," *Nanomaterials*, vol. 9, no. 2, pp. 1–17, 2019.

[83] Z. Wang, L. C. Ciacchi, and G. Wei, "Recent advances in the synthesis of graphene-based nanomaterials for controlled drug delivery," *Appl. Sci.*, vol. 7, no. 11, 2017.

[84] H. S. Jung, M. Y. Lee, W. H. Kong, I. H. Do, and S. K. Hahn, "Nano graphene oxide-hyaluronic acid conjugate for target specific cancer drug delivery," *RSC Adv.*, vol. 4, no. 27, pp. 14197–14200, 2014.

[85] S. M. Chowdhury *et al.*, "Graphene nanoribbons as a drug delivery agent for lucanthone mediated therapy of glioblastoma multiforme," *Nanomedicine Nanotechnology, Biol. Med.*, 2015.

[86] C. Wang, B. Chen, M. Zou, and G. Cheng, "Cyclic RGD-modified chitosan/graphene oxide polymers for drug delivery and cellular imaging," *Colloids Surfaces B Biointerfaces*, 2014.

[87] H. Gao, W. Yang, K. Min, L. Zha, C. Wang, and S. Fu, "Thermosensitive poly(N-isopropylacrylamide) nanocapsules with controlled permeability," in

Polymer, 2005.

[88] E. Ruiz-Hernández, A. Baeza, and M. Vallet-Regí, "Smart drug delivery through DNA/magnetic nanoparticle gates," *ACS Nano*, 2011.

[89] N. Y. Rapoport, A. M. Kennedy, J. E. Shea, C. L. Scaife, and K. H. Nam, "Controlled and targeted tumor chemotherapy by ultrasound-activated nanoemulsions/microbubbles," *J. Control. Release*, 2009.

[90] Z. Xiao *et al.*, "DNA self-assembly of targeted near-infrared-responsive gold nanoparticles for cancer thermo-chemotherapy," *Angew. Chemie - Int. Ed.*, 2012.

[91] Q. Yan, J. Yuan, Z. Cai, Y. Xin, Y. Kang, and Y. Yin, "Voltage-responsive vesicles based on orthogonal assembly of two homopolymers," *J. Am. Chem. Soc.*, 2010.

[92] E. Demirel, E. Karaca, and Y. Yuksel Durmaz, "Effective PEGylation method to improve biocompatibility of graphene derivatives," *Eur. Polym. J.*, vol. 124, no. November 2019, p. 109504, 2020.

[93] J. I. Paredes, S. Villar-Rodil, A. Martínez-Alonso, and J. M. D. Tascón, "Graphene oxide dispersions in organic solvents," *Langmuir*, vol. 24, no. 19, pp. 10560–10564, 2008.

[94] M. Morpurgo and F. M. Veronese, "Conjugates of peptides and proteins to polyethylene glycols.," *Methods Mol. Biol.*, vol. 283, pp. 45–70, 2004.

[95] V. Kuete, O. Karaosmanoğlu, and H. Sivas, "Anticancer Activities of African Medicinal Spices and Vegetables," *Med. Spices Veg. from Africa Ther. Potential Against Metab. Inflammatory, Infect. Syst. Dis.*, pp. 271–297, 2017.

[96] Y. Oz, A. Barras, R. Sanyal, R. Boukherroub, S. Szunerits, and A. Sanyal, "Functionalization of reduced graphene oxide via thiol-maleimide 'click' chemistry: Facile fabrication of targeted drug delivery vehicles," *ACS Appl. Mater. Interfaces*, vol. 9, no. 39, pp. 34194–34203, 2017.

[97] W. Zhang *et al.*, "Preparation of amino-functionalized graphene oxide by Hoffman rearrangement and its performances on polyacrylate coating latex," *Prog. Org. Coatings*, vol. 94, pp. 9–17, May 2016.

[98] and A. C. Dominic Chow†,§, Michelle L. Nunalee†,‡, Dong Woo Lim†,‡, Andrew J. Simnick†,‡, "Peptide-based Biopolymers in Biomedicine and Biotechnology," *Mater Sci Eng R Rep*, vol. 23, no. 1, pp. 1–7, 2008.

[99] X. Zhao, L. Liu, X. Li, J. Zeng, X. Jia, and P. Liu, "Biocompatible graphene oxide nanoparticle-based drug delivery platform for tumor microenvironment-responsive triggered release of doxorubicin," *Langmuir*, vol. 30, no. 34, pp. 10419–10429, 2014.x

[100] H. Kim, D. Lee, J. Kim, T. Il Kim, and W. J. Kim, "Photothermally triggered cytosolic drug delivery via endosome disruption using a functionalized reduced graphene oxide," *ACS Nano*, vol. 7, no. 8, pp. 6735–6746, 2013.

[101] Y. Zhang, C. Liu, W. Shi, Z. Wang, L. Dai, and X. Zhang, "Direct measurements of the interaction between pyrene and graphite in aqueous media by single molecule force spectroscopy: Understanding the π-π interactions," *Langmuir*, vol. 23, no. 15, pp. 7911–7915, 2007.

[102] Z. Medarova, L. Rashkovetsky, P. Pantazopoulos, and A. Moore, "Multiparametric monitoring of tumor response to chemotherapy by noninvasive imaging," *Cancer Res.*, vol. 69, no. 3, pp. 1182–1189, 2009.

[103] K. Chatterjee, J. Zhang, N. Honbo, and J. S. Karliner, "Doxorubicin cardiomyopathy," *Cardiology*. 2010.

[104] Q. Ban, T. Bai, X. Duan, and J. Kong, "Noninvasive photothermal cancer therapy nanoplatforms: Via integrating nanomaterials and functional polymers," *Biomater. Sci.*, vol. 5, no. 2, pp. 190–210, 2017.

[105] K. Ryu, J. Park, and T. Il Kim, "Effect of ph-responsive charge-conversional polymer coating to cationic reduced graphene oxide nanostructures for tumor microenvironment-targeted drug delivery systems," *Nanomaterials*, vol. 9, no. 9, 2019.

[106] S. Y. Qin *et al.*, "Theranostic GO-based nanohybrid for tumor induced imaging and potential combinational tumor therapy," *Small*, vol. 10, no. 3, pp. 599–608, 2014.

[107] W. Zhang, J. Dai, G. Zhang, Y. Zhang, S. Li, and D. Nie, "Photothermal/pH

Dual-Responsive Drug Delivery System of Amino-Terminated HBP-Modified rGO and the Chemo-Photothermal Therapy on Tumor Cells," *Nanoscale Res. Lett.*, vol. 13, 2018.

[108] A. H. Hung *et al.*, "Graphene oxide enhances cellular delivery of hydrophilic small molecules by co-incubation," *ACS Nano*, vol. 8, no. 10, pp. 10168–10177, 2014.

[109] S. C. Therapy, "Synergistic Cancer Therapy," pp. 1–14, 2020.

[110] M. D. Walsh, S. M. Luckie, M. C. Cummings, T. M. Antalis, and M. A. Mcguckin, "Heterogeneity of MUC1 expression by human breast carcinoma cell lines in vivo and in vitro," *Breast Cancer Res. Treat.*, vol. 58, pp. 255–266, 2000.

[111] E. Quagliarini, R. Di Santo, D. Pozzi, P. Tentori, F. Cardarelli, and G. Caracciolo, "Mechanistic insights into the release of doxorubicin from graphene oxide in cancer cells," *Nanomaterials*, vol. 10, no. 8, pp. 1–11, 2020.

DEVELOPMENT OF EPPT1 TARGETED BIOCOMPATIBLE DRUG DELIVERY SYSTEM AND INVESTIGATION OF ITS ANTICANCER ACTIVITY

ORIGINALITY REPORT

15%	11%	10%	4%
SIMILARITY INDEX	INTERNET SOURCES	PUBLICATIONS	STUDENT PAPERS

PRIMARY SOURCES

1	ejournals.library.ualberta.ca Internet Source	1%
2	Fatemeh Salahpour Anarjan. "Active targeting drug delivery nanocarriers: Ligands", Nano-Structures & Nano-Objects, 2019 Publication	1%
3	sens.medipol.edu.tr Internet Source	1%
4	pubs.rsc.org Internet Source	1%
5	www.freepatentsonline.com Internet Source	<1%
6	Submitted to Nashville State Community College Student Paper	<1%
7	"Handbook of Graphene", Wiley, 2019 Publication	<1%